

Interrogating the neurotransmitter system with fast-scan cyclic
voltammetry in an optogenetics context

by

Yao Lu

M.A., Chemistry, 2012

Brown University, Providence, RI, US

B.S., Chemistry, 2010

Tsinghua University, Beijing, China

A dissertation submitted in partial fulfillment of the
requirements for the Degree of Doctor of Philosophy
in the Department of Chemistry at Brown University

Providence, Rhode Island

May 2016

© Copyright 2016 by Yao Lu

This dissertation by Yao Lu is accepted in its present form by
the Department of Chemistry as satisfying the dissertation requirement
for the degree of Doctor of Philosophy.

Date _____

Dr. Arto V. Nurmikko, Advisor

Recommended to the Graduate Council

Date _____

Dr. Wilson Truccolo, Reader, Co-advisor

Date _____

Dr. Shouheng Sun, Reader

Date _____

Dr. Lai-Sheng Wang, Reader

Date _____

Dr. Wael Asaad, Reader

Approved by the Graduate Council

Date _____

Dr. Peter M. Weber

Curriculum Vitae

Yao Lu was born in Kaifeng, Henan Province of China on July 26th, 1987. He went to Tsinghua University for undergraduate study since 2006 and graduated with a B.Sc. in Chemistry in 2010. Yao started doctoral study in August, 2010 in the Department of Chemistry at Brown University. He joined Dr. Arto V. Nurmikko's neuroengineering lab and researched on various interdisciplinary projects.

Publications in scientific Journals, peer reviewed:

In time order:

[1]. Lu, Y., Driscoll, N., Ozden, I., Yu, Z., Nurmikko, A. V. (2015). Modulating dopamine release by optogenetics in transgenic mice reveals terminal dopaminergic dynamics. **Neurophotonics**, 2(3), doi: 10.1117/1.NPh.2.3

[2]. Jiang, M., Kurvits, J., Lu, Y., Nurmikko, A. V., Zia, R. (2015). Reusable Inorganic Templates for Electrostatic Self-Assembly of Individual Quantum Dots, Nanodiamonds, and Lanthanide-Doped Nanoparticles. **Nano Lett.**, doi: 10.1021/acs.nanolett.5b01009.

[3]. Lu, Y., Truccolo, W., Wagner, F. B. P., Vargas-Irwin, C. E., Ozden, I.,

Zimmermann, J. B., Nurmikko, A. V. (2015). Optogenetically-Induced Spatiotemporal Gamma Oscillations and Neuronal Spiking Activity in Primate Motor Cortex. **Journal of Neurophysiology**, doi: 10.1152/jn.00792.2014

[4]. Yin, M., Borton, D.A., Komar, J., Agha, N., Lu, Y., Li, H., Li, Q., et al. (2014). NeuroResource Wireless Neurosensor for Full-Spectrum Electrophysiology Recordings during Free Behavior. **Neuron**, 84, 1170-182, doi: 10.1016/j.neuron.2014.11.010

[5]. Ozden, I., Wang, J., Lu, Y., May, T., Lee, J., Goo, W., Nurmikko, A. V. (2013). A coaxial optrode as multifunction write-read probe for optogenetic studies in non-human primates. **Journal of Neuroscience Methods**, 219(1), 142-4, doi: 10.1016/j.jneumeth.2013.06.011

[6]. Nisar, A., Lu, Y., Zhuang, J., Wang, X. (2011). Polyoxometalate nanocone nanoreactors: Magnetic manipulation and enhanced catalytic performance. **Angewandte Chemie - International Edition**, 50(14), 3187-192, doi: 10.1002/anie.201006155

[7]. Nisar, A., Lu, Y., Wang, X. (2010). Assembling polyoxometalate clusters into advanced nanoarchitectures. **Chemistry of Materials**, 22(11), 3511-518, doi: 10.1021/cm100691a

Acknowledgements

It is to my great pleasure to deliver my sincere thanks to the numerous people I worked with at Brown University who are the best professors and colleges. I receive constant help and support from them, which makes my scientific research at Brown University extremely exciting and fascinating.

Firstly I would like to sincerely thank my advisor, the leader for our neuroengineering lab, Dr. Arto V. Nurmikko for his guidance and advisory in the development of my research interests, his help and encouragement through various challenges in the scientific study, and his unconditional support through all aspects in the academic and non-academic world.

I would like to thank my co-advisor Dr. Wilson Truccolo. Through the five years of my research, he has been supporting my scientific explorations in the neuron-related disciplines. As a computational neuroscientist, Dr. Truccolo has been always giving me great advisements and patiently answering my naive questions.

I would like to thank my committee members Dr. Lai-Sheng Wang, Dr. Shouheng Sun, Dr. Wael Asaad, all of whom have been supporting throughout my 5 years of

research with invaluable advices and resources. Dr. Shouheng Sun and Dr. Lai-sheng Wang are excellent chemists who have considerable professional knowledge and experience in electro-chemistry, and have been supporting me both through courses in the chemistry department and through research. Dr. Wael Asaad has been providing me with important guidance with his deep understanding of the Basal Ganglia and dopaminergic system, especially through the efforts of *in vivo* studies.

Finally, I would like to express my sincere appreciation to my wife, Zidan Wu, who has been unconditionally supporting me for my research activity in the lab. I'm also truly in debt and thankful for my parents for their love and encouragement. Without their support I would never be able to pursue my dream at Brown University.

Contents

List of Tables	xiii
List of Figures	xiv
1 Introduction	1
1.1 The mystery of the brain and the motivation of research	2
1.2 The brain's chemical messenger systems	5
1.3 Approaches for real-time monitoring of neuro-chemicals	8
1.4 Introduction to the work presented in this article	10
2 Electro-chemical sensing of neurotransmitters through Fast-Scan Cyclic Voltammetry with carbon based electrodes	12
2.1 Introduction to Fast-Scan Cyclic Voltammetry (FSCV)	13
2.2 Mechanism of FSCV and example of recorded chemical signals	15
2.2.1 Electric holding and scanning potentials	15
2.2.2 Generating background-subtracted cyclic voltammograms	17

2.2.3	Monitoring neuro-chemical concentration in real-time	19
2.3	Preparation of carbon fiber micro-electrodes for FSCV	21
2.4	Instrumentation and neuro-chemical signal acquisition	24
3	Chemical messenger dopamine dynamics interrogated through op-	
	togenetics in transgenic mice brain slices	27
3.1	Introduction: Investigating chemical messenger dopamine through light	
	stimulation	29
3.2	Optogenetic tools and characterizing the expression of opsins	32
3.2.1	Development of optogenetics	32
3.2.2	Cell-type specificity and transgenic animals	34
3.2.3	Use Immuno-chemistry to characterize the ChR2/EYFP ex-	
	pression	36
3.3	Experimental setup and methodology for studying dopamine dynamics	
	in healthy brain slices	42
3.3.1	Breeding transgenic animals and the brain slice technique . . .	42
3.3.2	Preparing FSCV recording chamber and optical stimulation	
	paradigm	44
3.3.3	Fast-scan cyclic voltammetry experiments	46
3.3.4	Post-processing of recorded neuro-chemical signals	48
3.4	Optogenetic stimulation is able to induced neuro-chemical dopamine	
	release	49

3.5	Modulating the dopamine release concentration by different light stimulation protocols	55
3.5.1	Effects of light power	55
3.5.2	Effects of stimulation pulse width	58
3.5.3	Discussion on stimulation parameters	60
3.6	The amplitude of transient dopamine response is critically dependent on the temporal profile of the light stimulus	62
3.7	Recovery of presynaptic dopamine revealed by optogenetics	67
3.8	Chemical kinetic analysis of dopamine release and uptake	71
3.9	Conclusions	73
4	A novel chronically implantable neuro-chemical sensing probe for real-time monitoring of neurotransmitters <i>in vivo</i>	75
4.1	Introduction: Motivation of the development of a chronic neuro-chemical sensor	76
4.2	Design of the chronically implantable neuro-chemical sensing probe .	78
4.3	Fabrication approaches	86
4.4	Characterizing the neuro-chemical sensing probe <i>in vitro</i> and comparison with traditional probes	91
4.4.1	Testing the neuro-chemical probe in dopamine standard solution	91
4.4.2	Testing the neuro-chemical probe in live transgenic mouse brain slices	93

4.5	Improvements made for adaptation of the chronic implantation environment	97
4.6	Conclusions	99
5	In vivo real-time electro-chemical sensing of dopamine activity in transgenic mice	101
5.1	Experiment protocols of FSCV recording in live transgenic mouse . .	102
5.2	Detecting endogenous dopamine in the dorsal striatum	108
5.2.1	In vivo FSCV Background activity in a passive state	108
5.2.2	Measuring dopamine through adsorption in dorsal striatum . .	110
5.2.3	Differences of dopamine concentrations in dorsal striatum and the cortex	112
5.3	Optogenetically induced <i>in vivo</i> dopamine activity	115
5.4	Dopamine activity in an environment with external physical-stress induction	117
5.5	Conclusions	120
6	Discussion and conclusions	121
6.1	Light stimulation modulated dopamine release	123
6.2	Specificity of neuro-chemicals	124
6.3	In vivo dopamine activity	126
A	Investigating induced brain rhythms through optogenetics	128

A.1	Background on brain’s gamma oscillations	129
A.2	Experimental methods	131
A.3	Optogenetic stimulation above a critical intensity level induces narrow band gamma oscillations	136
A.4	Induced gamma engage a larger network beyond the direct light stim- ulation region	141
A.5	Spatiotemporal patterns (waves) of optogenetically-induced gamma os- cillations	142
A.6	Neuronal spiking during induced gamma oscillations	143
A.7	Discussion and conclusions	148
	REFERENCES	152

List of Tables

3.1 Table of transgenic animal lines 35

List of Figures

1.1	Oxidation and reduction of the electro-chemically active dopamine.	9
2.1	Illustration of the scanning electric potential against the working electrode.	16
2.2	Recorded raw FSCV current signals.	17
2.3	Non-background-subtracted cyclic voltammogram.	19
2.4	Example of FSCV recording with dopamine solution.	20
2.5	Photo of a homemade carbon fiber electrode.	22
2.6	The FSCV instrumentation.	25
3.1	ChR2-EYFP expression in transgenic mouse brain slices.	37
3.2	High resolution fluorescent microscope images in SN/VTA region.	38
3.3	Immunocytochemistry analysis with Tyrosine Hydroxylase staining in the NAc.	40
3.4	Immunocytochemistry analysis with Tyrosine Hydroxylase staining in the VTA.	41

3.5	Illustration of the optical stimulation paradigm in brain slices dopamine FSCV experiments.	45
3.6	Insertion of CFE in brain slices.	48
3.7	Optically induced DA efflux by a 25 ms light pulse in transgenic mouse brain slices.	51
3.8	Background subtracted cyclic voltammogram at optical DA release peak	53
3.9	One control experiment where electrode is not inserted in the brain slices.	54
3.10	Optically induced DA peak level as a function of light power.	56
3.11	Eadie-Hofstee transformation of the mean DA peak response vs. light power density curve.	57
3.12	Effect of light pulse width on the evoked dopamine concentration.	59
3.13	Dopamine release levels from varies stimulation parameters.	61
3.14	FSCV 2D color plots in two stimulation conditions.	63
3.15	Correlation of light ramp duration and mean DA peak response.	66
3.16	Effects of stimulation inter-pulse interval.	68
3.17	Recovery of releasable presynaptic DA pool.	69
3.18	Kinetic analysis of dopamine release and uptake.	72
3.19	The Michaelis-Menten kinetics of dopamine uptake under optical stim- ulation.	72
4.1	Illustration of the probe design.	79

4.2	Intensity distribution simulation of light delivered through two types of optical fibers , in log10 scale, unit: mW/mm ²	82
4.3	Penetration test and additional electrophysiology electrode.	85
4.4	Fabrication process of the neuro-chemical probe.	87
4.5	Detailed structure of the probe tip.	90
4.6	Neuro-chemical probe testing in dopamine standard solutions.	92
4.7	Neuro-chemical probe with multiple carbon fibers.	93
4.8	Testing the probe in live brain slices.	94
4.9	Validating the neuro-chemical probe in brain slices	96
4.10	Comparison of induced dopamine in dorsal (left) and ventral (right) striatum.	97
5.1	The probe and head-fixed <i>in vivo</i> experiment configuration.	103
5.2	Reference wire and the neuro-chemical probe inserted in brain tissue at two locations on the skull.	105
5.3	A view of the chronically implanted assembly.	106
5.4	2D FSCV color plot in the cortex and dorsal striatum of live transgenic mouse brain.	109
5.5	FSCV recording of dopamine in dorsal striatum through adsorption.	111
5.6	FSCV signals as the probe is retracted from dorsal striatum back into the cortex, showing decreased dopamine signal.	113

5.7	Optogenetically induced dopamine release from a chronically implanted probe in a live animal.	116
5.8	Tail pinch stress applied as indicated by the blue stripe. Activities observed following the stress induction.	119
A.1	Polymer optical fiber microelectrode array (POF-MEA).	137
A.2	Gamma oscillations induced by constant (square) pulse light stimulation.	139
A.3	Gamma oscillations induced by ramp light stimulation.	140
A.4	Spatiotemporal patterns of optogenetically-induced gamma waves.	144
A.5	Modulation of neuronal spiking rates during optogenetically-induced gamma LFP oscillations.	146
A.6	Spike-LFP pairwise phase consistency analysis and predictive power of optogenetically-induced gamma oscillations on neuronal spiking.	147

Chapter 1

Introduction

1.1 The mystery of the brain and the motivation of research

The human brain is a complex electrical and chemical system which is composed of around 10^{11} individual neurons. Although technology today allows researchers to gain in-depth knowledge of the working mechanism for many of the body's organs, the brain remains the least understood. The brain is the vital central command center of the human body where all of human experience and thoughts are generated and experienced. Despite technological advances of the time, the united and coherent working of this complicated system is still largely concealed in mystery. I would like to begin with one story to take a brief peek at the mysteries of the brain.

Dr. Sperry:

It was a sunny day in 1979, Dr. Roger Sperry walked into his brain psychology lab at the California Institute of Technology. He had scheduled a meeting with a special 'guest' later today. It was one of his patients who had suffered massive epileptic seizures,. Dr. Sperry knew he needed a corpus callosotomy, a surgical procedure which disconnects the two hemispheres of the brain by slicing the thick bundle of nerve fibers that pass between..

The surgery had no complications and the patient's seizures had been fully contained in the time since surgery. The purpose of the visit today was to run a visual perception test, since the patient reported some strange symptoms. Dr. Sperry asked

the patient to fix his eyes at the center of the screen. Note that brain's visual system works in such a way that left and right side of the visual field projects to the opposite brain hemisphere. He flashed an image of a toothbrush on the right visual field, which can be perceived by the patient's left brain. The patient quickly responded saying it's a toothbrush that he saw. However, when the toothbrush was flashed on the left visual field in exactly the same way, the patient reported not seeing anything at all! The image was directed to the right side of the brain uninhibited but it seems he couldn't retrieve the information.

Dr. Sperry, confused since his patient's visual system was still intact, devised a modified experiment. He flashed an image of an object into the left eye, then asked the patient to use his left hand (controlled by the right brain) to pick out the item from an assortment. He correctly picked out the item in the image directed to his right brain, even though he reported seeing nothing. Dr. Sperry again asked the patient to explain what the item was, but the patient cannot vocally describe it.

This is now known as the 'split-brain' problem. While the two hemispheres of the healthy brain interact with each other closely via the major 'cable' – the corpus callosum - in the split brain patients, the cable is no longer functional which leads to the impaired communication of information, causing the two hemispheres to behave in dis-united ways, almost as if there are two brains working individually [64]. Since the language center is predominantly in the left hemisphere, information trapped in the right brain is not available for speech production, but the patient could still pick

out the object with the hand controlled by the right brain.

Another very interesting example in split-brain patients is the alien hand syndrome, where the patient lost conscious control of one of his hand, which can individually behave in unwanted ways, often leading the patient to use his other hand to physically stop the uncontrollable alien hand. This was also observed from the patients with split-brain.

Dr. Sperry won the Nobel prize in Physiology and Medicine with David Hunter Hubel and Torsten Nils Wiesel in 1981, for his research in the split-brain studies.

”Indeed a conscious system in its own right, perceiving, thinking, remembering, reasoning, willing, and emoting, all at a characteristically human level, and . . . both the left and the right hemisphere may be conscious simultaneously in different, even in mutually conflicting, mental experiences that run along in parallel.”

- Roger Wolcott Sperry, 1974

Dr. Sperry is also know for his study on the chemical guidance of neuronal connections, known as the 'chemoaffinity hypothesis'. He studied the guidance of visual neuron projections in African Clawed Frog. He concluded that the neurons used chemical markers to selectively direct their connections. This leads to the emerging of the research area of axonal growth guidance through chemical gradient of different molecules.

The above are only some of the examples to illustrate the mysteries of the brain. Many more burgeoning areas of research are just starting to aid in the long-term

battle to unveil the mysteries of this complex electrical and chemical system in our head. And eventually, to understand ourselves or our sophisticated minds better.

My research in this thesis focuses on the chemical messengers in the brain. These are a special family of molecules that are responsible for making the 10^{15} connections between individual neurons. I utilized electro-chemistry techniques to monitor the fluctuations of these chemical messengers in real time in brain slices or in the intact brain. Although it may be a small step in the generic research efforts towards understanding the nervous system, nevertheless, our study advances the understanding of the behavior of these important neuro-chemicals, potentially also contributing to the long term goal of revealing the mysteries of the brain.

1.2 The brain's chemical messenger systems

Despite the tremendous number of individual neurons, the brain cannot function if these neurons are not interconnected in a delicate and complex pattern. The connections between each cell are what's most important in establishing a conscious mind. 'I am my connectome', as Dr. Sebastian Seung, a faculty member now at Princeton University, asked his audience to read aloud repeatedly during his TED talk. What is responsible for enabling the communication between different cells are the synapses. The major mechanism for how synapses work is through the release and reception of chemical messengers. The activity evoked in the pre-synaptic neuron is the release of chemical messengers previously stocked in vesicles into the tiny gap at the synapse.

This leads to an increased concentration of these chemicals in the synapse. The post synaptic neuron senses the activity by using receptors which can bind specific chemicals, and it is then either excited or inhibited, i.e. it receives input information from the pre-synaptic neuron.

Understanding the chemical messenger systems in the brain is a major field of neuroscience study. These chemical messengers are called neurotransmitters and they can be divided into several groups: amino acids, gasotransmitters, monoamines, peptides and so on. The goal of this thesis is to use electro-chemistry methodology to investigate the electro-active monoamines, especially dopamine. As a major type of neurotransmitter, dopamine is primarily found in deep brain regions that has drawn considerable interest in recent years. Its role is closely related to behaviors involving reward seeking, motor control, learning, attention and emotion in both the healthy and diseased brain [29] [19]. Several neurological and psychiatric disorders such as depression, drug addiction, Attention Deficit Hyperactivity Disorder (ADHD) and Parkinson's disease are consequences of dopamine transmission deficiency or excessiveness [63] [24] [52]. Therefore, understanding the dopaminergic system is important in unfolding the underlying mechanisms and treating these disorders.

In the brain's dopamine messenger system, three major dopaminergic pathways dominate. In the mesolimbic pathway, the dopaminergic neurons in the ventral

tegmental area (VTA) project to the nucleus accumbens (NAc); in the nigrostriatal pathway projections originate in the substantia nigra (SN) and project to striatum; in mesocortical pathway projections run from the VTA to the prefrontal cortex [19]. In particular, on the dopamine system map, the NAc is known as the brain's 'reward center' [21]; alterations of dopamine level in the NAc can dramatically influence the animal's behavior. This is seen in experiments of intracranial electrical self-stimulation (ICSS). Animals continuously press the lever for stimulation to elicit dopamine release in the NAc at the expense of food consumption [31] [55], which is direct evidence of the significant role of mesolimbic dopamine in reward-related behavior.

Other chemical messengers such as serotonin also have vital functionality in the nervous system, and is also viable through electro-chemical sensing. For the scope of this thesis, we will focus on the electro-chemical sensing of dopamine in particular. Although we note that the tools and experimental framework developed in this thesis can be universally applied to other electro-active chemical species researches in brain slices or in the intact brain.

1.3 Approaches for real-time monitoring of neurochemicals

To study the chemical messenger system, one has to first gain a way of sensing the dynamics of these chemicals in the brain tissue. One method might be to surgically extract substances from the tissue and perform off-line analytics. However, this method is practically problematic because of the perturbation inflicted on the brain and the slow speeds at which these experiments can be performed. We can only gain the base chemical composition of the cerebro-spinal fluid, but have no access to the rich dynamical activity going on in the nervous system tissues.

Microdialysis has been one approach to studying neurotransmitter dynamics. A microdialysis probe is sufficiently small to cause minimal damage to the brain. The semi-permeable membrane at the tip of the probe allows passive diffusion of certain chemicals. Solution is collected in the probe over a range of minutes to gain a measurement of neurotransmitter concentration. The research using this technique has generated many interesting results regarding how neurotransmitters interact with various factors [1].

However, measuring neurotransmitter concentration every several minutes is still far less interesting for neuroscience research. Consider the other signals in the brain, such as the neuronal spiking activity: one spiking event takes only around 1 ms in total. Even slower dynamics of brain rhythms, such as some slow wave oscillations,

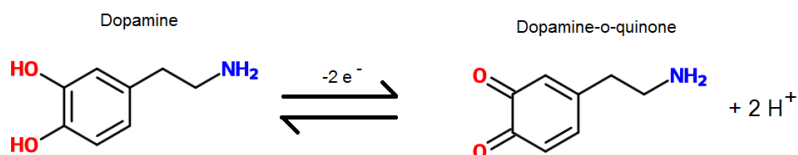


Figure 1.1: Oxidation and reduction of the electro-chemically active dopamine.

happen on a time scale of hundreds of milliseconds. To get close to this time scale, researchers have to invent a faster way of sensing neurotransmitters in the brain.

Electro-chemistry methods has been an innovative approach in neurotransmitter sensing. Because some of the chemical messengers are electro-active, for example, dopamine can be oxidized at carbon electrodes around electric potential of + 0.6 V. This makes it possible to measure the tiny oxidation / reduction currents through the electrodes to gain knowledge of the neurotransmitter concentration.

We adapted the Fast-Scan Cyclic Voltammetry (FSCV) as the electro-chemistry method to monitor neurotransmitter in real-time both in brain slices and *in vivo*. FSCV is better in terms of the speed and chemical identifiability compared to other electro-chemical techniques such as amperometry and pulsed voltammetry. We will spend the next chapter to explain and explore fast-scan cyclic voltammetry in detail.

1.4 Introduction to the work presented in this article

The work is presented here in the following order:

Firstly, the FSCV technique is introduced. Example of FSCV recording using home-made carbon fiber electrodes are shown. The electro-chemical signatures of dopamine molecules are explained with example recordings.

Next, we deployed optogenetic tools in a home-bred transgenic mouse model. This enables artificial induction of dopamine activity through activation of opsins. The neurons in these animals express opsin channelrhodopsin-2 in dopaminergic neurons only.

In the brain slices of these transgenic animals, we explored terminal dopamine release dynamics in response to temporally and spatially controlled optical stimulation. Dopamine signal was probed by FSCV using carbon fiber electrodes. We found that optogenetic stimulation applied directly at dopaminergic neuron terminals at e.g. nucleus accumbens in brain slices can effectively evoke dopamine release. Our results show that the temporal features and the level of dopamine release are non-linearly dependent on the optical power, pulse width and the shape of the waveform.

Later, for the purpose of monitoring neurotransmitter *in vivo*, we proceed to develop a novel two-way neuro-chemical sensing probe capable of both delivering controlled light stimulation and performing FSCV recording in deep brain regions.

Carbon and optical fibers are integrated together to achieve same-site stimulation and recording.

Lastly, this chronic implantable probe is used for *in vivo* experiments to study the dopamine transmission in mouse's dorsal striatum. Optogenetics successfully induced elevated dopamine response in live animals. Some observations of dopamine activity in a physically stressed state is also reported.

Overall, our systematical investigation of the dopamine dynamics *in vitro* and *in vivo* using a simple optogenetic framework provided important insights for neurochemical research, and demonstrated the capability to interrogate dopamine transmission using the combination of electro-chemistry and optogenetic tools. Part of the work in this thesis is published in [44]. The appendix session includes material from the publication [45] by the author.

Chapter 2

Electro-chemical sensing of
neurotransmitters through

Fast-Scan Cyclic Voltammetry

with carbon based electrodes

2.1 Introduction to Fast-Scan Cyclic Voltammetry (FSCV)

Cyclic Voltammetry (CV) has been a popular technique in studying electro-chemical properties of certain chemical species in the solution, understanding redox processes, as well as characterizing electrode surfaces of different materials [41]. In this technique, the applied electric potential of a working electrode is controlled with respect to a reference electrode whose potential is constant [40]. As the name cyclic voltammetry suggests, the voltage potential of the working electrode is scanned in a 'cyclic' way. It is first ramped up against the reference electrode, often linearly, to a certain value (switching potential) and then decreased to the initial potential. As the potential of the electrodes change, current flowing through the working electrode is being measured and plotted against the scanning potential to give a 'cyclic voltammogram' trace. This trace contains all sorts of information regarding both the chemicals in the solution and the electrode itself.

In the 1980s, Julian Millar developed a new technique, called Fast-Scan Cyclic Voltammetry to specifically target the applications for neuro-chemicals [13]. He has enhanced the traditional CV technique by increasing the temporal resolution of voltammetry scans by a few orders of magnitude. It is a significant step forward for the neuro-chemical research, because that the brain's chemical signals are often

very fast in nature, ranging from milliseconds to seconds, which is practically impossible for the traditional CV to keep record of. Since the development of FSCV, there have been vast research efforts involved in solving the myths of the brain's chemical messenger systems: dopamine, noradrenaline, serotonin, etc. Numerous publications have reported the discoveries in the rapid neurotransmitter transmission and its correlation with pharmacological and behavioral research.

There are some major advantages on using FSCV for neuro-chemical detection [58]. Some techniques such as micro-dialysis, works well for measuring long-term, tonic neuro-chemical fluctuations because of their low sampling rate (in minutes); however brain's fast, phasic neuro-chemical activity plays significant functional role in the neuronal systems. Another advantage of FSCV is its chemical identifiability. Non-cyclic electro-chemistry techniques such as amperometry [73] and pulsed voltammetry is able to perform fast measurement, but may provide less additional information regarding the redox processes. Note that in FSCV, different chemicals can be easily distinguished by their distinct signature oxidation and reduction peaks, because they start being oxidized at varies electric potentials on the electrode surface. Therefore, FSCV is the technique best suitable for studying fast, phasic neuro-chemical transmission in a complex chemical environment of the brain.

2.2 Mechanism of FSCV and example of recorded chemical signals

2.2.1 Electric holding and scanning potentials

We will first start by introducing how FSCV works in very practical examples. In conventional cyclic voltammetry, a scan cycle often takes minutes to hours to complete [40]. Here we use a sampling rate of 10 Hz, which means 10 scan cycles would be finished in 1 second time. Between each voltammetry scan, we have to leave enough time for the neuro-chemicals at the working electrode surface to exchange with the neuro-chemicals in the solution (the brain), so that the signals from the electrode can accurately reflect the real neuro-chemical concentration in the surrounding tissue. Figure 2.1 shows the working electrode potential, or command voltage, controlled by the voltameter. The holding potential is at -0.4 V to promote neuro-chemical dopamine adsorption at the working electrode surface. For each 100 ms, a voltammetry scan starts; the applied potential is ramped up against the reference electrode until a switching potential of + 1.2 Volts at a speed of 400 V/s, and then ramped down at the same speed. The entire scanning potential lasts for 8 ms only. Then it goes back to the holding potential of - 0.4 Volts. Because the oxidation of electroactive neuro-chemicals such as dopamine happen at around + 0.6 Volts on a carbon electrode [56], we would need to raise the potential well above that value so that the neuro-chemical molecules around the working electrode surface can be fully oxidized.

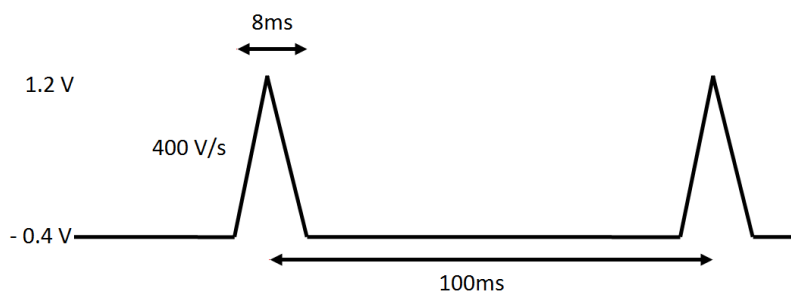


Figure 2.1: Illustration of the scanning electric potential (FSCV command voltage) against the working electrode in an FSCV recording experiment. Each 'peak' generate one cyclic voltammogram recording.

This will generate a very well defined oxidation current peak.

Remember that the useful information regarding the extracellular concentration of neuro-chemicals is gained during the electron exchange process happening at the working electrode surface, during the oxidation of these molecules. The voltmeter is able to record such current flow in real time during voltammetry scans. Figure 2.2 demonstrates the recorded current during 2 voltammetry scans (intentionally scanned at slower speed for the ease of observation) in one of my experiments. The general trend of the current is similar to the command voltage, i.e. increasing in the first half and decreasing in the later half of one scan cycle. The somewhat strange temporal profile of this current trace, or the shape of the cyclic voltammogram, is related to both resistive current and capacitive double layer charging. [37]

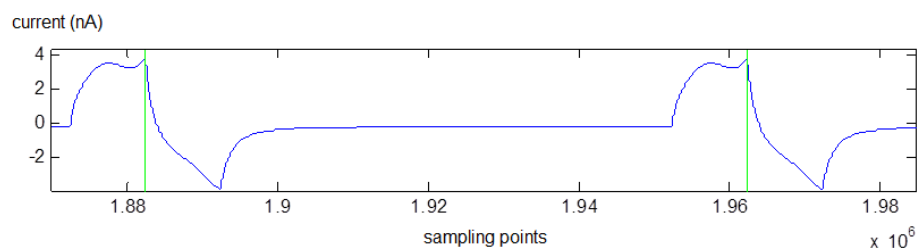


Figure 2.2: Recorded electric current going through the working electrode during 2 voltammetry scans. Green line denote the switching point of the scanning voltage from forward to reverse directions.

Regarding the capacitive charging, an electric double layer is usually formed between the electrode and the conductive solution [59], especially when it's a micro-electrode. The charges into or out of the electrode quickly formed an electric gradient at the surface of the electrode, preventing further charge movement. An equilibrium is reached in this process, leading to an electric double layer that have certain capacitance. Each time the voltage is varied, charging of the double layer capacitor leads to extra currents which could influence the cyclic voltammogram. This large background current in FSCV is present no matter neuro-chemical molecules exist or not.

2.2.2 Generating background-subtracted cyclic voltammograms

In each FSCV scan cycle, the recorded current is extracted and plotted against the scanning voltage, resulting in a cyclic voltammogram. Let's now take a closer look

at what a neuro-chemical signal would look like in a cyclic voltammogram, again with very practical examples. Here is an example of a single cyclic voltammogram extracted when the working electrode is sitting in a 25 μM standard dopamine solution in a beaker. As can be seen in figure 2.3, two small 'bumps' appear on the cyclic voltammogram, corresponding to the oxidation (during increasing potential) and the reduction (during decreasing potential) of dopamine molecules on the electrode surface. This is an extreme case because the dopamine concentration is very high compared to any physiological concentrations (usually below 1 μM). Therefore, in the real brain, the two redox current peaks would be significantly smaller, and would be difficult for observation in this kind of voltammograms. The solution to this issue is to use background subtraction when plotting cyclic voltammograms. Because the background, non-dopamine current is stable over time, we can subtract this constant pattern from all the voltammograms. Usually this background pattern is determined by averaging over a passive recording period, where no stimulation of dopamine release is performed in the brain tissue.

After background subtraction, tiny amount of currents can be detected despite the existence of large background current. Here we present an example of our FSCV recording during which the electrode is moved from control solution (artificial cerebrospinal fluid, ACSF) to the standard solution containing 1 μM dopamine in ACSF. Figure 2.4 upper panel shows the background subtracted single voltammogram when the working electrode is in 1 μM dopamine solution, where primarily only the currents

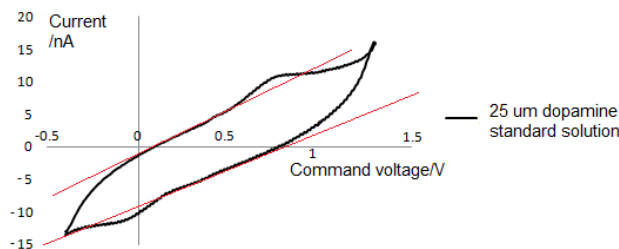


Figure 2.3: Non-background-subtracted cyclic voltammogram in high dopamine concentration. This is a single cyclic voltammogram showing recorded current plotted against command voltage, in a 25 μM standard dopamine solution. Oxidation and reduction current causing abnormalities in the CV.

caused by dopamine oxidation (around + 0.6 V) [41] and reduction (around - 0.3 V) are left on the plot. These signature oxidation and reduction peaks are important in validating the identity of the recorded chemical species in a complex environment in the brain.

2.2.3 Monitoring neuro-chemical concentration in real-time

Because we are aiming at real-time monitoring of the neuro-chemical activity, individual voltammograms only represent the activity at certain time points and is not sufficient. Therefore, it is common practice to plot all the single voltammograms vertically in a 2D FSCV color plot (Figure 2.4, lower panel), where the x-axis is elapsed time; y axis is the command voltage; color coding in the z direction represent the amplitude of redox currents. Each vertical line of the 2D plot should be considered one cyclic voltammogram at a given time point. Therefore, in the 2D color plot, we

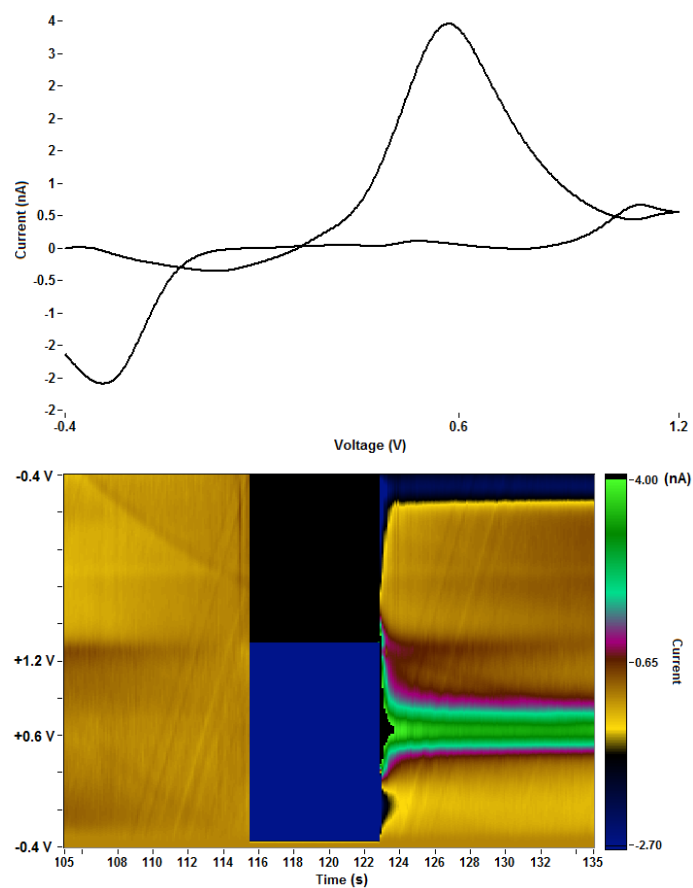


Figure 2.4: Upper: background subtracted voltammogram when the electrode is in 1 μM dopamine solution. Lower: 2D FSCV color plot, x-axis is in seconds. Electrode is in control solution first half of the recording, switched to 1 μM dopamine solution in the later half.

are watching the evolving cyclic voltammograms over time. We can see no activity is present when the electrode is in the control solution, while oxidation and reduction current present when the electrode is moved to the dopamine solution.

The actual neuro-chemical dopamine concentration depends on the amplitude of the oxidation and reduction peaks. Because oxidation peak is bigger, the concentration is therefore usually calculated based on the FSCV signals at + 0.6 V in particular. Taking a horizontal line at + 0.6 V in the 2D FSCV plot, the amplitude of the signals at this line is the estimated time-lapsed dopamine concentrations. We could also extract the voltammogram and calculate the area of the oxidation peak as the metric rather than the absolute value of the peak, but the two generate very similar results. Eventually, our calculated real dopamine concentration would depend on an additional calibration experiment with standard 1 μ M dopamine solution as described in later chapters.

2.3 Preparation of carbon fiber micro-electrodes for FSCV

Carbon fiber electrodes has been the electrode of choice for electro-chemical neurotransmitter sensing because of the high sensitivity. Due to carbon's adsorptive characteristics [8], neurotransmitter dopamine can be adsorbed at the surface of working electrodes, promoting electron exchange. This adsorption especially tends to happen

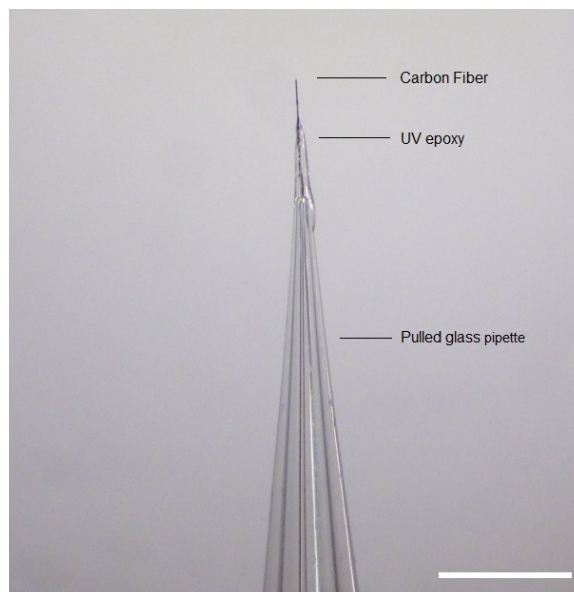


Figure 2.5: Photo of a homemade carbon fiber electrode. After heat assisted pulling, the glass pipette is tapered at the tip. Carbon fiber is trimmed to around $200\ \mu\text{m}$ to ensure optimal neuro-chemical detection sensitivity. Bar denotes 1 mm.

during holding potential between voltammetry scans at $-0.4\ \text{V}$ [56]. In addition, the tiny size of carbon fibers ($7\ \mu\text{M}$) has unbeatable advantage in terms of *in vivo* neuro-chemical monitoring. It is potentially interesting to develop novel materials or new carbon-based electrodes for the purpose of neuro-chemical sensing, which may or may not increase the sensitivity to dopamine and the mechanical properties of the electrode, but the topic is beyond the scope of this work. We are aiming at applied neuro-chemical research questions, therefore choose to utilize the currently most suitable and viable electrode material to fabricate our home-made carbon fiber electrodes and chronic implantable probes.

For our home-made carbon fiber electrodes, we adapted the procedures reported

in several previous publications [56] [47] [37]. Firstly, carbon fibers (Goodfellow, Coraopolis, PA) were vacuum aspirated into glass pipettes of 1.5 mm in diameter (Sutter Instrument, Novato, CA) and subjected to heat assisted pulling (Micropipette puller P97, Sutter Instrument). After pulling, the pipette was tapered for 2 mm at the tip, and tightly fit the diameter of the carbon fiber, resulting in a nearly closed encapsulation. We applied a small amount of UV epoxy at the contacting area between the carbon fiber and the pipette to further ensure that during recording, no solution can move up into the glass pipette through capillary effects. This is important in that additional contacting electrode surface with the solution will cause a large change in the impedance of the electrode. While impedance usually needs to be kept extremely stable to guarantee a consistent baseline of FSCV. Exposed carbon fibers were then carefully trimmed under microscope with a blade to around 200 μm long. Lastly, electric connections were made at the other end of the pipette between the carbon fiber and a copper wire. Silver epoxy is used for this purpose. In a typical electrode fabrication process, around 10 such CFEs were made simultaneously for reserve of future experiments.

2.4 Instrumentation and neuro-chemical signal acquisition

The electronic instrumentation we used for FSCV is described in this section. Home-made carbon fiber microelectrodes were connected to a Dagan CHEM-CLAMP voltammetry amplifier through a 1 MOhm head stage ($N=0.01$). We used two National Instrument PCI cards: NI PCI 6024e was used for voltammetry data acquisition and command voltage waveform output; NI PCI 6321 was used for synchronization and triggering an analog pulse generator for optical stimuli. Analog signals were sent directly to the laser driver. The data acquisition software used was Demon Voltammetry [81]. The head stage, electrode and the recording media were placed inside a Faraday cage to prevent extraneous electric noise. A temperature sensor is also placed in the recording chamber ACSF solution to monitor the temperature change for brain slice experiments. The figure 2.6 shows our electronic instrumentation used for FSCV.

In a typical recording experiment, firstly the working electrode and reference electrode (Ag/AgCl wire) is placed in the ACSF solution or in the brain slices, and connected to the head-stage. To acquire FSCV signals, the command voltage was scanned from -0.4 V to 1.2 V and back to -0.4 V at 400 V/s with a sampling frequency of 10 Hz. Cyclic voltammograms in the 1 second before stimulation onset were averaged and used as the baseline for background subtraction. We examined

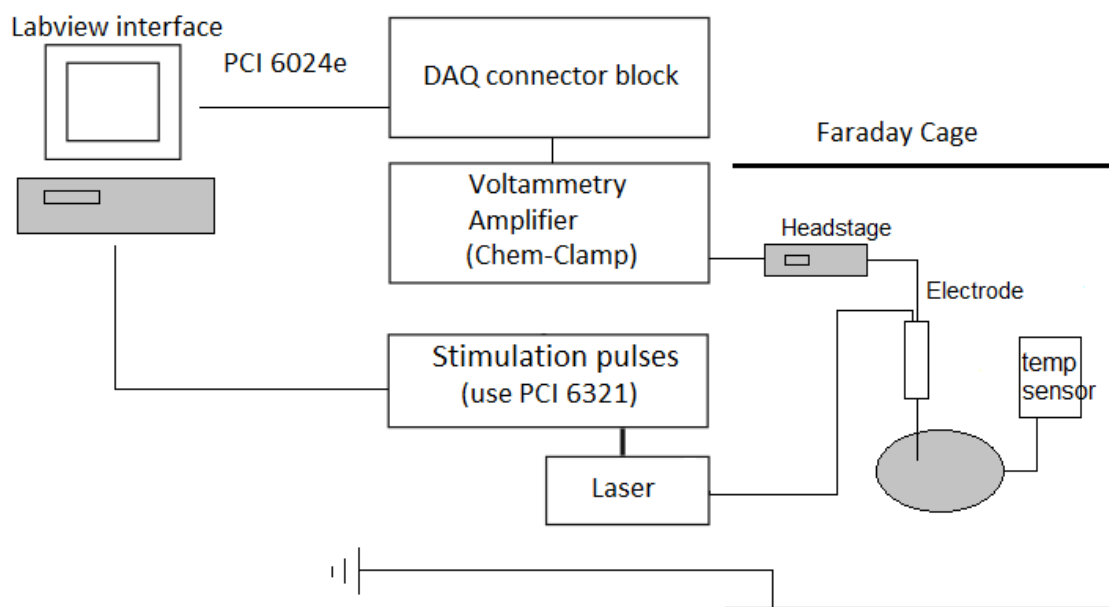


Figure 2.6: The FSCV instrumentation. On the left side is the computer with two NI data acquisition cards. It is connected to the DAQ connector block / voltammetry amplifier and the analog pulse generator respectively. On the right side in the Faraday cage is the recording chamber with either ACSF solution or live brain slices. The head-stage is also situated inside the Faraday cage.

background subtracted cyclic voltammograms in each recording to identify the typical oxidation peak at 0.6 V and reduction peak at -0.3 V respectively to confirm that the recorded chemical species is dopamine, with minimal interference from other chemicals [78]. If we would like to calculate absolute concentration of dopamine, before FSCV experiments, electrodes need to be calibrated by 1 μ M standard dopamine solution [74] [36]. The concentration traces of recorded DA were generated using the calibration factors. The FSCV setup was turned on 10 minutes before actual recording to ensure a stable baseline in each recording session.

In the next chapter we will introduce the FSCV experiments protocol in an *in vitro* environment: the transgenic mouse brain slices. The experimental setup will be the same as described in this chapter, but extra steps are required to breed transgenic animals, prepare health and live brain slices, stimulating the targeted brain region with light stimulus and so on.

Chapter 3

Chemical messenger dopamine
dynamics interrogated through
optogenetics in transgenic mice
brain slices

In this chapter, we demonstrate the use of fast-scan cyclic voltammetry in brain slices in conjunction with cell-type-specific optogenetic targeting. The animal model we used is specifically tailored transgenic mice, which conditionally express the opsin Channelrhodopsin-2 (ChR2) in dopaminergic neurons, enabling light activation of dopamine (DA) activity. We begin with introducing the principles and utility of optogenetic tools and their cell-type-specificity. Immuno-chemistry is used to characterize the expression of opsins in the brain slices.

With the powerful electro-chemistry technique, we systematically studied effective neuron-terminal-targeting induction of neuro-chemical dopamine release at physiological levels. We also achieved direct manipulation of induced dopamine concentration by controlling light intensity, pulse width, and the shape of stimulation waveforms. In addition, it was also found that the temporal shape of the stimulus waveform at light onset is critically related to induced dopamine concentrations. Furthermore, dopamine uptake kinetics as well as the recovery of the presynaptic releasable dopamine pool are studied and modeled.

More broadly, our experimental findings provide important further evidence for effectively applying electro-chemistry tools to interrogate the neurotransmitter dynamics in live brain tissue, especially in the behaviorally relevant regions of the brain such as the nucleus accumbens (NAc) and the striatum in a highly cell-type specific context.

3.1 Introduction: Investigating chemical messenger dopamine through light stimulation

In traditional neuro-chemical studies, the modulation technique of release used most extensively is electrically stimulating the neurons carrying these chemicals, in particular dopamine. Electrical stimulation produces a non-cell-type-specific excitation. However, since there is a significant population of non-dopaminergic neurons coexisting with dopaminergic neurons [43], recruiting all subtypes of neurons may result in complex neuro-chemical system dynamics, as well as evoking electrical and chemical consequences not related to dopamine, which may be undesirable in potential therapeutic treatment. An alternative approach for more controlled manipulation of the dopaminergic system is to use optogenetics which allows cell-type specific manipulation of neural activity through light-gated ion channels. Optogenetics has been employed in recent studies for targeted DA release. Specifically, Threlfell et al. [68] demonstrated light induced DA release from cholinergic interneurons and dopaminergic neurons in mouse striatum. Bass et al [7] studied the DA release in rat striatum with different quantities and durations of light pulses, and compared optical and electrical stimulation. Melchior et al [49] has recently compared optically and electrically induced DA release utilizing pharmacological methods. A few *in vivo* studies have used light induced DA as an indicator to investigate behavioral conditioning ([2] [71]).

However, there has not been a detailed study to bring in all the key aspects of optogenetic stimulation, such as the light power density, light waveform shape and the temporal pattern of delivered stimuli. Additionally the DA dynamics in the NAc are much less well understood than those in the striatum [65]. The DA dynamics in the NAc are also especially important for many animal behaviors because of the central functional role of the NAc. Therefore, an understanding of these dynamics is crucial for developing physiologically realistic stimulation paradigms for future *in vivo* studies.

In this chapter, a detailed quantitative electro-chemical study is presented, focusing on neuron terminal dopamine dynamics and their manipulation by light stimulations of varying parameters. Note that previous studies on optically induced DA release have been using virus injection to induce opsin expression [7] [66]. In our transgenic opsin-expressing animals, expression does not depend on the viral diffusion or efficacy of transduction in the physically heterogeneous brain, and therefore is more stable and has better cross-animal consistency. In this model, we were able to electro-chemically record the elicited transient high concentrations of extracellular DA by light at a particularly low power density of 0.1 mW/mm^2 compared to the previously used value of around 10 mW/mm^2 [68] or other typical levels used across *in vitro* and *in vivo* mammalian studies [23] [34]. Importantly, minimal light artifacts were observed under this regime of low power density, which allows simultaneous and overlapping light stimulation and FSCV. By controlling stimulation parameters such

as light power and pulse width, optically induced DA concentrations can be precisely modulated across the dynamical range of 10 nM to sub- μ M. Surprisingly, optogenetically induced DA release was observed to also depend significantly on the temporal shape at the rising edge of stimulus waveform. We also found that the optogenetically induced DA efflux, as a consequence of direct axonal and terminal excitation, is attenuated during various temporal patterns of consecutive light stimulation. Details of such behavior were investigated by studying the kinetics behind the recovery of the releasable DA pool after an initial DA release event. We further estimated a number of key time constants that define DA clearance in the uptake process, during which a transporter protein pumps DA back into the cytosol. The time constants are expected to be dramatically different between the DA uptake process and the recovery of the releasable DA pool since more complicated mechanisms are involved in the latter case. In general, we provide a detailed terminal dopaminergic dynamics study using optogenetics tools in the NAc. The different light stimulation parameters discussed here will provide guidance for designing practical stimulation paradigms to induce DA release. Our results therefore set the stage for future studies on reward, motivation and emotion related behaviors where the modulation of dopamine level in the NAc is important.

3.2 Optogenetic tools and characterizing the expression of opsins

In the past 10 years, neuroscience research has been reforming and reorganizing in a tremendous scale, all due to a single milestone invention: optogenetics [9]. The development of application of these light-gated ion channel proteins in neuroscience research has enabled researchers in any sub-fields to control neurons and brain circuits by light, rather than electrical pulses that were used traditionally. This is a huge step in the study of neural systems, because of the cell-type specificity brought by utilizing optogenetics. Opsins are expressed selectively on certain types of cells by the control of promoters that are capable of conditionally initiate expressions.

Neuro-chemical research has not been studied in detail in an optogenetic context, despite optogenetics is being applied among all the areas of neuroscience research and has contributed to unprecedented scientific findings. Here, our work in the field of neuro-chemical research is based on optogenetic control of neurotransmitter dynamics recorded by FSCV. The first step is to successfully deploy the optogenetic tools like in any other sub-fields of neuroscience research.

3.2.1 Development of optogenetics

Although Optogenetics is a new and emerging field that is recognized recently, the necessity of it has been proposed long before its development. Francis Crick in 1979

[20] have put forward the idea that a method to selectively activate certain type of neurons rather than all of them is very crucial in the next step advancements in neuroscience research. Because of the huge complexity of brain's circuits, different type of cells form a complex network which makes it almost impossible to tackle the myth and understand the individual neuron type's functional role. Before the development of optogenetics, no other techniques had been able to achieve such goals. The application of microbial opsins in controlling neuron activity, in particular affecting membrane potentials has led to the development of optogenetics [22].

These opsins are first discovered in various microbes, in which the power of evolution have invented the functionality of sensing light in the environment and create a neuronal signal to the nervous system, like in the retina. Among these different types of opsins, perhaps the light-gated ion channel proteins are the most important family, especially the uses of channelrhodopsins as the early hugely success cases of optogenetic control of neuron activity [9]. There are mainly three families of opsins: excitatory opsins such as the Channelrhodopsins that conduct cations, inhibitory opsins such as the Halorhodopsins that conduct chloride ions, and rhodopsin-G-protein-coupled receptors which activate selective biological functions. Many variants of the above opsins have been invented aiming at improvements in neural activation power, latency etc. Next we will introduce how to apply these tools in the experiments.

3.2.2 Cell-type specificity and transgenic animals

In order to have any of these membrane proteins to affect the neural activity, first step is to through certain approaches manage to incorporate these proteins on the cellular membranes of specific types of neurons. As the molecular biology “central dogma” teaches us, the membrane proteins are from the beginning produced intracellularly by the processes of transcription (DNA to mRNA) and translation (mRNA to protein). This means the incorporation of external membrane proteins requires the delivery of related external genes. A natural thought would be to use artificially engineered virus, which is indeed one of the most common approaches adapted by neuroscientists. Inactivated virus is able to infect the neurons and deliver desired genes designed to produce light gated ion-channel proteins. This requires injection of virus into the brain tissue in live animals. There are two most common types of virus used in optogenetics: the lentivirus and the adeno-associated virus (AAV) [28]. Viral injection is very widely adapted in research; however, we would not dig into further details as I adapted a different approach in this work.

Transgenic animals, in particular transgenic rodents, have become a more advanced and innovative way of incorporating opsins in neurons for lives animals. In 2007 and 2008, Arenkiel [5] and Zhao [83] reported the development of transgenic opsin-expression (Thy1) mice line which become very popular in studying cortical neural circuits in rodents. The advantages of transgenic animals are significant in that:

A. Considerably reduced the complexity of experiments by removing the viral transduction step weeks before the neural recording experiments.

B. Transgenic animals have more consistent and robust opsin expression targeting dopaminergic cells.

C. Better cross-animal consistency compared to the virus injection approach, because the diffusion of virus in the brain tissue can vary greatly among different experiments.

In sum, we finally choose to adapt the transgenic mice approach to deliver opsins to specific cells i.e. the dopaminergic neurons. In order to achieve such cell-type specificity, which is one of the big advancements – to selectively stimulate dopaminergic neurons while monitoring chemical messenger dopamine release, we specifically home-bred transgenic mouse lines at university’s animal care facility. In detail, we utilized the tool of Cre-dependent optogenetic transgenic mice, as developed by Hongkui Zeng’s group [46]. Briefly, the Cre recombinase is an intracellular enzyme that is capable of recombine specific pieces of DNA.

floxed-ChR2 mouse line	DAT-Cre mouse line
Allele name: Ai32(RCL-ChR2(H134R)/EYFP	Allele name: DAT ^{iresCre}
Gene symbol: Gt(ROSA)26Sor	Gene symbol: Slc6a3
Type: homozygous	Type: heterozygous

Table 3.1: Table of transgenic animal lines

3.2.3 Use Immuno-chemistry to characterize the ChR2/EYFP expression

The DAT-Cre X ChR2 transgenic mouse is expected to selectively express channel-rhodopsin 2 in all dopaminergic neurons across the entire brain. This includes any of the three major pathways discussed: the mesolimbic pathway where the dopaminergic neurons in VTA project to NAc, the nigrostriatal pathway where projections originate in SN and end in striatum, and finally the mesocortical pathway where projections originate in VTA and end in prefrontal cortex [19]. Although the expression mechanism for opsins is solid, for scientific robustness, we still would like to experimentally verify the actual opsin expression condition in individual transgenic animals.

A quick understanding of the general opsin expression location can be gained by utilizing the fluorescence microscopy technique in transgenic mouse brain slices. Because in these transgenic animals, the membrane protein ChR2 is fused with enhanced yellow fluorescent protein, the brain tissue expressing opsins would have yellow fluorescence under a peak excitation wavelength of around 500 nm, and have a peak emission wavelength of around 540 nm. We used fluorescence filters with particular wavelength windows that ensure we are observing the fluorescence of YFP. The details of the instrumentations are described in the next section.

Below is our observation of the ChR2/EYFP fluorescence in one of the transgenic animals. Coronal brain slices (Bregma +1.00 mm AP) were prepared to examine the brain regions of striatum, nucleus accumbens, and SN/VTA.

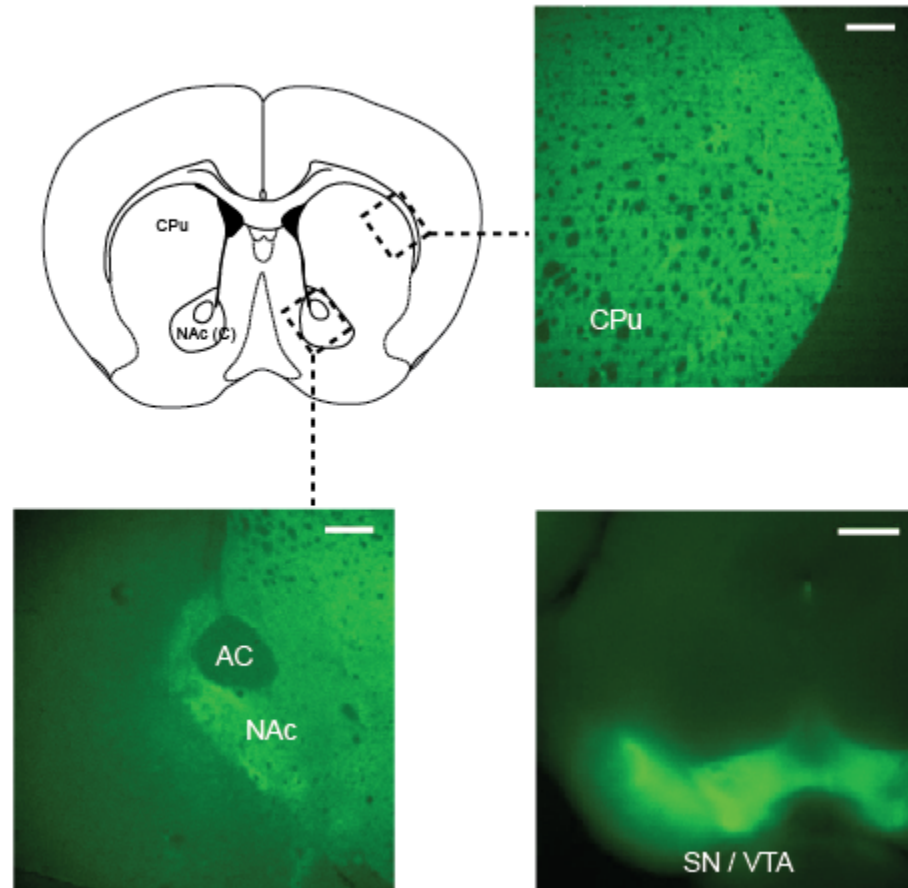


Figure 3.1: Fluorescent microscope images (excitation wavelength for YFP: 490 nm) show existence of YFP fluorescence in Caudate Putamen (CPu, upper right) and Nucleus Accumbens (lower left; AC stands for anterior commissure) in forebrain coronal slices (+ 1.0 mm AP; scale bars are 0.2 mm). Expression is also seen in mid-brain coronal slices of SN/VTA (lower right; -3.1 mm AP; scale bar is 0.5 mm).

As can be seen, the green-colored fluorescence mainly present at NAc, CPu, and SN/VTA area (which is in a different slice at the mid brain). This corresponds to the dopaminergic neuron's projection terminal fields at NAc, CPu, and the cell bodies at SN/VTA. Because the production of ChR2/EYFP of this transgenic mouse is happening intracellularly, ChR2/EYFP membrane proteins can reach the projection terminal fields through axonal transportation. To further examine in detail, high resolution fluorescence imaging is performed with a 40 X objective lens at the area of SN/VTA. We are able to observe the individual dopaminergic neurons and the projections originate from these neuron cell bodies.

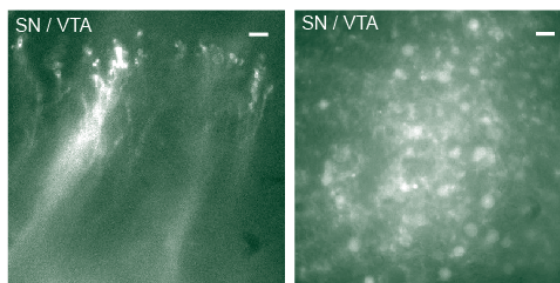


Figure 3.2: High resolution fluorescent microscope images in SN/VTA region both coronal (left) and sagittal (right); scale bar is 10 μm .

However, using fluorescence imaging technique alone is not sufficient to scientifically validate the successful cell-type specific expression of opsins in dopaminergic neurons only. We therefore choose to use immunochemistry methods to further investigate the expression of opsins in our experimental subjects. The main goal of the immunochemistry analysis is to:

1. Observe the detailed structure of opsin expressing dopaminergic neurons, including soma, axons and dendrites.

2. Use immunostaining of tyrosine hydroxylase to understand the types of neurons (dopaminergic vs. non-dopaminergic). Compare the localization of dopaminergic neurons and opsin expressing neurons.

To successfully utilize immunochemistry, we adapted the experimental procedures as follows [17]. Firstly, the DAT-Cre X ChR2/EYFP transgenic mouse was terminally anesthetized with Beuthanasia-D. Perfusion was performed transcardially with saline followed by 4% paraformaldehyde in PBS (phosphate buffered saline) solution. The brain was extracted and sequentially fixed in 4% paraformaldehyde in PBS solution (1 day) and then 30% sucrose solution (until brain sunk in solution). The brain was then frozen with dry ice and cut into 40 μm coronal slices with a microtome. For tyrosine hydroxylase (TH) immunostaining, slices were sequentially washed in PB (phosphate buffer; twice, 5 min each), PBS (three times, 5 min each), and then left in block solution for 1hr. The block solution was prepared with 0.1% Tween (Sigma-Aldrich, MO), 0.25% Triton-X (Sigma-Aldrich, MO), and 10% normal donkey serum (EMD Millipore, MA) in PBS. Slices were then immersed in primary antibody (1:1000 AB152 Anti-Tyrosine Hydroxylase in block solution, EMD Millipore, MA), covered with tin foil, and rotated for 2.5 days in a cold room (4 °C). Slices were thoroughly washed five times in PBS (5 min each) and again blocked in block solution for 1 hr. The slices were then transferred to secondary antibody solution (1:500, Alexa

Fluor $\text{\textcircled{R}}$ 594 donkey anti-rabbit IgG in block solution; Life technology, CA) for 2 hrs. Afterwards, they were again washed in PBS (three times, 5 min each) and PB (twice, 5 min each), and mounted on microscope slides. Specific slices containing VTA (-3.2 mm Anterior-Posterior) and NAc (+1.0 mm AP) were selected and examined under a Zeiss LSM 510 Meta Confocal Laser Scanning Microscope to verify the co-localization of ChR2-EYFP with TH. The figure below is the resulting confocal microscopy images from the forebrain slices at the NAc area.

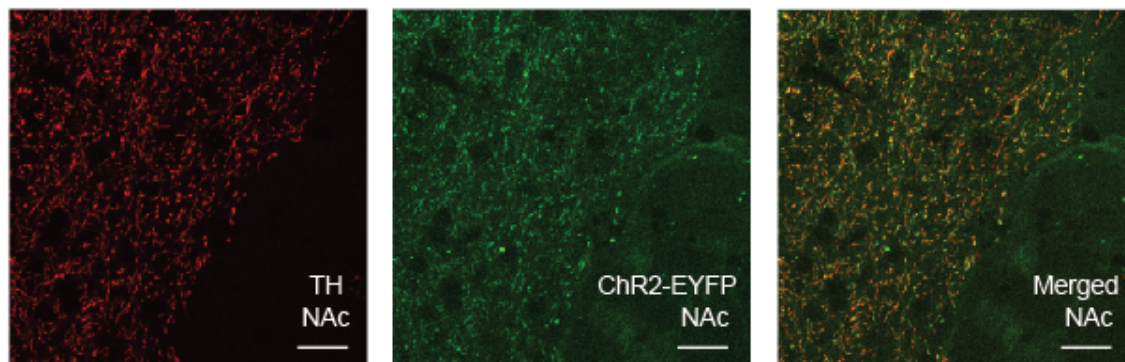


Figure 3.3: Immunochemistry analysis with Tyrosine Hydroxylase staining in the NAc (+1.00 mm AP) where DA dopaminergic neuron projections (but not cell bodies) can be observed. TH is shown in red (left); YFP fluorescence is in green (middle); merged image is on the right. Scale bars indicate 20 μm .

In the NAc, which contains the axons and terminals of DA neuron, YFP fluorescent neuronal projections overlapped well with the TH-labelled structures shown above. This overlap indicates that the neurons that express opsins, and the neurons that are TH-labelled are the same group of neurons – i.e. the dopaminergic neurons.

Such traces were not seen in the anterior commissure (bottom right corner of the images), which does not contain dopaminergic projections. These histological results confirmed that our optogenetic stimulation of ChR2 was indeed affecting dopaminergic projections, as expected in these transgenic animals conditionally express ChR2 by the control of DAT-Cre. We also examined the dopaminergic neuron cell bodies at the SN/VTA region.

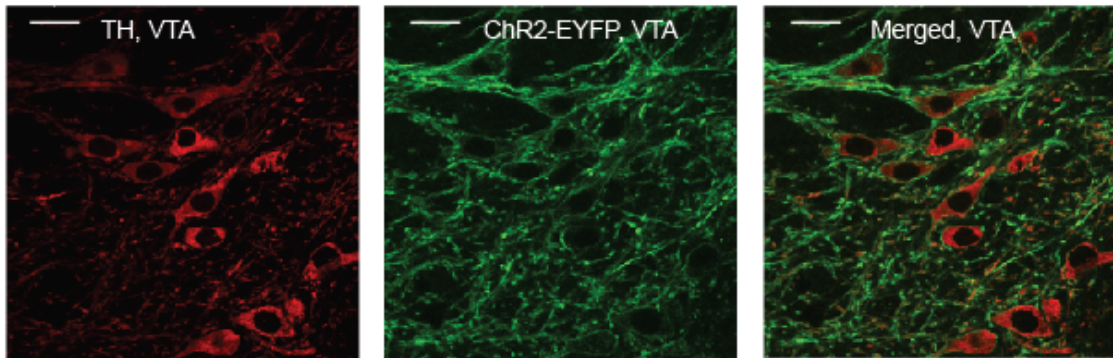


Figure 3.4: Immunocytochemistry analysis with Tyrosine Hydroxylase staining in the VTA (-3.2 mm AP) where DA cell bodies can be seen. TH is shown in red (left); YFP fluorescence is in green (middle); merged image is on the right. Scale bars indicate 20 μm .

One can observe the existing dopaminergic cell bodies and their dendrites in the left TH-labelled confocal microscopy image, where the round black object is the cell nucleus. These cell structures also present YFP fluorescence, which means they are expressing opsins. We note that the YFP existence is slightly stronger in the dendrites vs. the soma. This is because ChR2/EYFP is naturally transported to the

membrane of the neuron because of its functional role. In summary, the histology experiments were done with immunostaining of tyrosine hydroxylase (TH) to verify the colocalization of ChR2-EYFP with TH in both the VTA and NAc. Dopaminergic cell bodies stained with TH and showing YFP fluorescence were found in the VTA (Fig 1B). This immunochemistry analysis is of vital importance because it ensures our light stimulation is exclusively affecting dopaminergic projections in the transgenic mouse brain slices, as expected in these DAT-Cre x ChR2 transgenic animals.

3.3 Experimental setup and methodology for studying dopamine dynamics in healthy brain slices

In this section, we will introduce the generic procedures of performing the neurochemical sensing experiments in transgenic animal brain slices. The animal model and brain slice technique are firstly described, followed by the optical stimulation protocol and the electro-chemistry recording technique.

3.3.1 Breeding transgenic animals and the brain slice technique

The entire process from purchasing breeding pairs of transgenic animals to genotyping the litter and wait for maturity usually took around 2 month time. It is therefore important to plan in advance to ensure a steady supply of experimental subjects.

After purchased from the Jackson Laboratory, animals were housed in Brown University's animal care facility. Then the transgenic DAT-Cre mouse line was crossed with the floxed ChR2(H134R)-EYFP mouse line to produce offspring. These offspring were subsequently genotyped. At postnatal day 5 – day 10, mice was labelled by toe clipping under conventional numbering policy. Then we sampled mouse tails of 2 - 3 mm long to store in electrostatic spray treated boxes. The labels of the animals and tail samples were carefully kept in record. The mouse tail samples were shipped for genotyping to Transnetyx Inc. The company used automated polymerase chain reaction (PCR) technique with Cre probes to identify which specific animals carry Cre gene. The animals carrying Cre gene is capable of expressing ChR2/EYFP in the brain tissue. After genotyping is finished, those transgenic mice that are tested positive for the presence of Cre were used in experiments. Note that animals from 1 4 month age are best for neuro-chemical sensing experiments.

For preparing healthy slices, brain slices were cut from adult mice 2-3 months in age, both male and female. In the detailed procedure, the mice were firstly anesthetized with a solution of Ketamine (10 mg/ml) and Xylazine (1 mg/ml) and decapitated. The brain was quickly removed and submerged in an ice-cold oxygenated ACSF cutting solution containing (in mM): 125 NaCl, 2.7 KCl, 25 NaHCO₃, 1.22 NaH₂PO₄, 10 dextrose, 2 CaCl, 2 MgSO₄·7H₂O, 1 ascorbic acid. Coronal slices, 300 μ m in thickness, were cut with a vibrating blade microtome (Leica VT1000S,

Leica Biosystems) in the same ice-cold ACSF cutting solution. The slices were incubated for 30 min at 32 °C and then maintained at room temperature (20 °C) in oxygenated ACSF cutting solution [58]. Animal care and experiments were performed in accordance with the National Research Council Guide for the Care and Use of Laboratory Animals (Brown University Institutional Animal Care and Use Committee). The healthiness of the brain slices is extremely important for *in vitro* experiments because it's necessary to keep the neurons in the slice healthy and alive, while the membrane proteins and dopamine transporter (DAT) proteins should be active as well. The time it takes from decapitating the animal until the brain slices are transferred to the oxygenated incubating ACSF is the most important factor in keeping the brain slices healthy. Therefore, extra practice is required to successfully prepare the slices that are suitable for dopamine sensing experiments. Notes: may add all brain slices

3.3.2 Preparing FSCV recording chamber and optical stimulation paradigm

In order to perform *in vitro* dopamine FSCV experiments under optogenetic stimulation, firstly slices containing the nucleus accumbens (+1.0 mm AP) were placed in a recording chamber under a microscope (Eclipse E600FN, Nikon, Melville, NY) and superfused with room temperature oxygenated ACSF recording solution containing (in mM): 125 NaCl, 2.7 KCl, 25 NaHCO₃, 1.22 NaH₂PO₄, 10 dextrose, 1 CaCl, 1

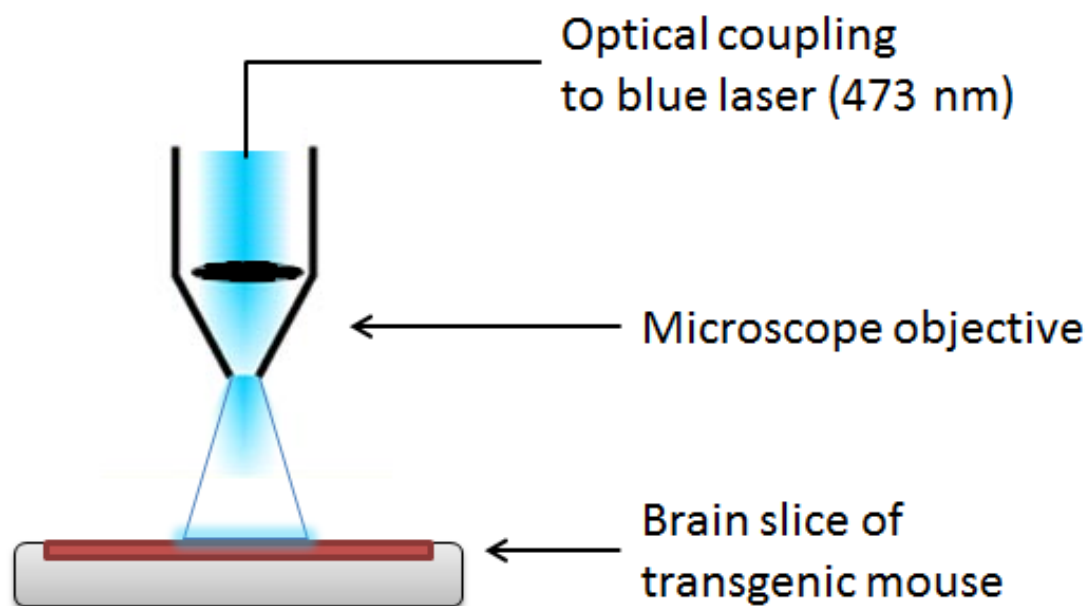


Figure 3.5: Illustration of the optical stimulation paradigm in brain slices dopamine FSCV experiments. The blue light is delivered through microscope objective and illuminated area is indicated on the slices.

MgSO₄·7H₂O. For validation purpose, the expression of ChR2-EYFP was checked under the microscope with an excitation wavelength of 490 nm by a Polychrome 5000 lamp from Till Photonics (Bavaria, Germany). After confirming opsin expression in the slices, we would compare between different slices and different brain regions for the expression. We have found that the brain slice around +1.00 mm AP from bregma is best for the study of dopamine FSCV sensing.

The optogenetic excitation of the dopaminergic cells was carried out by a blue laser (473 nm, CrystaLaser, Reno, NV) the output of which was coupled to the

microscope and projected through the objective onto the slice. Since the light is delivered through the microscope objective, this results in a 2.4 mm by 2.4 mm illuminated circular area on the brain slices. The illuminated area is carefully aligned to be around the recording FSCV electrode. This optical stimulation paradigm ensures the dopaminergic neuron projections around the dopamine sensing electrode are receiving the strongest light stimulation. Our purpose is to sufficiently excite all the dopamine terminals to induce a high extracellular dopamine concentration that can be detected by FSCV (higher dopamine concentration is also potentially behaviorally significant for the consideration of the later *in vivo* experiments).

3.3.3 Fast-scan cyclic voltammetry experiments

After the brain slices from DAT-Cre X ChR2/EYFP transgenic mouse is prepared properly according to above procedures, we then run neuro-chemical sensing FSCV experiments in the slice medium. Briefly, home-made carbon fiber electrodes (CFE) were inserted under the microscope into the NAc area close to the anterior commissure of the coronal forebrain slices (+1.0 mm AP) with the aid of a micromanipulator. Under constant light from the laser, we centered the light around the CFE to ensure that the dopaminergic projections in the NAc are receiving the light excitation when laser pulses are sent through the objective. The light power was measured by a power meter (PM100D, Thorlabs, Newton, NJ). The details of the FSCV recording is provided in Chapter 2.

Next, we would need to place the CFE in the targeted brain tissue. To record the concentration of dopamine molecules released, the CFE has to be inserted properly into the tissue. Carbon fibers have a diameter of $7\ \mu\text{m}$, and are strong enough for penetration. However, shear stress should always be minimized. We use a micro-manipulator (Sutter instruments) in the fine motion mode to precisely control the movement of the CFE, under the microscope. The CFE is held at around 30 degree with respect to the brain slice. We slowly move the CFE to approach the slice surface at NAc. Once the tip of the carbon fiber starts contacting the slice surface, we carefully move the CFE in a zig-zag fashion. The CFE is moved down and forward alternatively to penetrate the tissue. It can be estimated how much of the carbon fiber tip is inside the tissue by observing the blurring of the fiber. Once most of the exposed fiber tip is inserted in the tissue (for better chemical sensing); FSCV recording can be started. The recording chamber is under constant oxygenated ACSF flow to support the healthiness of the brain slice. External ACSF is kept at 31 degree (Centigrade). If the experiment involves optogenetic stimulations to evoke dopamine release, we paused for at least 5 minutes between each FSCV recording session to allow DA recovery and ensure consistency among multiple DA release events. As a control, we performed the FSCV recording experiment with the electrode placed in the NAc in wild type animals without ChR2, and did not observe any induced DA signals. Throughout the experiments, we ensure our FSCV electrode was in the NAc area of the slices, while the light is focused around the FSCV electrode and

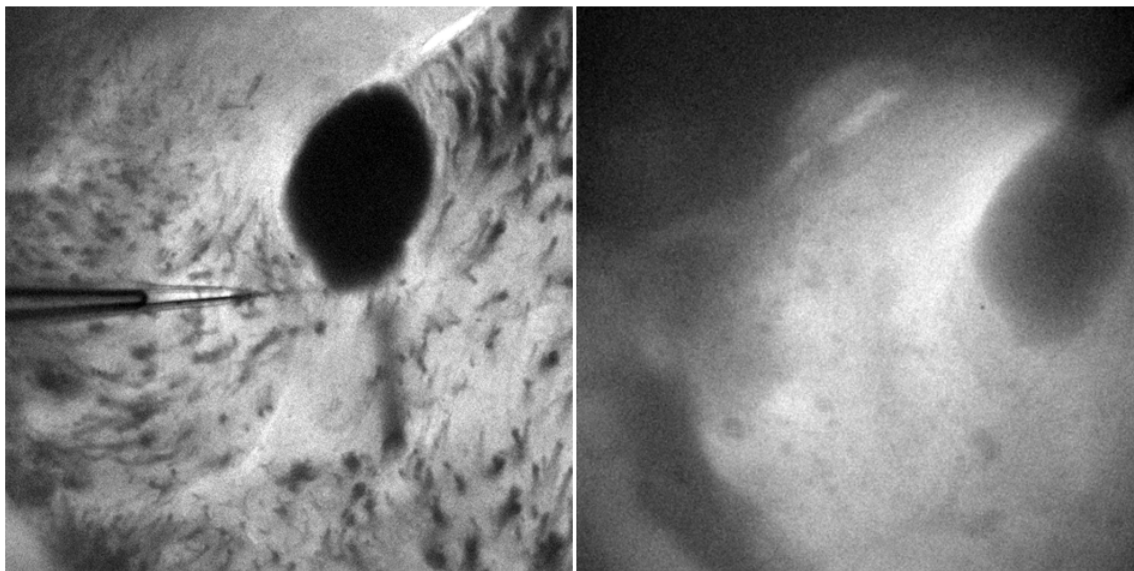


Figure 3.6: Insertion of CFE in brain slices. Left: The CFE inserted into the NAc of a brain slice. Right: corresponding fluorescence image proving the CFE is at a place with ChR2/EYFP expression.

illuminating NAc.

3.3.4 Post-processing of recorded neuro-chemical signals

After FSCV data acquisition from the brain slices, additional processing is needed to interpret the raw signals. Essentially, dopamine concentration traces recorded by FSCV were calculated using the signal at + 0.6 V with respect to the calibration factors. The FSCV color plots follow the standard 2D representation with time along the X axis, command voltage along the Y axis and pseudo color along the Z axis showing the oxidation current measured from electrodes (background subtracted). These 2D

color plots were generated in Demon Voltammetry [81]. Data across multiple animals was grouped together for investigation of different light stimulation parameters; the amplitudes of DA release were normalized to allow comparison across animals with respect to one highest value we recorded in each animal. The exact peak DA levels depend on factors such as local density of dopaminergic neuron terminals; and therefore vary with the electrodes' different position in the NAc tissue, among different slices, and across animals. The average peak DA level observed was estimated by electrode calibration to be 524 nM (S.E.M. = 53 nM; N = 8). For curve fitting and modeling, data was exported and analyzed in Matlab. The model we adapted for kinetic analyses is the Michaelis-Menten model, which is the classical enzyme kinetics model commonly used to characterize DA uptake [77]. To fit the model, an objective function calculating the sum of squared error between recorded data and simulated data was created in Matlab. Simulated data was obtained by Matlab differential equation solver, given the Michaelis-Menten equation.

3.4 Optogenetic stimulation is able to induced neuro-chemical dopamine release

We used electro-chemistry to monitor the transient, relatively high concentrations [82] extracellular dopamine release evoked by light in the Nucleus Accumbens (NAc) area of 10 adult transgenic mice. Only mice identified as positive (+) for Cre (i.e.

expressing ChR2(H134R)-EYFP) by genotyping were used. Brain slices were checked under a fluorescent microscope to confirm opsin expression before each FSCV recording experiment. As described already in Chapter 3.2.3, expression was mainly found in the VTA and SN in the midbrain, and in the NAc and CPu in the forebrain, in agreement with previous studies on dopaminergic cell distribution in the mouse brain [27]. Expression in other areas was not observed in the forebrain and midbrain slices.

To electro-chemically measure phasic terminal dopamine release events modulated by optogenetics, as described above, FSCV electrodes were inserted into brain slices at the NAc. Light was delivered through the objective forming a $d = 2.4$ mm illuminated spot around the electrode tip. As analog input controlled laser pulses were delivered onto the brain slices, simultaneous FSCV recording tracked the extracellular concentration of dopamine.

With the electrode sitting in NAc tissue, we turned on the laser and applied a 25 ms, square waveform light pulse. The region around the CFE electrode is very briefly illuminated, almost unnoticeable to the naked eye. However, a very strong abrupt change of FSCV signal was recorded as shown in figure 3.7. This abnormal activity was followed by a gradual decay over a few seconds until the FSCV plot relaxed to the baseline level before the stimulation is applied.

Recall that this FSCV 2D color plot shows the time-lapsed cyclic voltammogram. Each vertical line indicates one CV at a certain time point. Therefore the x-axis is the time and y-axis stands for FSCV scanning voltage (triangle waveform, from -0.4

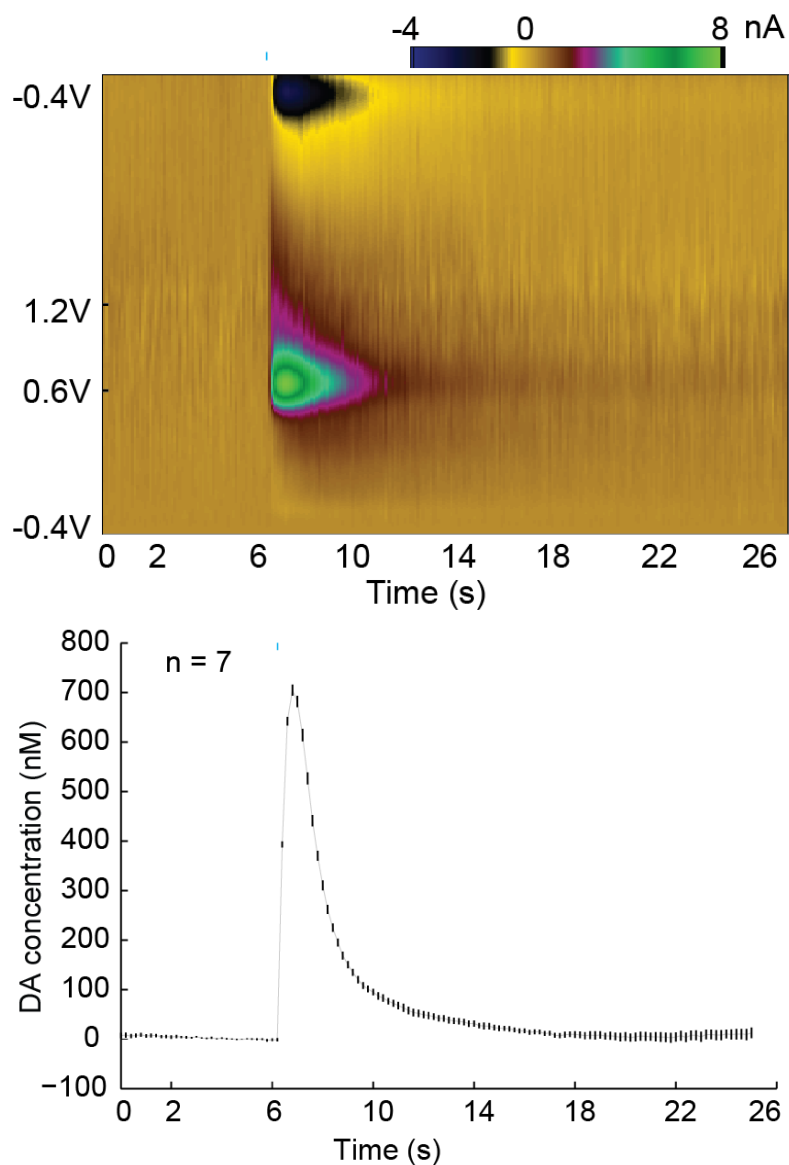


Figure 3.7: Optically induced DA efflux by a 25 ms light pulse in transgenic mouse brain slices. Upper panel: Recorded standard FSCV 2D color plot with stimulation at $t = 6.2$ s. Z axis shows background-subtracted voltammetry current in pseudo color. Lower panel: Converted mean DA concentration trace under the same stimulation parameter with small vertical bars represent \pm S.E.M. ($n = 7$ recordings in the same slice). (peak concentration at 705 ± 11 nM).

V to 1.2 V back to -0.4 V). The converted DA concentration vs. time plot is the average DA concentration trace calculated according to the FSCV signal at +0.6 V (which corresponds to a horizontal line on the left FSCV color plot), with error bars (vertical bars) as plus minus standard error of the mean (S.E.M). Error bars are small because of the good cross-trial consistency under same stimulation parameters. The sample size is $n=7$ FSCV recordings under exactly the same stimulation condition in one brain slice.

Next, we verified the identity of detected chemical signal is indeed a result of extracellular dopamine concentration increase. This is done by taking a single cyclic voltammogram at the ‘peak’ of the evoked activity by light. The background subtracted cyclic voltammogram below displayed clear oxidation and reduction peaks at +0.6 V and -0.3 V 3.8. These are the signature peaks known to correspond to dopamine. Therefore, our observed change in FSCV signal is a large extracellular dopamine concentration increase in the slice tissue, but not a result of other chemicals in the brain.

Overall, the optogenetic induction of immediate DA release was reproducible in all $N = 10$ adult transgenic animal subjects with different peak concentrations. During multiple stimulation events in one brain slice when the electrode was maintained at the same position, the time profiles of DA release showed little variation. This demonstrates that the induced DA release was highly reproducible and consistent among different stimulation events.

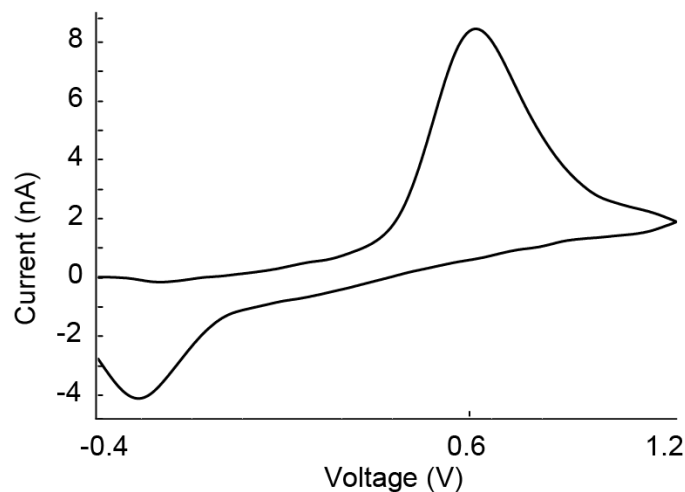


Figure 3.8: Background subtracted cyclic voltammogram at optical DA release peak; oxidation current is seen at 0.6 V and reduction current around -0.3 V.

In addition, dopamine signals were not seen in control experiments with the CFE placed out of the brain slice as shown below 3.9, nor do redox peaks. The optical stimulation power required to induce DA release was measured to be relatively low (<1 mW/mm²), which minimizes potential light artifacts at our typical stimulation parameters. The absence of any artifacts during induced DA release combined with the cell-type specificity in optogenetics enables us to investigate clean dopamine dynamics in the NAc, as well as to obtain accurate estimates of any kinetic parameters.

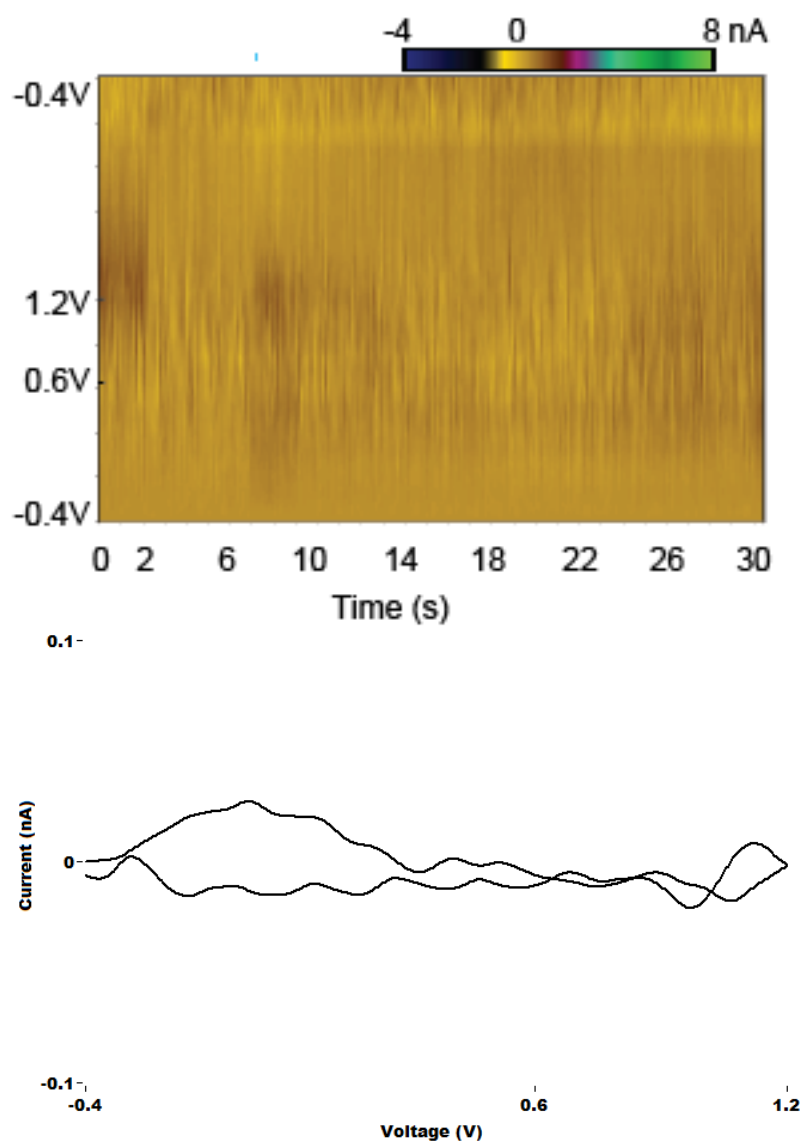


Figure 3.9: One control experiment where electrode is not inserted in the brain slices but under same light stimulation parameters shows no DA signals and minimal light artifact.

3.5 Modulating the dopamine release concentration by different light stimulation protocols

After successfully utilizing cyclic voltammetry methods to record the evoked dopamine release, we quantitatively studied the dopamine dynamics under constant FSCV monitoring while changing the light stimulation. It is known that the spontaneous release of DA during animals' natural behaviors has more variability and is often lower in concentration [18] than the DA release induced by an electrical pulse. This indicates that only a portion of the stored presynaptic DA pool is typically released into the extracellular space during natural behavior. To mimic the DA release events in naturally behaving animals, it is essential to achieve scalable DA release with certain precision.

3.5.1 Effects of light power

Firstly, we investigated the effects of altering the optical stimulation power. Across 3 transgenic animals, a series of stimulations with different light powers were delivered with simultaneous FSCV, ranging from 0.09 mW/mm^2 to 1 mW/mm^2 . To minimize the effects brought by light pulse width, we used square pulses fixed at 100 ms long. As demonstrated in figure 3.10, the amplitude of the induced DA concentration increased as the light power was increased.

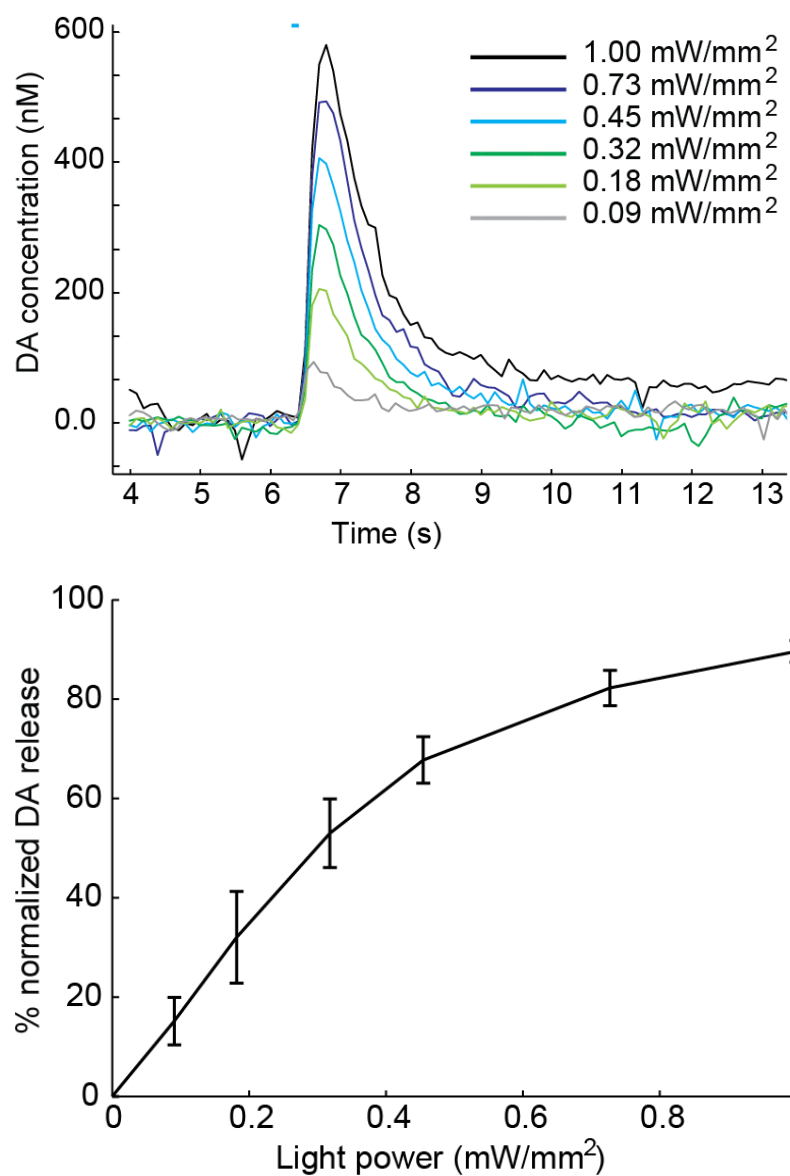


Figure 3.10: Upper panel: Stacked DA concentration traces under the 6 different light stimulation power. Lower panel: optically induced DA peak level as a function of light power, across 3 animals. ($n = 3 \times 6 = 18$ recordings in total; recordings are separated by 5-10 minutes to allow DA recovery. Vertical bars represent \pm S.E.M. Pulse width is fixed at 100 ms.)

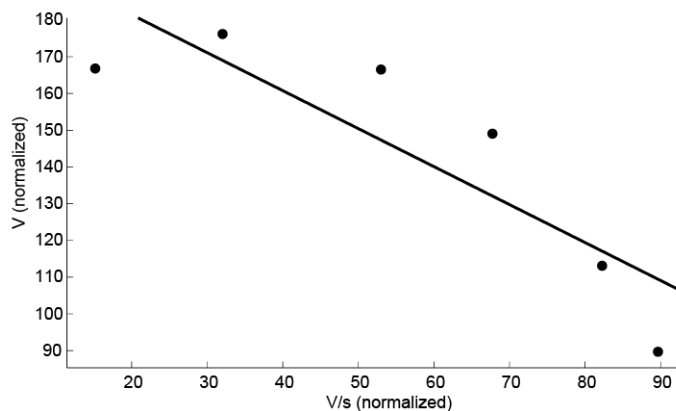


Figure 3.11: Eadie-Hofstee transformation of the mean DA peak response vs. light power density curve. The fitted linear model of $f(x)=a*x+b$ has coefficients: $a = -1.034 \pm 0.829$, $b = 202.1 \pm 52.0$, $R^2=0.750$

It appears that the relationship between stimulation power and the evoked concentration has a saturable trend. To look in detail, we performed an analysis using Eadie-Hofstee transformation, which is a linearization of the Michaelis-Menten equation. However, a sufficiently good linear fitting was not achieved (R^2 value of 0.750). This indicates that even through the DA peak response increases with the light power density; their correlation is more complicated than that described by the typical enzyme kinetics.

We speculate this may be due to the nature of the light ‘receiver’ protein, Channel-rhodopsin-2, which interprets the light power density in mW/mm^2 in a complex way beyond common protein kinetic models. This results in a sub-linear or non-linear correlation of dopamine peak concentration to light power in an Eadie-Hofstee diagram. Nevertheless, the DA peak and light power still correlate positively, and

have saturable characteristics.

3.5.2 Effects of stimulation pulse width

Next, we also observed an increased DA response as the light pulse width was increased while the light power was held constant (1 mW/mm^2) across 4 transgenic animals. In figure 3.12, short light pulses of 3 ms induced relatively small DA release. However, a sharp increase of DA level was seen as the light pulse width increased. This increased DA release reached a plateau around 15 ms. This indicates that when the light stimulation is sufficiently long ($\geq 15 \text{ ms}$), the amount of released DA reaches a saturation point for the effect of pulse width. Previous studies in electrically elicited DA release [77] [30] have been using the number of stimulation pulses as the primary approach to modulate DA release concentrations. We found that increasing the pulse width in optogenetics can result in a similar effect as multi-pulse stimulations.

Optical stimulations appear to be more versatile and effective since longer pulse width or stronger light power both can lead to increased DA release, in addition to increasing the number of pulses in the electrical stimulation case. However, we think applying large quantity of stimulation pulses over an extended period has the potential to result in even higher DA release [77] [49]; while increasing the pulse width beyond 15 ms does not seem to further increase DA release concentrations.

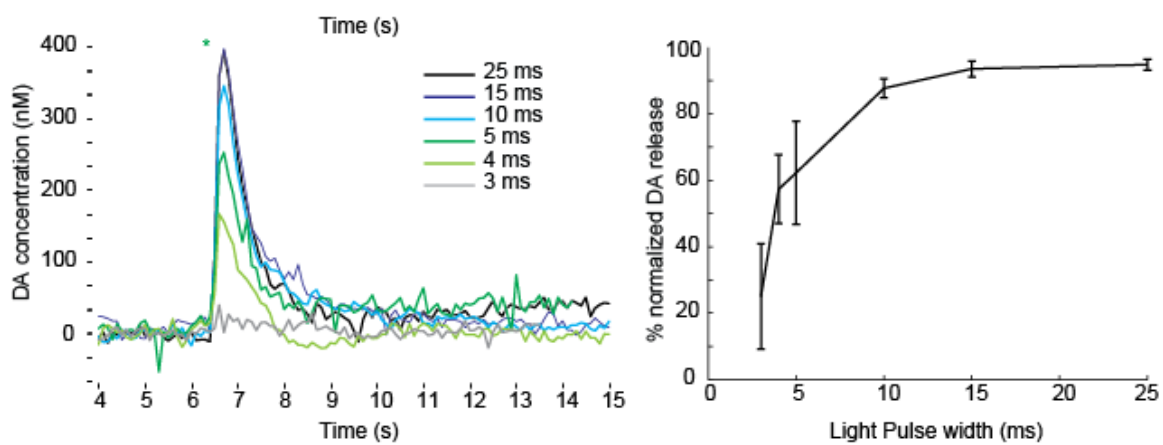


Figure 3.12: Effect of light pulse width on the evoked dopamine concentration. Left: recorded dopamine concentration traces in one brain slice under different pulse widths. Right: induced dopamine peak level as a function of light pulse width across 4 animals ($n = 4 \times 6 = 24$ recordings in total; recordings are separated by 5 10 minutes to allow DA recovery. Vertical bars represent \pm S.E.M. Light power is fixed at 1 mW/mm²).

3.5.3 Discussion on stimulation parameters

The rationale for choosing the parameters are firstly described below. The pulse width of 100 ms used for analyses of power-DA peak correlation was to avoid the modulation effects brought by the pulse width. Because the DA response reaches a plateau as the pulse width increases to 15-25 ms, usage of longer pulse width such as 100 ms or 1s will not interfere with the study of other parameters. The same situation applies to light power density of $1\text{mW}/\text{mm}^2$. We found $0.1\text{ mW}/\text{mm}^2$ represents the dynamic range of optically evoked DA, from release around the noise level to maximum release. More generally, the parameters chosen are in similar range with other optogenetic experiments [7], which reliably evoked robust spiking modulation or DA release.

Additionally, DA responses under different stimulation patterns of single pulse or pulse trains were compared across 3 transgenic animals (figure 3.13). The total three light patterns used were a 4 ms pulse, 4 pulses of 4 ms (25 Hz), and a 25 ms pulse, respectively (all under $1\text{ mW}/\text{mm}^2$). As seen, 4 pulses of 4 ms (25 Hz) stimulation increased the amount of DA release to around 200% of that from a single 4 ms pulse; while a longer 25 ms pulse also elicited higher DA release. The release levels between 4 pulses of 4 ms (25 Hz, takes a total time of 124 ms) and a single 25 ms pulse is similar (one-way ANOVA and multiple comparison test, $\alpha=0.05$).

This is in accordance with previous reports [7] [68] in the rat/mouse striatum. Therefore in contrast to electrical stimulation where pulse trains are usually necessary

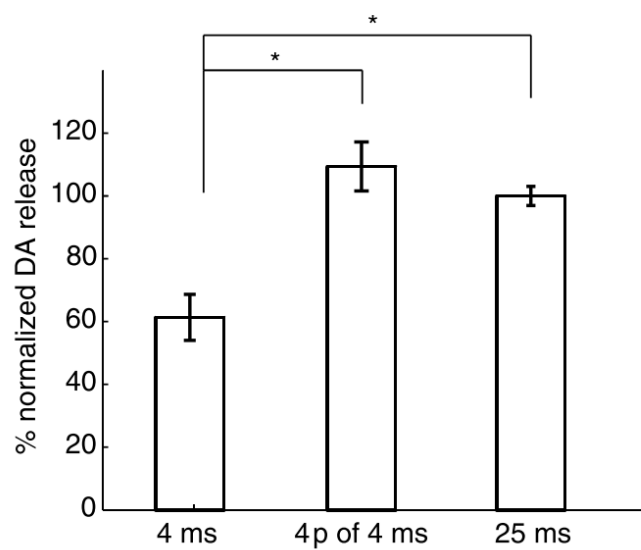


Figure 3.13: Dopamine release levels from varies stimulation parameters. The induced dopamine levels from light stimulations of a 4 ms pulse, 4 pulses of 4 ms (25 Hz), and a 25 ms pulse; $n = 7, 10, 22$ recordings respectively, across 3 animals. DA level evoked by the 4 ms pulse is different than the other 2 cases (one-way ANOVA and multiple comparison test, $\alpha=0.05$); concentration normalized with respect to DA release of 25 ms pulses.

[30], optical stimulation effectively reaches high DA level with a single square pulse of 25 ms. In fact, more than 50% of the maximum DA was released by a brief 4 ms light pulse. This seems to differ from the case of electrical stimulation where one 4 ms biphasic pulse elicits less than 10% of the maximum DA release [80]. Thus the optogenetic direct targeting of the dopaminergic neuron axons and terminals appears to be a very efficient way to evoke saturated DA release events.

3.6 The amplitude of transient dopamine response is critically dependent on the temporal profile of the light stimulus

Our results indicate that higher extracellular DA concentrations can be induced by increasing either the intensity, the duration or the number of light pulses, all of which correspond to increased light energy delivery into the targeted brain area.

However, we found that controlling the energy delivery is not the only way to modulate DA release; the light pulse waveform also plays an important role. We demonstrate in this section that the optogenetically evoked transient DA signal is significantly dependent on the stimulus waveform at the onset of the light stimulus. We performed a series of FSCV recordings where the temporal shape of the rising edge of the light pulse was varied. The abrupt rising edge of a square pulse was replaced by a short linear ramp of varying slope at the onset of 1s light stimulations.

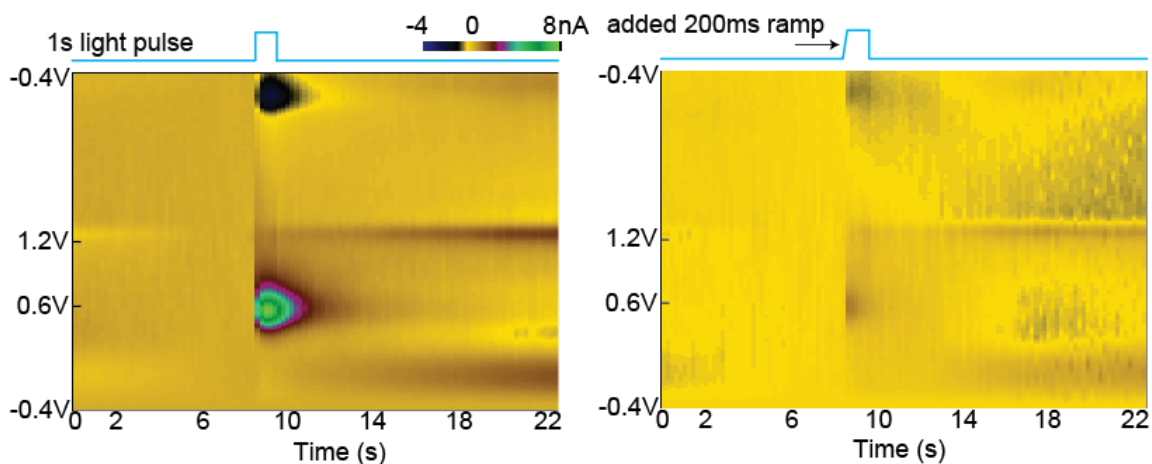


Figure 3.14: Standard FSCV 2D color plots under a 1 s square pulse (left) versus a 200 ms ramp + 1 s square pulse stimulation (right). Z axis shows background-subtracted voltammetry current in pseudo color; data is from single recordings.

These temporal waveforms with initial ramps ranging from 12.5 ms to 300 ms were applied as analog inputs to the blue laser driver. All stimulations shared the same 1s square pulse shape after the initial ramp. A comparison is shown in figure 3.14 between a stand-alone 1 second square pulse and a 1s square pulse with a 200 ms initial ramp. (We chose 1 s pulse since it was long enough to rule out the influence of later waveforms other than the onset waveform. Yes, we have observed that the effect is same for longer pulses. In fact, we have found that any persistent light after the initial few hundred milliseconds do not have any influence on the DA concentration recorded, no matter what kind of waveform is applied.)

Very interestingly, lower DA response is observed in the latter case despite the

fact that more total light energy was delivered to the targeted brain area. More systematically, we investigated this effect in 4 transgenic mouse subjects by gradually increasing the ramp duration (figure 3.15). Results show that peak DA concentration varies dramatically with ramp duration. For example, the released DA concentrations are significantly different between waveforms with 50 and 75 ms added-ramp (one-way ANOVA and multiple comparison test, $\alpha=0.05$). In fact any of the DA release from 12.5, 25, 50 ms ramp waveforms is larger than that from 75, 100, 300 ms ramp waveforms (one-way ANOVA and multiple comparison test, $\alpha=0.05$). Longer ramps preceding the square pulse invariably resulted in lower peak DA concentrations, even though more total light energy is delivered. Our findings thus demonstrate the induced transient DA efflux is critically dependent on the shape of temporal waveforms of optogenetic stimulation at the moment of light onset. On the other hand, difference in induced extracellular DA concentration is not necessarily a result from change in the amplitude and length of light stimulations.

Since the relationship between ramp time and dopamine level seems sigmoidal, We suspect that to use a logarithmic plot would be a better representation. $\log(\text{ramp})$ is used instead of the ramp duration on the x-axis of the ramp plot 3.15. The new x-axis ranges from $\log(12.5)=2.5$ to $\log(300)=5.7$ while y axis remains unchanged. It can be observed the transformed plot is still slightly sigmoidal shape (figure 3.15), though it's closer to linear than the original curve. This may indicate the ramp duration - DA peak correlation is on a higher order or more complicated than sigmoid. It could

be interesting to explore this correlation in detail in future studies. Especially use simulation methods to study the number of activated light gated ion channels (ChR2) under a slowly ramped up light power. Then calculate the depolarization caused by activation of ChR2 to determine DA molecule release. This is also interesting in other phenomenon generated by light ramp such as cortical oscillations [3].

In sum, this observation indicates that optogenetic induction of terminal DA release apparently requires a “shock” effect:, i.e. a fast rising edge at the onset of stimulation. This may have resulted from both characteristics of the opsins receiving light stimulation and terminal DA vesicle release conditions. It’s known that light power is related to the activation probabilities of the ChR2 opsins is related to light power. As light power is increasing during the ramp, expressed opsins on the dopaminergic cell terminal may be activated at different timestamps. On the other hand, while a square pulse immediately imposed a higher activation probability on all opsins in one cell, which leads to a larger depolarizing current. On the other hand It is also known that DA vesicle release is promoted by larger cell depolarization (ref Raiteri). We speculate that this effect is likely a general property of dopaminergic cell response, and that a simultaneous activation either by opsins or synaptic inputs can result in high extracellular DA release in physiologically conditions.

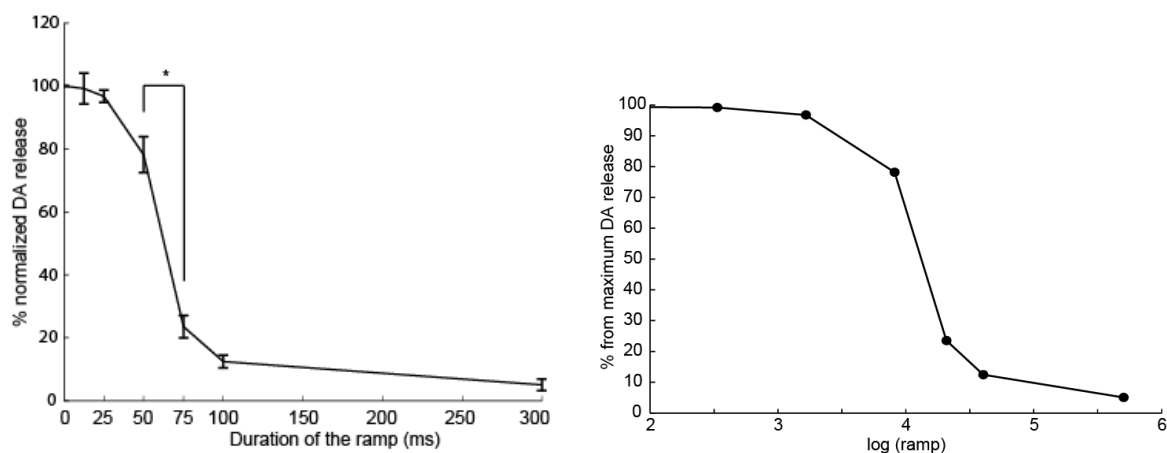


Figure 3.15: Correlation of light ramp duration and mean DA peak response. Left: DA peak level as a function of added ramp time to the 1s square pulse. (In $n=4 \times 6 = 24$ total recordings across 4 different animals. Recordings are separated by 5 10 minutes to allow DA recovery.) Y-axis is normalized with respect to the DA release induced by non-ramp square pulses in each animal. Among adjacent ramp durations, DA peak level is significantly different between 50 ms and 75 ms ramp waveforms (one-way ANOVA and multiple comparison test, $\alpha=0.05$). Right: Average dopamine response under different added ramp time. X-axis is replaced with log of ramp duration (from $\log(12.5)$ to $\log(300)$).

3.7 Recovery of presynaptic dopamine revealed by optogenetics

Upon the onset of optical stimulus, stored presynaptic dopamine is released, causing a transient local high concentration of extracellular DA in the sub- μM range. The extracellular DA then returns to the cytosol through DAT uptake to be prepared for a future release event. The DA must also be sequestered into synaptic vesicles to be recovered into a readily releasable state, in addition to simply being transported back into the cytosol [10]. The releasable presynaptic DA pool is recovered dynamically during this process. Optogenetics is an ideal tool to unfold the dynamics behind the recovery of releasable presynaptic dopamine because conventional electrical stimulation also excites non-dopaminergic neurons in the brain which may interfere with extracellular DA release, whereas optogenetics allows the selective activation of dopaminergic cells.

For this purpose, we used stimulation protocols with series of two consecutive light pulses applied at varying intervals while electro-chemically monitoring the dopamine activity. The voltammetry signature of dopamine is validated by FSCV colorplot. As shown in figure 3.16, the initial light pulse in each recording always elicits about the same peak DA concentration. While as the inter-pulse interval is increased from 2 s to 40 s, the second pulse elicits DA concentrations of gradually increasing amplitude. At short inter-pulse intervals of 2, 3, and 4s, the readily releasable DA is less than

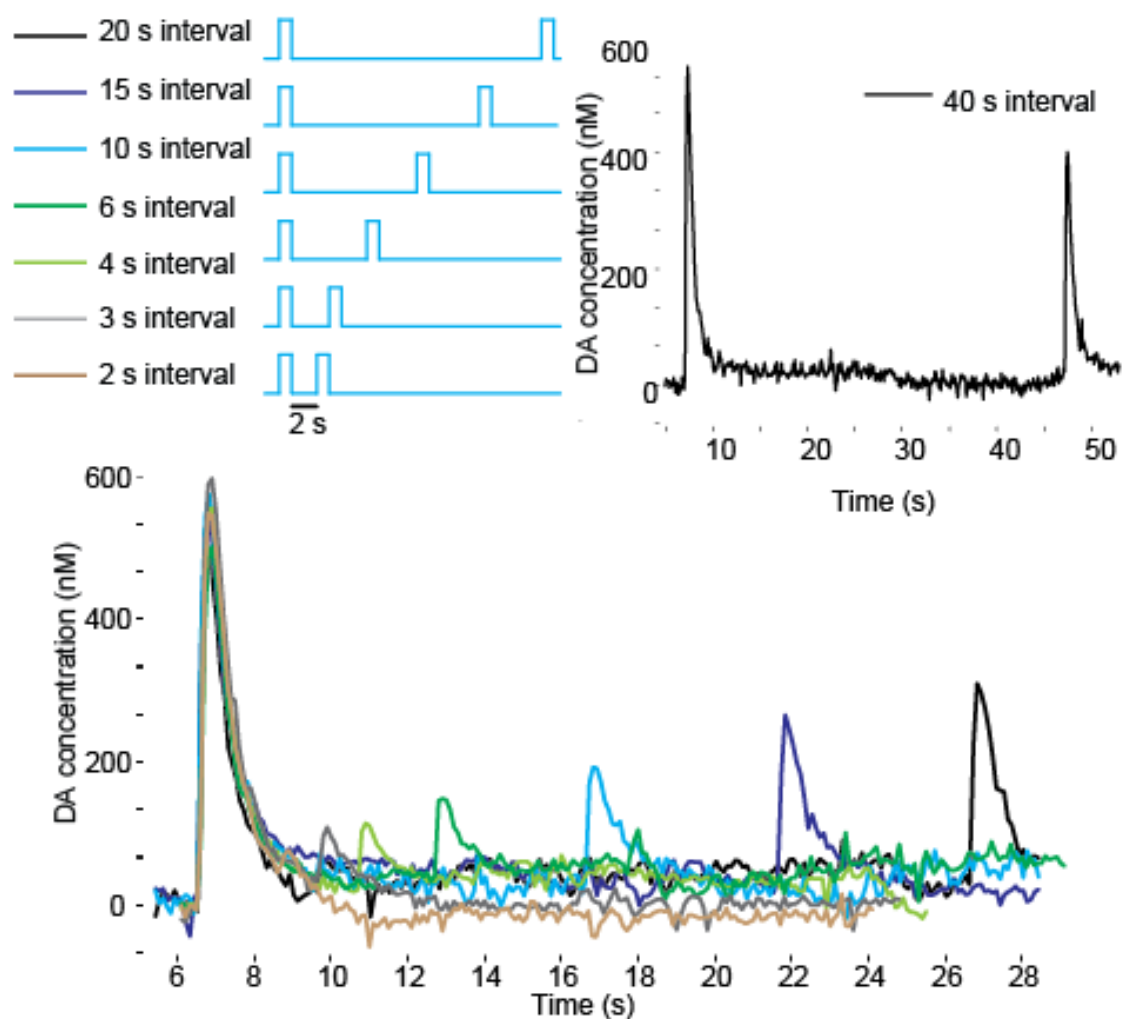


Figure 3.16: Effects of stimulation inter-pulse interval. Series of recorded DA concentration traces under two light pulses with inter-pulse intervals of 2, 3, 4, 6, 10, 15, 20, 40 seconds. Stimulations were kept at 1 mW/mm^2 power and 1 s in length; data is from a set of 7 recordings in one of the animals from 4D. Recordings are separated by 5-10 minutes to allow DA recovery.

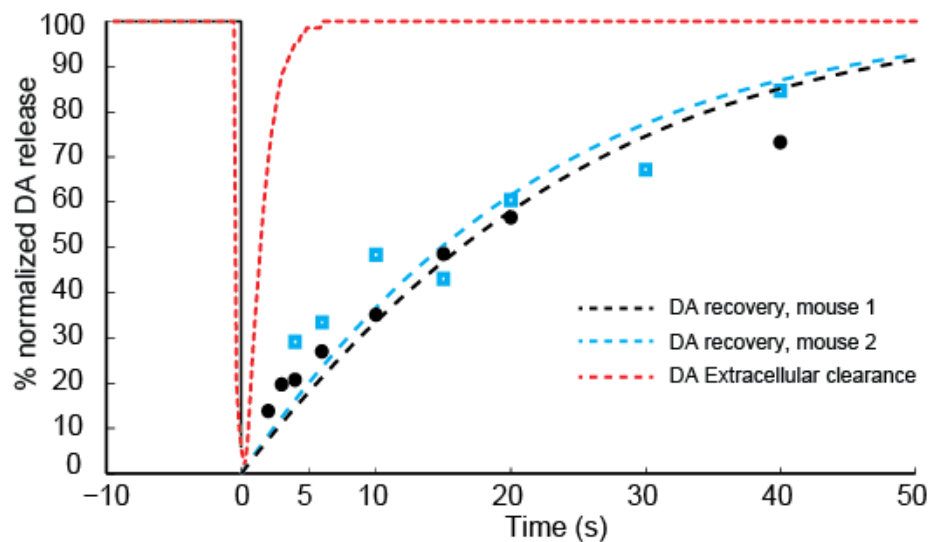


Figure 3.17: Recovered releasable presynaptic DA on second pulses as a function of inter-pulse interval in 2 adult transgenic mice (blue and black). Red line indicates the clearance of extracellular dopamine molecules (i.e. DA concentration recorded by FSCV).

20% of the original amount, indicating depletion of releasable presynaptic DA. For recording with 40s inter-pulse interval (Fig 3.16), the second pulse elicits DA level to 70% of that from the initial pulse, suggesting most of the releasable DA pool is restored.

Complete recovery can be achieved on a scale of minutes, since 5 minute intervals between the trials were sufficiently long so that the initial DA peak for each trial remained nearly constant in magnitude (543 ± 27 nM).

We plotted the recovery of DA against inter-pulse time, in the two transgenic

mouse subjects studied (sometimes referred as paired-pulse inhibition [38]) . Consistent results were observed (figure 3.17, blue and black). Also, when compared with the extracellular clearance of dopamine recorded by FSCV (figure 3.17, red line), the recovery of readily releasable presynaptic DA takes place on a much longer time scale.

Compared to similar studies which employ electric stimulation [57], we observed a stronger dopamine release inhibition effect 2–10 s after an optical pulse; while the qualitative trend of recovery is similar. We speculate that light stimulation may achieve better clearance of the releasable DA pool at the first pulse, since it can be delivered on a longer time scale due to the absence of artifacts. In addition, these results proved that the paired-pulse inhibition effect in electrical stimulations can be reproduced in the cell-type specific environment in optogenetics without recruiting other non-dopaminergic neurons in the brain, thus excluding the possibility of other neuron types causing this effect.

During the recovery of presynaptic DA pool, a number of processes are involved such as the DA transportation from the cytosol to presynaptic vesicles [26], docking of DA vesicles [54], or autoreceptor inhibition. Autoreceptor inhibition is shown to primarily happen within around 0.5–2 s after the first DA release, and therefore should not contribute to the general recovery effect seen on longer time scale [57]. Therefore, our observed DA recovery is more likely related to the formation of presynaptic DA vesicles. A vesicular monoamine transporter-2 protein, which mediates DA transportation from cytosol to synaptic vesicles, also primarily obeys the Michaelis-Menten

kinetics, which we modeled in the next section.

3.8 Chemical kinetic analysis of dopamine release and uptake

We further performed kinetic analyses on the uptake and recovery process of optogenetically induced DA concentration data. Michaelis-Menten kinetics (Methods) is used to model the DA uptake. The estimated best fit parameters were found to be the following: V_{max} is $0.969 \mu\text{M/s}$ taking K_m of $0.21 \mu\text{M}$ (Ross, 1991) ($R^2 = 0.918$, Fig 3.18); the first order rate constant k ($k = V_{max}/K_m$) is 4.6 s^{-1} . This estimation is similar to the previously reported electrically evoked DA uptake rate constant k of $4.0 - 7.8 \text{ s}^{-1}$ in the mouse NAc area [12] and also lower than the reported rate constant in the CPu area [65]. In addition, several other parameters describing the uptake kinetics such as full-width at half height (FWHH), T20 (the time of 20% substrate clearance), and T80 (the time of 80% clearance) [81] were also extracted from the data. Optogenetically induced DA release peaks by single 1s square pulses have a mean FWHH of $1.48 \pm 0.02 \text{ s}$, T20 of $0.68 \pm 0.03 \text{ s}$, and T80 of $2.52 \pm 0.10 \text{ s}$.

We also applied Michaelis-Menten kinetics analysis to the releasable DA pool recovery data. In this case, a K_m value of $1 \mu\text{M}$ is used [25] [39] to fit the model, yielding V_{max} values of 0.0585 and $0.0592 \mu\text{M/s}$ respectively for the two transgenic animals (figure 3.17, $R^2 = 0.922, 0.881$). The recovery of releasable presynaptic DA

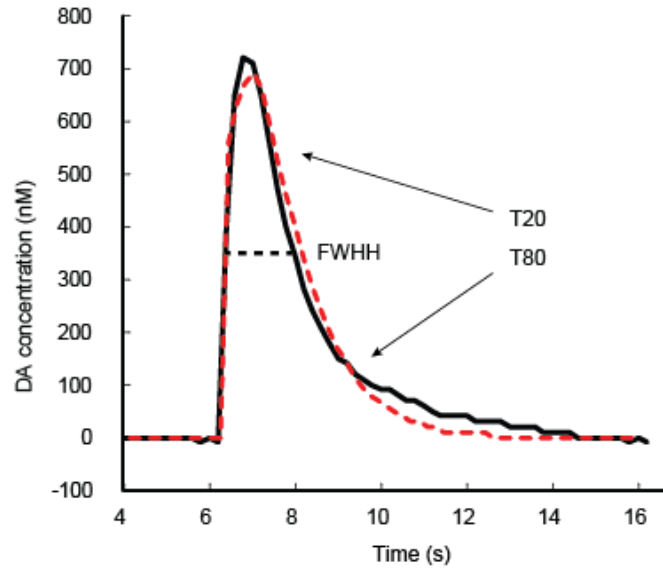


Figure 3.18: In the uptake kinetic analysis, simulated (red) versus recorded (black) FSCV DA concentration signal. FWHH, T20, T80 is shown.

$$\frac{d[DA]_{EC}}{dt} = [DA]_o - \frac{V_{\max}}{K_m / [DA]_{EC} + 1}$$

Figure 3.19: The Michaelis-Menten kinetics of dopamine uptake under optical stimulation.

seems to be adequately fitted with the Michaelis-Menten model. The V_{\max} value obtained for recovery of releasable DA was much lower than the value obtained for DA uptake, which indicates that uptake into cytosol alone is not sufficient to prepare DA molecules for another immediate release. Therefore, this validates that other processes are involved in the recovery of releasable presynaptic DA.

Beyond our basic studies, such quantitative understanding of DA dynamics has

potential relevance for understanding drug addiction and reward driven behavior, since the timing of DA release relative to behavioral events and the extent of attenuation is important. In addition, our results demonstrated that both the slower kinetics of recovery of the presynaptic DA pool and the faster kinetics of DA uptake by DAT can be studied using optogenetics in a cell-type specific stimulation context. With less interference from non-dopaminergic cells and other artifacts, more accurate DA terminal kinetic analyses can be performed, which may contribute to future theoretical and/or modeling studies. DA transmission in the NAc in particular is critically involved in an animal's reward driven behavior, learning, emotions, etc. A transient DA release in the NAc is often seen at anticipation or receipt of natural reward stimuli (such as for food [62]). Artificially induced transient DA release events (or 'rewards') can be an effective way for optogenetics to play a significant role in animals' natural behaviors. Thus quantitative understanding of the interaction between the light and the terminal dopaminergic dynamics in the NAc is an important step forward. Behaviorally realistic stimulation paradigms can be developed accordingly in the application of future *in vivo* experiments.

3.9 Conclusions

In sum, our results demonstrate the feasibility using electro-chemistry to quantitatively study the optogenetic modulation of DA release events in the NAc under

various stimulation conditions, in a simple framework using transgenic animals. Optogenetics is shown to be both capable and efficient in eliciting high concentration extracellular dopamine release events, through targeted stimulation of exclusively dopaminergic cell axons and terminals in the NAc. A remarkably low light power of around 0.1 mW/mm^2 is required to elicit measurable DA release. Extracellular concentrations of DA release can be manipulated by controlling various parameters such as the light power, light pulse width, shape of waveform onset, or the temporal pattern of pulses delivered. Kinetic time constants and parameters for the recovery of the readily releasable DA pool as well as for DA uptake were obtained under this cell-type specific stimulation scenario. These results suggest that the combination of targeted optogenetic stimulation and simultaneous FSCV in transgenic animals provides a useful approach for the quantitative study of terminal dopaminergic dynamics. Further studies may utilize this approach to investigate various questions related to dopamine transmission in both healthy and diseased brain, or to design potential behavioral experiments with optogenetically modulated dopamine release.

Chapter 4

A novel chronically implantable
neuro-chemical sensing probe for
real-time monitoring of
neurotransmitters *in vivo*

4.1 Introduction: Motivation of the development of a chronic neuro-chemical sensor

As explained in previous chapters, the brain's chemical messengers (neurotransmitters such as dopamine and serotonin) have a central role in various aspects of animal behavior, such as motor control, reinforcement learning and emotion [79]. While understanding the chemical transmission in an *in vitro* environment explains the neurotransmitter terminal behavior and its chemical dynamics, it has its own drawbacks and restrictions.

First and foremost, the correlation of certain characteristics such as dopamine transmission with animal behavior cannot be investigated in an *in vitro* environment. To study behavior related scientific questions in an *in vivo* experiment setting, a freely moving experimental approach is necessary.

Secondly, the dopaminergic neuronal terminals and axons in the brain slice tissue lack mid-brain input. Brain's native commands are sent from the mid-brain regions such as Ventral Tegmental Area (VTA) and Substantia Nigra (SN) through Medial Forebrain Bundle (MFB) to the neuronal terminals and axons in the striatum and nucleus accumbens. Lacking afferent neural inputs, the *in vitro* dopamine signals would not demonstrate the same spontaneous temporal profiles as those signals in a live animal would. Therefore, *in vitro* recording reveal less interesting neuro-chemical information in the intact brain.

Lastly, we are interested in studying the chronic changes in dopamine release characteristics and fluctuation in extracellular concentrations. This requires a recording approach that can last for days, weeks, even months. Brain slices obviously do not last for more than a few hours, thus prevent us from understanding changes that happen on a longer time scale. Chronic changes in dopamine basal level are particularly of interest in several neural degenerative diseases. [43] A probe that have the potential to monitor chronic changes is therefore a very valuable tool in both fundamental and clinical research context.

Therefore, to overcome above restrictions and while gaining a deep understanding of these dopaminergic pathways and how they interact with animal's behavior, researchers have to be able to in real-time monitor the fluctuations of dopamine *in vivo* and chronically. In recent years, attempts have been made by improving the traditional carbon fiber pipette probe in terms of its size and bio-compatibility for implantation in rodents [18]. Clark et al. have fabricated an implantable sensor that consist of a fused silica encapsulation and one single carbon fiber exposed around 150 μm at the tip. Through tissue histology analysis post implantation, they have demonstrated that the carbon fiber, with a diameter of 7 μm , barely leave any visible trace in the brain tissue in a chronic implantation context. This result indicates that the carbon fiber is able to acquire the genuine chemical messenger transmission in the undamaged tissue. Although their results demonstrate the chronic recording capability of carbon fiber, however, this approach does not have the capability to deliver optical

stimulation *in vivo*, therefore making it impossible to integrate with the optogenetic tools whose cell-type specificity is very powerful in studying neuronal systems. In addition, with a single “read-only” design, it requires a second ‘stimulation probe’ implantation in order to drive the dopamine release events [42], which greatly adds surgical challenges and affect the post-surgical survival of the experimental subject.

4.2 Design of the chronically implantable neuro-chemical sensing probe

The progress in optogenetics and the development of a variety of transgenic rodent models have provided a powerful tool set to study the functional role of specific dopaminergic pathways on neural activity and behavior. Effective application of this tool set for *in vivo* studies requires the development of a novel opto-chemical probe for simultaneous light delivery and cyclic voltammetry dopamine recording.

Below, we summarized the necessary functional components and their roles in an chronic implantable neuro-chemical sensing probe (in this chapter we use the shorter name neuro-chemical probe for simplicity):

A. Electrode capable of detecting dopamine with fast-scan cyclic voltammetry.

Carbon based electrode is necessary for detecting dopamine because of the specific electrical and mechanical properties. It has been so far the most successful family of materials in neurotransmitter detection. As explained above, carbon electrode surface

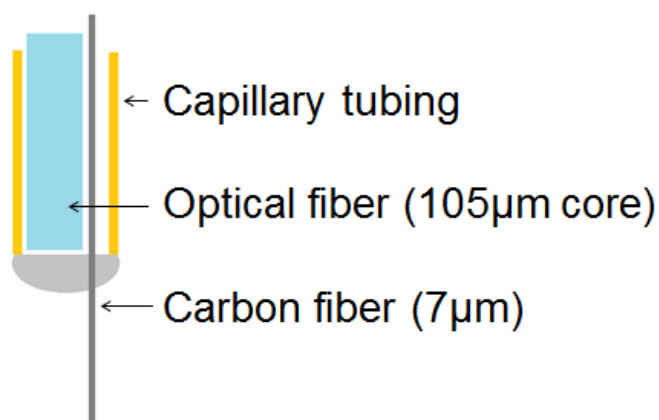


Figure 4.1

promotes dopamine adsorption at electric potential at -0.4 V. We have experimented for different ways of integrating the carbon-based electrode into our device, including utilizing graphene coated optical fiber. Despite the innovation in these techniques, the carbon fiber is more reliable because of its high resistance to mechanical and chemical damage. In addition, the $7 \mu\text{m}$ size ensures minimal tissue damage and specificity in local dopamine recording. Because our work focus on result-driven, applied neuro-chemical research, we therefore choose to adapt the most reliable way to record *in vivo* dopamine. We integrated the $7 \mu\text{m}$ carbon fiber in our neuro-chemical sensing probe as the electrode for FSCV recording.

B. Optogenetic stimulation delivery targeted at the local dopamine terminal field

We utilize the optogenetic tools to study cell-type specific stimulation, where light delivery into the brain tissue is crucial. Unlike in brain slice studies, where we deliver light on to the slice through microscope objective. For *in vivo* environment, because

the transparency of the brain is low (see recent efforts to make the brain optically transparent by the technique of CLARITY [48]), an optical fiber is often used to deliver light in the targeted region. When designing our optogenetic neuro-chemical probe, the stimulation objective is to elicit a dopamine release by the dopaminergic neuron terminal field, such that the carbon fiber is able to measure this dopamine release by FSCV. Therefore, the light illumination is best to cover the brain tissue surrounding the exposed carbon electrode. We adapted two improvements in our design to facilitate targeted light delivery:

1. Positioning the optical fiber behind the exposed carbon fiber electrode. Since light is delivered in front of the optical fiber, the recessed optical fiber can better target the tissue around the electrode.
2. Switching from 10 μm core diameter optical fiber to 105 μm core diameter fiber.

Our typical construct for delivering light into the brain involves using a 10 core diameter, 125 outer diameters, polymer coated optical fiber. For neuro-chemical sensing experiment in particular, we have made a modification which is to substitute the 10 core fiber with 105 core optical fiber (outer diameter remain unchanged).

The reason is from both quantitative and qualitative point of view. The ideal light illumination should have a reasonably large 3D volume in the brain to stimulation a sufficient number of dopaminergic terminals for a more robust dopamine release. At the same time, we would like the light spread to be more uniform rather than

concentrated at the very tip of the optical fiber, because high intensity light can cause strong electric artifact which interferes with the FSCV recording, diminishing our ability to assess the extent of dopamine release accurately.

From a quantitative point of view, simulations of light spread were performed in both the 10 and 105 core diameter fiber cases. We adapted the same approach for intensity distribution simulation in the 2013 paper which I co-authored [53]. Both types of optical fiber were simulated under a 6 mW laser power input. The color plots below show the Monte-Carlo intensity distribution when light is escaped from the tip of optical fibers. Determining factors for this distribution are the core diameter of the fiber (10 and 105), numerical aperture (NA, 0.075 and 0.22) of the optical fiber, and laser power input (6 mW). Color indicates the intensity of the light in unit of mW/mm^2 , on a \log_{10} scale.

This quantitative analysis of the light distribution shows that using a large core (105) optical fiber significantly facilitates the light spread, leading to larger illuminated area. In addition, the intensity is less concentrated at the tip of the optical fiber, which reduces potential light artifacts in the FSCV recording. Therefore, we have changed the design for the probe to using 105 core optical fiber, for the purpose of better optogenetic stimulation delivery.

C. The third functional component for the neuro-chemical sensing probe is electrical insulation and mechanical support for tissue penetration.

The carbon fiber electrodes have to be electrically insulated from the conductive

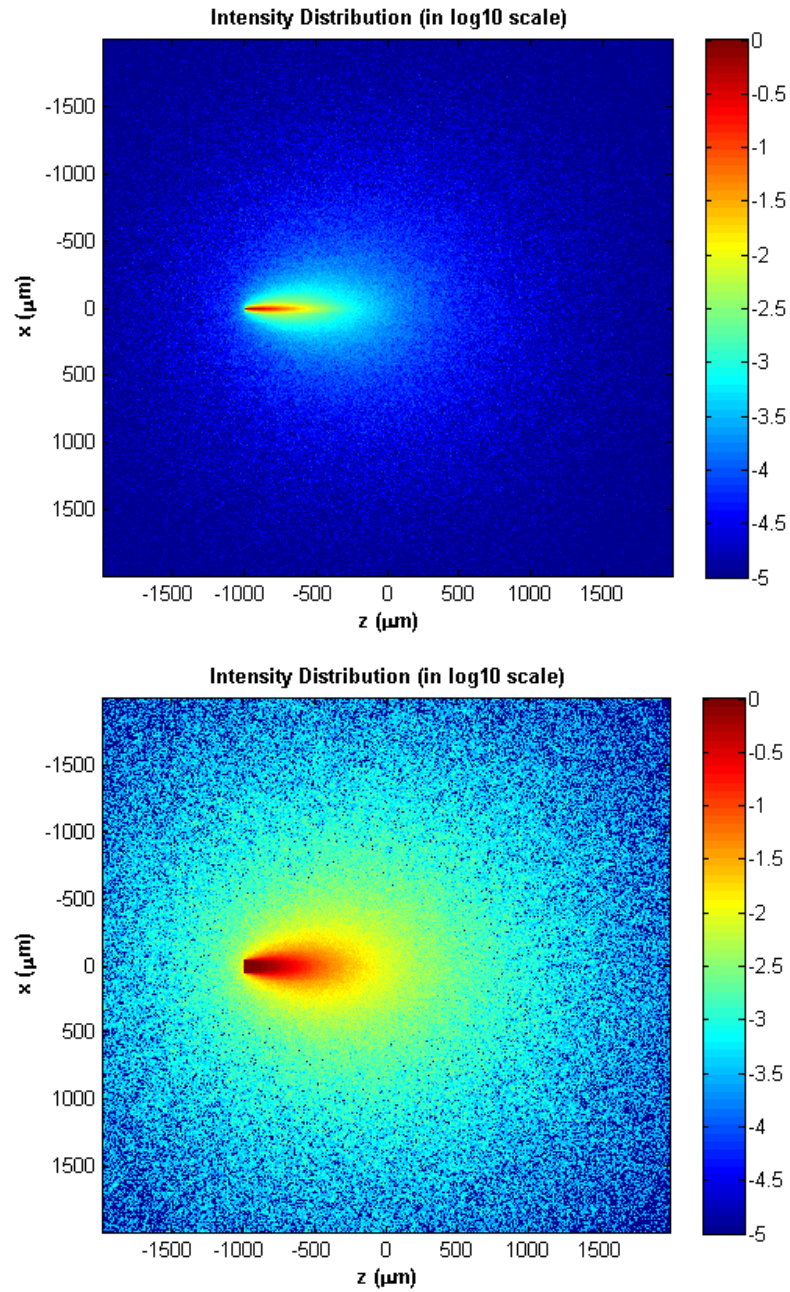


Figure 4.2: Upper panel: light distribution pattern in the brain at the tip of a $10 \mu\text{M}$ core, 0.075 NA optical fiber. Lower panel: light distribution pattern in the brain at the tip of a $105 \mu\text{M}$ core, 0.22 NA optical fiber. Both cases have laser input power of 6 mW. Generated by matlab code from our previously published results [53] (code courtesy of Dr. Ozden and Dr. Wang).

brain tissue except at the tip. In addition, with a 7 diameter, the carbon fiber itself do not have the mechanical strength to penetrate brain tissue. Therefore, in our design we utilize thin capillary tubing as the exterior of the probe, which bundles the carbon fiber and the optical fiber as an integral. We experimented with several different types of capillary tubing and have summarized their properties here:

Table capillary tubing,

Out of the above different types of capillary tubing, the 33 AWG small parts translucent amber miniature polyimide tubing has the smallest outer diameter, which is helpful in reducing tissue damage in an *in vivo* setting; while also have the necessary mechanical strength. Therefore, we adapted this type of capillary tubing as the exterior material of our neuro-chemical probe.

D. The last question is to determine the exposed electrode tip. In the setting of Fast-scan Cyclic Voltammetry, the exchange of electrons due to dopamine oxidation is happening at the exposed area of the carbon fiber electrode. One crucial procedure is to determine the size and distribution of this exposed area, i.e. the length of the exposed carbon fiber electrode directly contacting the tissue without insulation.

In case of smaller exposed electrode area, the sensitivity to extracellular dopamine concentration will be compromised, because the number of dopamine molecules in the adsorption process is proportional to the surface area of the carbon electrode. Although attempts have been made by researchers to increase the effective surface area of carbon fibers by modifications with innovative approaches such as utilizing

carbon nanotube [50] or graphene[6], the mechanical reliability (as 7 microfibers) and effects in increased sensitivity have not been very consistent for *in vivo* applied neuroscience experiments. It could be an interesting topic to pursue on increasing the sensitivity of dopamine electrodes, but is a completely different research direction. In sum, a restricted exposed electrode area will lead to limited dopamine sensing sensitivity; longer exposed carbon fiber electrode is beneficial.

On the other hand however, the length of exposed 7 μm carbon fiber is subject to practical concerns. Longer exposed carbon fiber is extremely vulnerable during the tissue penetration process in an *in vivo* recording setting. The brain contains numerous micro structures including resistant biofilms and membranes which all add to the difficulty of tissue penetration. In addition, the shear stress caused by inhomogeneity of the tissue is a concern in longer electrodes due to the force vector component vertical to the carbon fiber. One other reason electrodes cannot be too long is because we would like to observe a local effect of dopamine efflux caused by optical stimulation around the optical fiber tip, rather than the dopamine activity over a large non-specific region.

Integrating all the practical concerns described in the above argument, we have experimented with a few neuro-chemical probes that have exposed carbon fiber electrodes ranging from 50 μm – 300 μm ; and have determined that exposed carbon fiber less than 200 μm is less susceptible to breaking during tissue penetration while maintaining a high extracellular dopamine sensitivity. Therefore we use an exposed

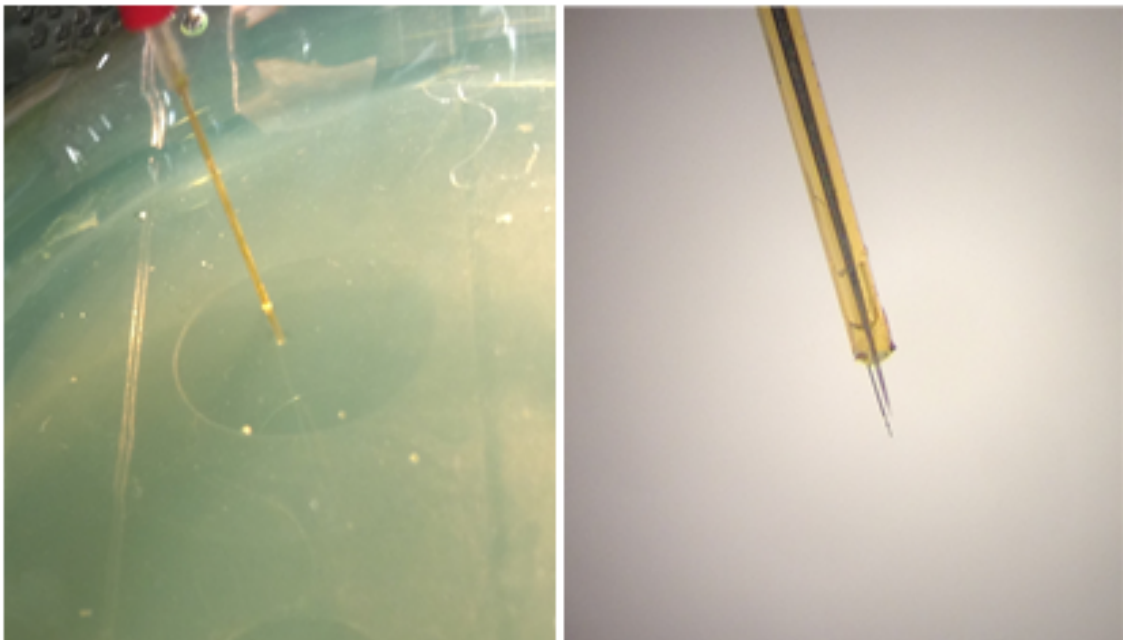


Figure 4.3: Left: Penetrating agarose gel as the brain equivalent, testing the mechanical strength of the probe. Right: attached an additional tungsten electrode for optional electrophysiology purpose along side the neuro-chemical probe.

electrode tip length of 200 μm .

Additionally, if we would like to acquire electrophysiology signals at the same time, it is possible to attach an additional tungsten electrode to the exterior of the neuro-chemical sensing probe. As shown, a tungsten electrode is glued on to the capillary tubing forming a pitch-fork construct with the existing carbon fiber electrode. Note that we do not require electrophysiology signals during our experiments, the tungsten electrode is therefore optional.

In summary, in our design for a novel two-way neuro-chemical probe, we focus on integrating the capability of both delivering controlled light stimulation and chemical sensing of dopamine by FSCV recording. Carbon fiber electrodes and optical fibers are built into thin capillary tubing. Same-site stimulation and recording is possible in this novel set-up, instead of the conventional experimental scheme in which stimulation is applied at the mid-brain (SN, VTA) while recording is done at the forebrain area of NAc or CPu. The probe is designed to be used for chronic *in vivo* experiments to study the dopamine transmission in rodents, and potential behavioral modulatory effects related to the dopamine system in various physiological conditions.

4.3 Fabrication approaches

In the above section on the design of the neuro-chemical sensing probe, the construct and different components of the probe is reasoned in detail. Given this design, fabrication of the probe was done in the following sequence of procedures.

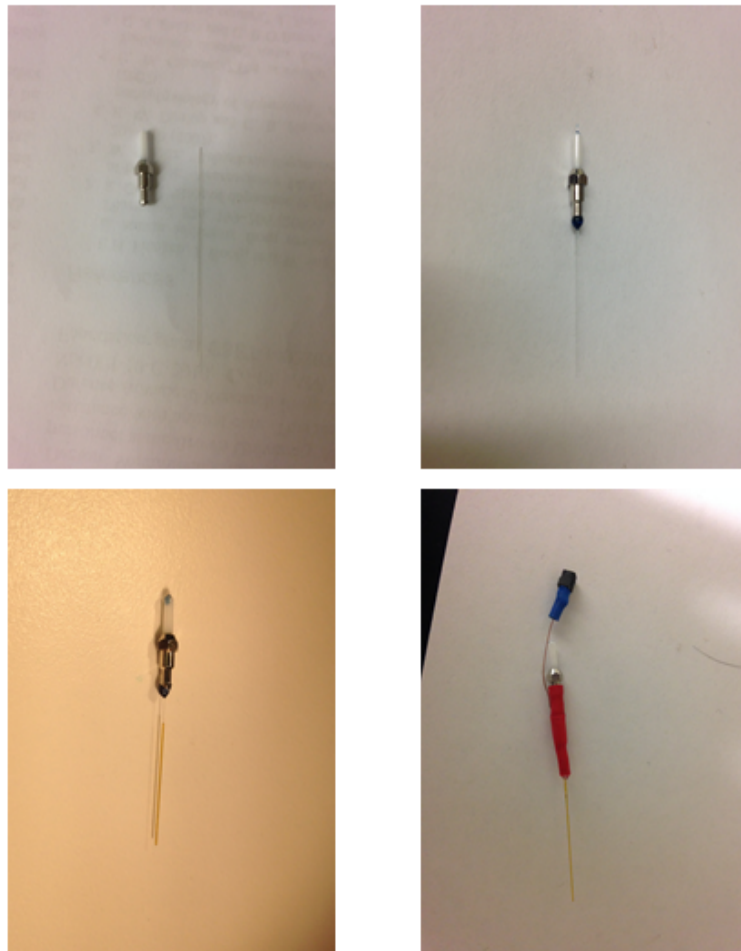


Figure 4.4: Top two: stage I. Bottom left: stage II. Bottom right: stage III.

Stage I, assembling optical coupling components

The first step in fabrication of the probe is to couple the optical fiber with the LC ferrule connector (Optoequip). The LC connector then can be coupled again to the outlet of the 473 nm blue laser. The LC connector we bought is designed to work with the optical fiber with 125 μm in diameter. We use the specific fiber stripping tool for 125 μm fibers (Thorlabs) to remove about 0.5 cm of the polymer coating at one end of the optical fiber. Then the fiber is dipped in heat epoxy (Thorlabs) and then carefully inserted into the LC connector from the metal end. Tiny amount of additional heat epoxy is applied to the two ends of the LC connector to ensure a complete fill of the gap between the fiber and the connector. The entire assembly is then placed on a hot plate at 100 degree (Celsius) for 2 hours to allow the heat epoxy to cure. The epoxy should be solid after curing, tightly holding the optical fiber in place. Lastly, the optical fiber is dipped in acetone overnight; afterwards all the polymer coating is removed with cotton q-tips.

Stage II, attaching carbon fiber and encapsulation with capillary tubing

In previously reported home-made carbon fiber probes, the 7 μm carbon fiber is vacuum aspirated into glass pipettes [67], because it's too small for manual manipulation or in fact, barely visible to the naked eye. Here, we invented another approach to incorporate this tiny fiber into our optogenetic neuro-chemical probe.

Essentially, we firstly cut a small bunch of carbon fibers from its original bulk ensemble. This bunch of fibers is then glued onto a clean white paper for higher visual

contrast. Under a microscope, we wet the optical fiber (with the LC connector) with water, and then carefully approach the carbon fibers. After one of the carbon fibers is adhered to the optical fiber, we cut it from the bunch with a surgical precision blade. We would need to make sure that the carbon fiber is long enough on both ends. Afterwards, the entire optical fiber - carbon fiber assembly is threaded into capillary tubing for electric insulation and physical protection. There should be a certain length of carbon fiber protruded outside the tubing, but not the optical fiber.

Stage III, make electric connection for FSCV

The third step of neuro-chemical probe fabrication (the last image in the figure), is to make electric connection from the carbon fiber to a copper wire and connector, so that we are able to connect it to the head-stage for FSCV recording. Under microscope, the copper wire is placed against the exposed carbon fiber at the non-tip end. Silver epoxy (epotek) is applied to glue the wire and the fiber together. After 2 hours curing on a hot plate, the silver epoxy solidifies. An extra layer of protection is provided by a heat shrinking tubing (alternatively can use Torr seal, Thorlabs) on the exterior of the assembly.

Stage IV, finish and testing

Lastly, the exposed carbon fiber tip is trimmed to the desired length around 200 μm under the microscope. Then a small amount of UV epoxy is applied at the end of the capillary tubing forming a half-circle. However, extra care should be taken not to apply epoxy on the carbon fiber, because exposed carbon surface is essential to

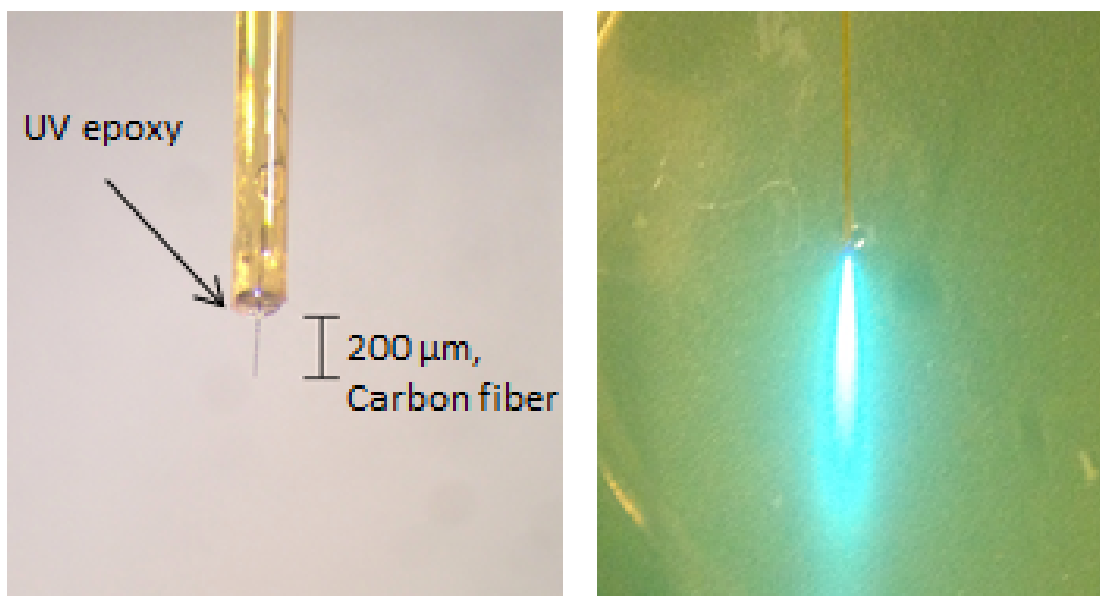


Figure 4.5: Left: view under a microscope for the detailed structure of the neurochemical probe tip. Right: In an agarose gel medium, after connecting the probe to a blue laser, light is escaping from the tip of the probe. (The light spread is different than in a real brain due to the lack of light scattering.)

dopamine sensing in FSCV. See below figure for details.

The light is confined within the optical fiber in the probe, while escaping at the probe tip, into the surrounding brain tissue. We aim at delivering optical stimulation to the neural structures immediately surrounding the exposed carbon fiber, so that more dopaminergic terminals can be activated, causing a higher extracellular dopamine efflux.

4.4 Characterizing the neuro-chemical sensing probe *in vitro* and comparison with traditional probes

4.4.1 Testing the neuro-chemical probe in dopamine standard solution

After a batch of neuro-chemical probes are fabricated, dopamine detection is tested with 1 μM dopamine standard solutions. Firstly, artificial cerebro-spinal fluid (ACSF) is prepared and separated into two identical glass dishes. One of the dish is set as the control, while the other is added with standard dopamine solution, resulting in 1 μM in concentration. The recording-ready neuro-chemical probe is initially sitting inside the control solution. FSCV recording is turned ON and kept running for 10 minutes for a stable baseline. Then the solution is manually switched to the glass dish that contain 1 μM dopamine. Background subtracted 2D FSCV color plot reveal large dopamine activity after the switch. It is further verified by the cyclic voltammogram obtained in the dopamine standard solution. A well-defined oxidation peak around + 0.6 V and a reduction peak around -0.3 V is seen on the cyclic voltammogram, indicating pure dopamine red-ox activity.

One variation of the probe is to incorporate multiple carbon fibers in one probe. Since the carbon fiber only have a diameter of 7 μM , multiple carbon fibers can easily fit into a single capillary tubing. This has both upsides and downsides in terms of the utility in dopamine detection.

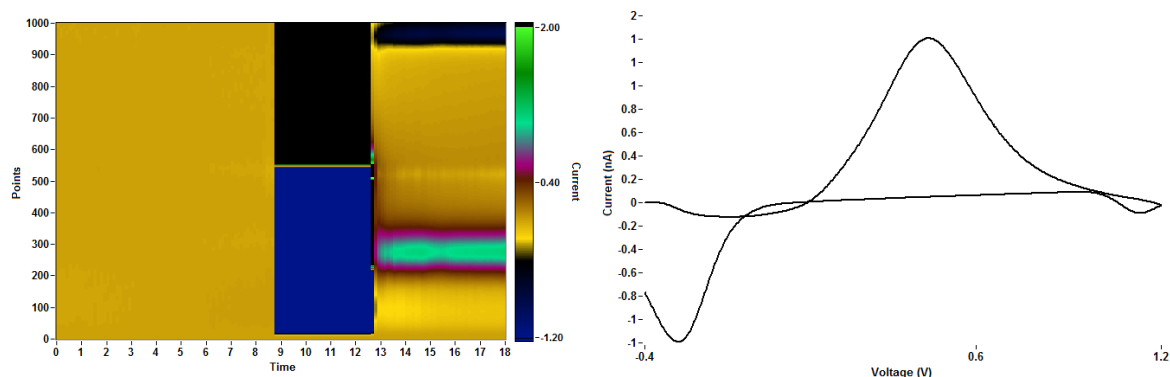


Figure 4.6: Left panel: 2D FSCV color plot, 1-8 seconds in control solution, and 13-18 seconds in 1 μ M dopamine standard solution. Right panel: the cyclic voltammogram taken in the 1 μ M dopamine standard solution.

The Benefits of multiple carbon fibers include: 1. Greatly enhanced mechanical strength. 3-4 carbon fibers bundle is much less susceptible to breaking during penetration of brain tissue. In addition, one broken carbon fiber will not forfeit the entire probe's FSCV recording capability. This increases the probe reliability for *in vivo* implantation experiments. 2. Larger surface area, potentially sensing released dopamine from a greater number of surrounding neuronal terminals.

If we record dopamine from two single carbon fibers, the oxidation peaks are slightly shifted. This also applies to a multi-carbon-fiber probe. Using more than one carbon fiber to detect from dopamine may introduce a broader oxidation peak. As shown below, the oxidation peak is much broader as if multiple peaks are combined together. This may not an issue if we are recording from a brain region where dopamine is the only dominant chemical messenger, such as NAc. However, it adds

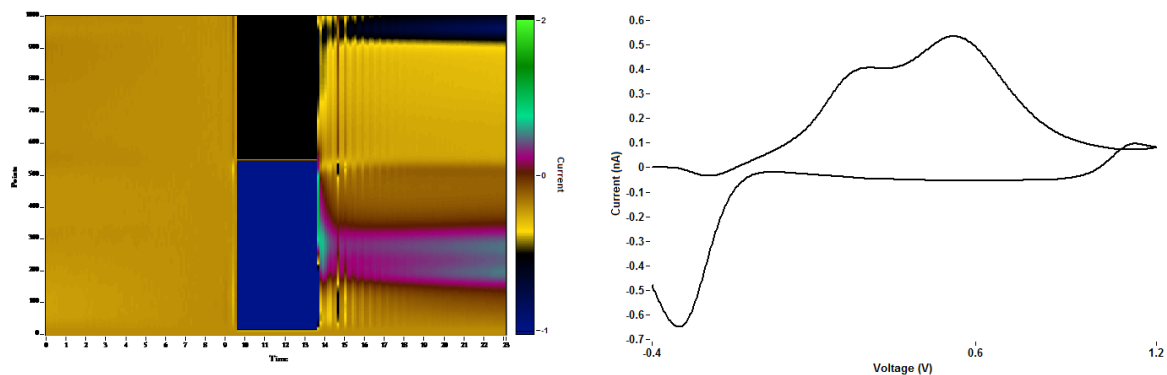


Figure 4.7: Left panel: 2D FSCV color plot, 1-9 seconds in control solution, and 14-23 seconds in 1 μM dopamine standard solution. Right panel: the cyclic voltammogram taken in the 1 μM dopamine standard solution.

difficulty to distinguish between dopamine and other chemical messengers such as serotonin, since the cyclic voltammogram profile is the primary way to differentiate between electro-chemically active molecules.

4.4.2 Testing the neuro-chemical probe in live transgenic mouse brain slices

We have extensively studied the chemical messenger dopamine release under optogenetic stimulation in brain slices in the last chapter. This neuro-chemical probe is designed for chronic, implantable, *in vivo* dopamine sensing. However, it is necessary to validate its dopamine sensing functionality in live brain slices before any surgical implantation work.

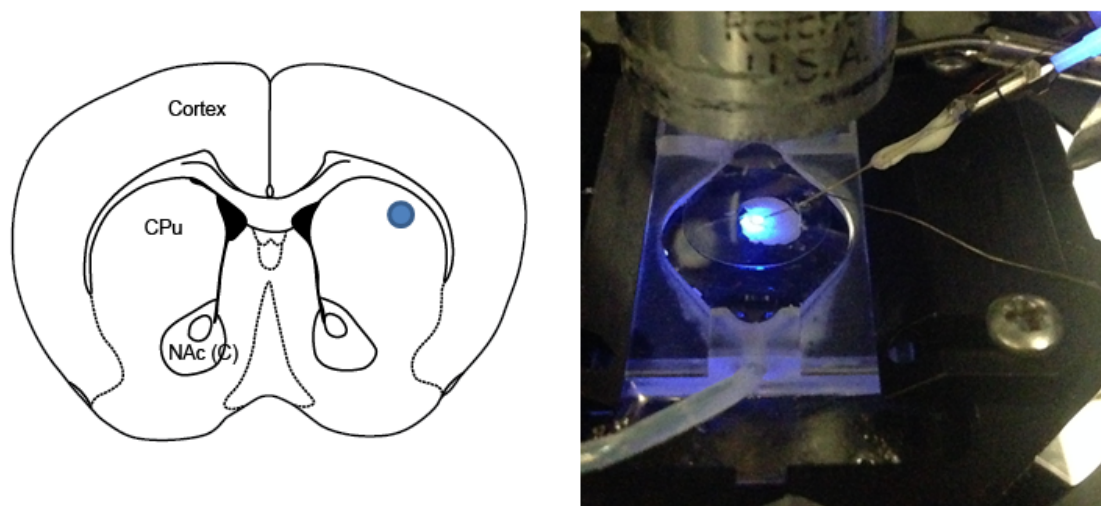


Figure 4.8: Left: region of interest for optically induced dopamine detection. Right: Photograph of the recording chamber and the probe.

The same brain slice experimental procedure was used, except that this implantable neuro-chemical probe is connected to the head-stage instead of the glass pipettes CFE. Brain slice containing the NAc and CPu area was prepared and placed in the recording chamber. The neuro-chemical probe was controlled by a micromanipulator to approach the brain tissue. The region of interest in this setting is the caudate putamen (CPu), or the dorsal striatum, which is closely related to some behavioral aspects like the motor control.

Under microscope, as shown in the figure above, the probe was inserted into the brain tissue in a zig-zag fashion, leaving most of the carbon fiber side the tissue.

Then a light stimulation is applied. However, the light was not delivered through microscope objective this time. Laser was coupled to the neuro-chemical probe at the other end, while optical stimulation was done by the light escaping from the probe tip.

The pattern of light delivery is a major factor of consideration in terms of the probe design. *In vivo* environment does not allow simple scheme of external light delivery such as through microscope objectives, because of the non-transparency of the brain. Therefore, delivering light through wave-guide optical fiber is essential for *in vivo* study. Here we tested this in a brain slice setting, using the light from optical fiber as the stimulation source.

We successfully recorded light induced transient dopamine release from the brain slices. As shown, a light pulse of 50 ms delivered through the probe evoked dopamine activity on the FSCV 2D color plot. A closer examination of the cyclic voltammogram confirms the chemical species recorded is dopamine molecules with signature oxidation peak at + 0.6 V and reduction peak at - 0.3 V.

Additionally, utilizing these probes in brain slices, we did research on the dopamine release differences in the dorsal striatum vs. the ventral striatum. The dorsal striatum is the part of striatum that is more close to the cortex, while ventral striatum is deeper in the brain, more close to NAc and other deep structures. Respectively, we placed the neuro-chemical probe in the dorsal striatum tissue and ventral striatum tissue and applied the same light stimulation of 50 ms. We observed that the dopamine

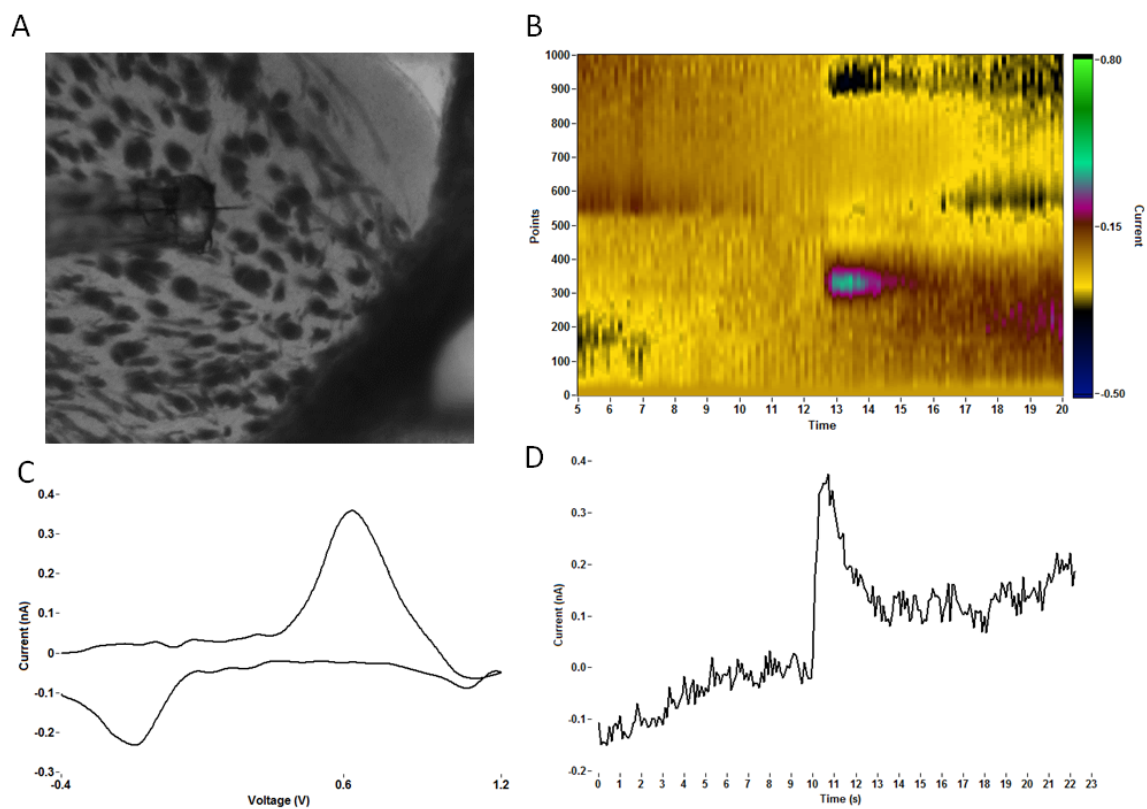


Figure 4.9: A. View from the microscope when inserting the probe tip into the dorsal striatum tissue. B. Optogenetically induced dopamine release measured by the probe. C. cyclic voltammogram validating the identity of dopamine recorded. D. calculated dopamine fluctuation according to B.

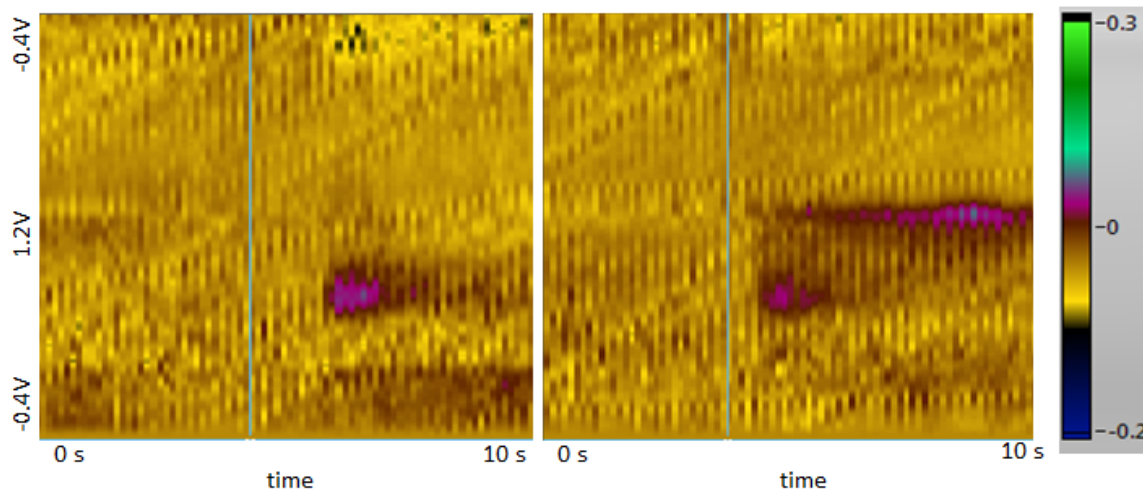


Figure 4.10: Comparison of induced dopamine in dorsal (left) and ventral (right) striatum.

response from the FSCV color plot is much smaller in the ventral striatum case. This result is consistent with previously reported electrically induced dopamine study [60]. According to this result, we decide to focus on dorsal striatum for the *in vivo* experiments.

After validation of the dopamine sensing capability of this chronic implantable probe in brain slices, we were ready to move on to *in vivo* recording in live animals.

4.5 Improvements made for adaptation of the chronic implantation environment

The existing design is functioning properly in a brain slice setting. We decide to make a few improvements for the purpose of enhancing surgical implantation compatibility.

A. Adapting the length of the neuro-chemical probe for suitability of mouse model.

Due to the small size of our animal model, we decide to use a shorter shank length in the probe. The distance from the surface of mouse skull to the dorsal striatum is around 2 mm in total, depending on the age of the mouse. We therefore aimed to make the shank (the capillary tubing part of the probe) with a length of 0.5 cm. Effectively reducing the total length of the probe is important in the survival of the probe after implantation, since the protruded probe can hit cage walls repetitively as the animal is living with the implantation in a long term.

B. Implantation of the reference wire.

Just as *in vitro* FSCV experiments, an Ag/AgCl reference wire is always needed to do the electro-chemistry properly. This reference wire needs to sit in the same conductive medium as the recording probe, which is the brain itself. After craniotomy, if we implant the reference wire in the same open skull region, it would be physically too close to the working electrode. This may cause problems such as short circuits etc. Therefore, we have to individually implant the reference wire at the contralateral side of the brain, which requires another craniotomy. Although this adds to the complexity of the surgical procedure, but it is definitely necessary.

C. Mechanical protection of the implanted assembly.

A temporary implantation does not require any extra protection methods. However, in this situation we are considering a chronic implantable situation, where the

probe may need to be functioning in the brain for weeks, even months in a live animal. Mice are active and constantly in physical interaction with the environment. In any chronic implantation, it has been important to protect the implanted assembly, including the probe, connectors and the reference wire mechanically. We use a plastic tube of 1 cm in diameter as a protection of the implanted assembly. This plastic tube is fixed on the animal's head by meta-bond dental acrylic. This method has been proven working properly to protect the implantation as mentioned in the next chapter.

4.6 Conclusions

In summary, here we report the development of a novel device with capabilities of local light delivery and dopamine sensing *in vivo*. This probe is designed to be chronic implanted in free moving animals. In this chapter we have shown the dopamine sensing capability of this probe in brain slices in the striatum area. We are going to use the probe for real *in vivo* applications in the next chapter. The detailed fabrication procedure is described for this probe, as well as the detailed rationales in the design process. Its two-way characteristic – both stimulating and recording from the neurotransmitters in the brain, make it a valuable tool in studying the optogenetically induced dopamine release in deep brain regions. Furthermore, its chronic implantation compatibility opens the opportunity of research in freely moving, behaving

animals, contributing to the effort of understanding the neurotransmitter's significant functional roles in various animal behaviors such as reward-seeking, reinforcement learning, depression etc.

Chapter 5

**In vivo real-time electro-chemical
sensing of dopamine activity in
transgenic mice**

5.1 Experiment protocols of FSCV recording in live transgenic mouse

The development of the chronic implantable neuro-chemical probe described in the last chapter opens up the opportunity for us to monitor dopamine in a live transgenic mouse. The motivation of the *in vivo* experiments has been discussed in more detail in Chapter 4.1. Here we mainly introduce the specific methodology and protocols in these experiments.

Firstly, the chronic implantable neuro-chemical probes are tested for FSCV and calibrated in dopamine standard solution to understand their electro-chemistry sensitivity to dopamine. These probes are the ones already adapted the changes describe above for the ease of surgical implantation. At least 5 working implantable probes must be kept in reserve for any *in vivo* session because the experiment has to be finished in the same day. The FSCV instrumentation used are the same as in brain slices recordings.

Secondly, the animals will be prepared for the experiments by mounting a head plate on top of their skull. We used surgical procedures from other rodent experiments [35]. Basically, the animal is initially anesthetized with ketamine/xylazine prepared according to the ACF guidelines. The animal is then head fixed on a rodent surgical setup and being cleaned with Povidone-iodine (Betadine) to prevent potential infection. The skin at the top of the skull is opened to reveal the skull

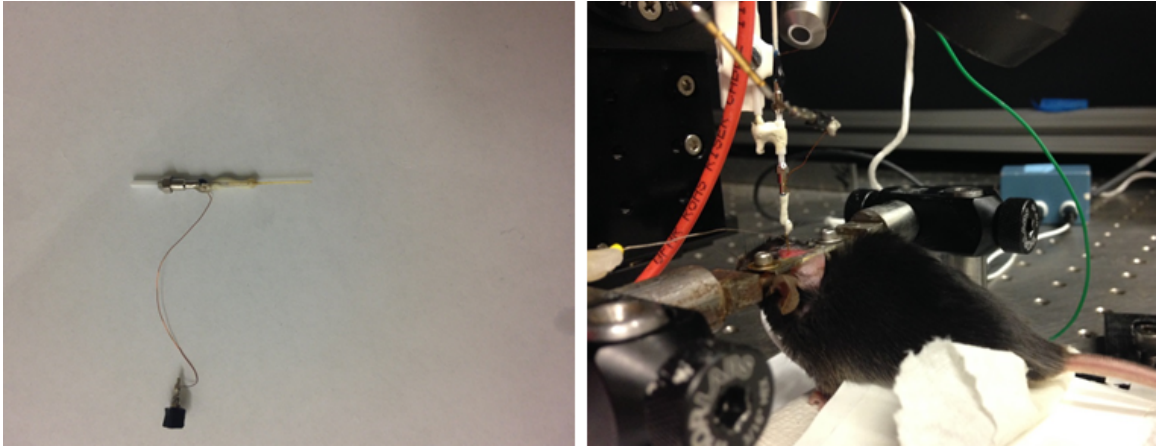


Figure 5.1: The probe and head-fixed *in vivo* experiment configuration.

surface. To ensure the neuro-chemical probe can reach the dorsal striatal area of the brain, the geometric signature bregma on the skull should be at the center of the open area. A commercial mouse head plate is held above the exposed skull and adjusted / measured to be precisely horizontal. Then dental cement Metabond (Parkell, inc.) is prepared and applied around the head plate. The Metabond should glue the head plate to the exposed skull but not the skin. Continue to apply Metabond until the head plate is securely fixed to the skull, but do not spill Metabond to the bregma area of the skull (center of the head plate opening). After the Metabond is solid enough, remove the head fix assembly to release the animal. Wait until the animal is fully awake before proceeding to next steps. Other detailed procedure please see similar protocols published [51] for any head fixed mouse experiments. The head-plate mounted animal is fixed to head plate holders during anesthesia as shown in figure 5.1.

Next, craniotomy must be performed to create openings on the skull for both neuro-chemical probe and reference wire to reach the brain. According the mouse brain atlas, dorsal striatum is a relatively large area on both sides. We typically use surgical drill to create an opening at 0.5 mm anterior to bregma, 2 mm lateral which is right above the dorsal striatum. Another craniotomy is made at the contralateral side of the brain at any location convenient, for the insertion of a Ag/AgCl reference wire.

After craniotomy, the skull is cleaned with saline to reveal the two openings for insertion. FSCV instruments are turned ON. The probe is again controlled by a micro-manipulator(Sutter Instruments, Inc.) as in brain slice experiments, except that here we need to ensure the probe is perpendicular to the horizontal line or rather, the head plate. The neuro-chemical probe is carefully lowered and inserted into the brain tissue while watching for FSCV response. The scale of cyclic voltammogram should not suddenly change by magnitudes (indicating the carbon fiber breaks). Meanwhile the reference wire is placed in the other hole on the skull in contact of the tissue. Figure 5.2 shows both the probe and the reference wire in place for an *in vivo* experiment.

The FSCV recording can now be performed under any condition such as optogenetic stimulation sessions. The depth of the probe is controlled by the micro-manipulator and should be recorded along side the FSCV signals. The probe can be carefully lowered in the targeted dorsal striatum region of the brain where endogenous dopamine can be measured and light stimulation can be performed. Detailed FSCV

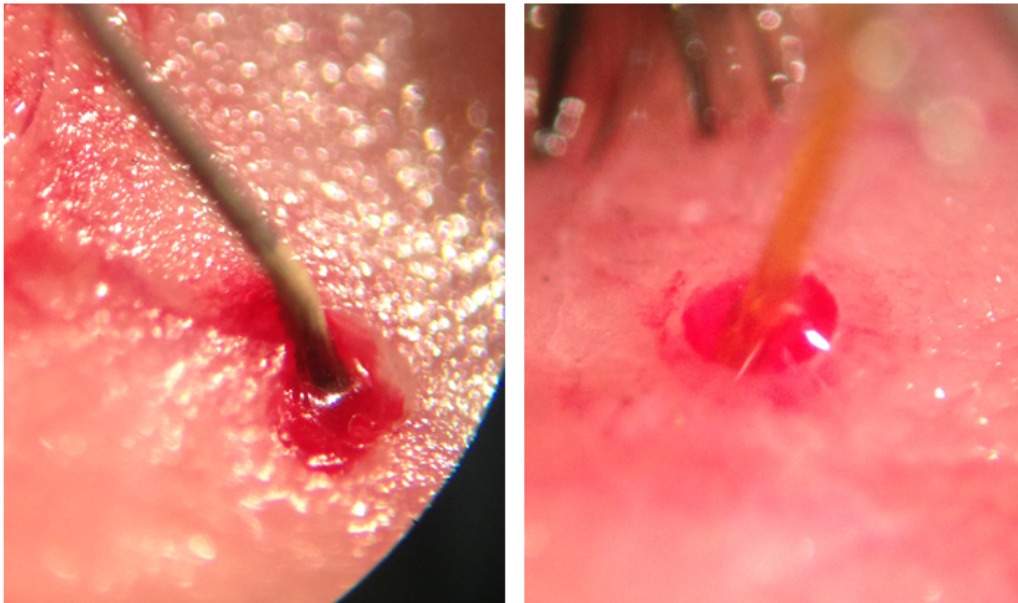


Figure 5.2: Reference wire and the neuro-chemical probe inserted in brain tissue at two locations on the skull.

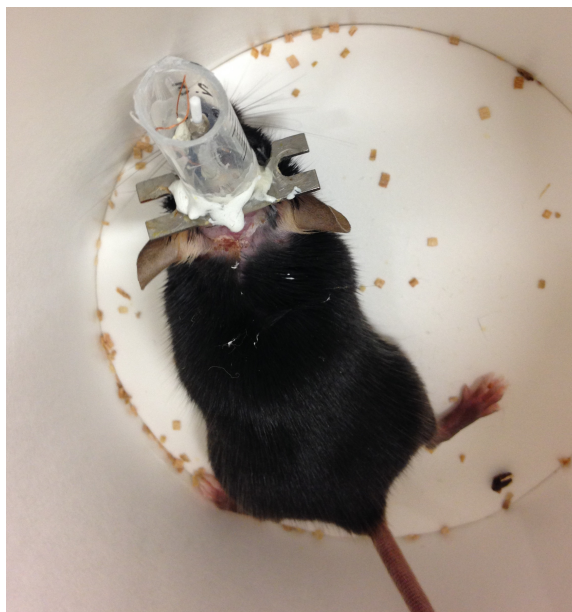


Figure 5.3: A view of the chronically implanted assembly.

results are presented later in this chapter.

It is convenient to perform FSCV recording in a head fixed configuration without implanting the probe. If a chronic experiment is desired, implantation of the neurochemical probe can be done at this stage. Once the probe is situated at an appropriate location in the dorsal striatum where dopamine activity can be evoked by light stimulation, the exposed skull and craniotomy can be closed by excessive Metabond application. Apart from closing the craniotomy, when applying the Metabond, care should also be taken to fix the neuro-chemical probe shank and the reference wire firmly on top of the skull. Continue to apply Metabond until it covers the entire exposed skull and the base of the probe/reference wire.

Finally, for physical protection against bumping into cage wall and ceiling when

the animal is awake, an extra plastic tubing should be fixed around the implanted probe/wire as shown in figure 5.3. The entire assembly is light weight so that the mouse can move around freely in the cage without any difficulties.

For chronic experiments, the neuro-chemical probe is kept implanted in the brain for up to 4 weeks. We did not observe obvious degradation or changes in this time scale, possibly due to the chemical inertness of the carbon electrode material. Carbon fiber has a structure similar to graphite, which is inert to almost all chemicals. And carbon have been a material of choice to manufacture heat and chemical resistant containers or use as a refractory material. The benign chemical environment in the brain tissue is unlikely to cause any change to the carbon fiber electrode [18]. Therefore, theoretically our carbon based electrode can survive as long as the life span of a mouse. There are nevertheless other practical factors in consideration, such as potential infection at the implantation, the health condition of the animal etc, but is rather generic for any surgical implantation. Furthermore, considering the normal length of mouse *in vivo* experiments, even if some form of behavior study, usually ranges from days to weeks. The long term stability of the implantable probe we developed is sufficient for the research purpose of mouse neuro-chemical dynamics in optogenetic or behavior contexts.

5.2 Detecting endogenous dopamine in the dorsal striatum

5.2.1 In vivo FSCV Background activity in a passive state

It is known that large concentration of chemical messenger dopamine mainly reside within a few specific regions of the brain, among them is the dorsal striatum. To investigate the endogenous dopamine in this area, we have performed FSCV recordings through our implantable probe.

In figure 5.4 we show two examples of the FSCV 2D color plot from both the cortex area of the brain and the dorsal striatum. Cortex is from 0 - 1.6 mm deep into the brain and do not possess massive dopaminergic projections. The 2D color plot in the cortex (372 μm) did not present any activity pattern except for noise background. We next carefully lower the probe further more down into the dorsal striatum (2457 μm), and start the FSCV recording again. From the lower panel, we see the 2D color plot present some subtle activity: positive current around + 0.6 V (points 300 in y-axis) and some negative current around - 0.3 V (points 950 in y-axis). These activity corresponds to the electro-chemical response of dopamine at carbon fiber electrodes, but the amplitude is rather small. This is because the animal was in a quite state when endogenous dopamine fluctuation is subtle.

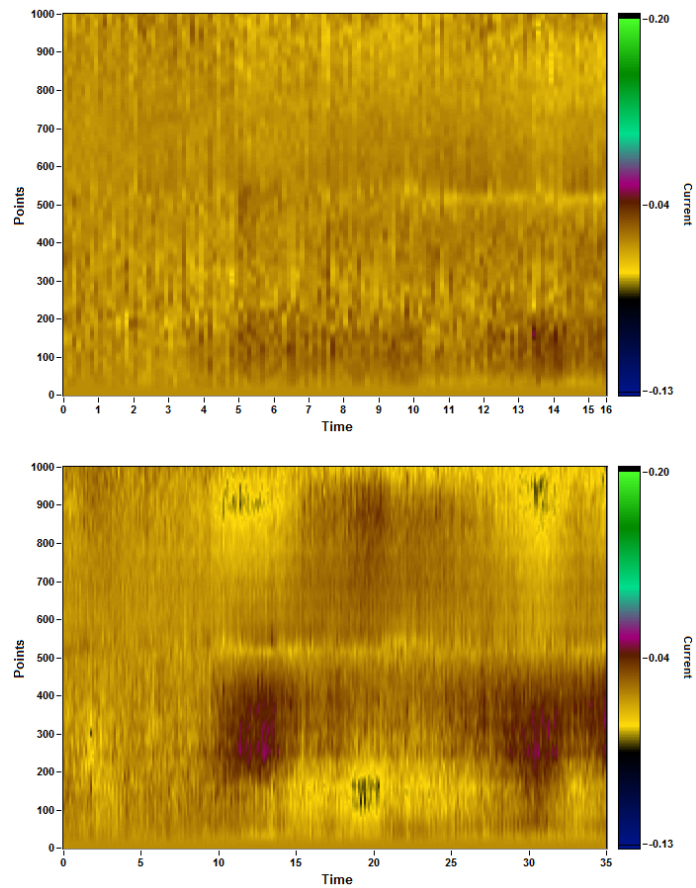


Figure 5.4: Upper panel: 2D color plot at the depth of $372 \mu\text{m}$ from the surface of the brain. Lower panel: same plot at $2457 \mu\text{m}$ depth, in the dorsal striatum area.

5.2.2 Measuring dopamine through adsorption in dorsal striatum

Note that the FSCV is a relative recording technique, it is background subtracted with respect to a control - often the start of the recording. This means we are actually measuring only the changes in dopamine concentration. Therefore, also the dopamine baseline level could be high in the dorsal striatum area, the endogenous fluctuations can be small in a passive state. Before we move on to stimulate the dopamine release with optogenetics or perform any behavioral experiments, it would be necessary to validate that the probe is situated in a region where baseline endogenous dopamine present. We use two distinct experimental ways to validate the presence of endogenous dopamine in the dorsal striatum.

Recall that the FSCV command potential have two components: a holding potential at -0.4 V and scanning potential from -0.4 V to $+1.2$ V back to -0.4 V. The holding potential is constantly on, and during FSCV scans last for 92 ms out of the 100 ms of a voltammetry cycle. The purpose of this long holding potential is to promote dopamine adsorption at the carbon electrode surface. This adsorption behavior is one of the major reasons to utilize carbon as the material of choice to monitor dopamine activity. Here we run the experiments in a different way so that adsorption of the dopamine can be observed. Before a recording session, firstly the working electrode potential is kept at 0 V for 3-5 minutes, the adsorption of dopamine is limited at this stage.

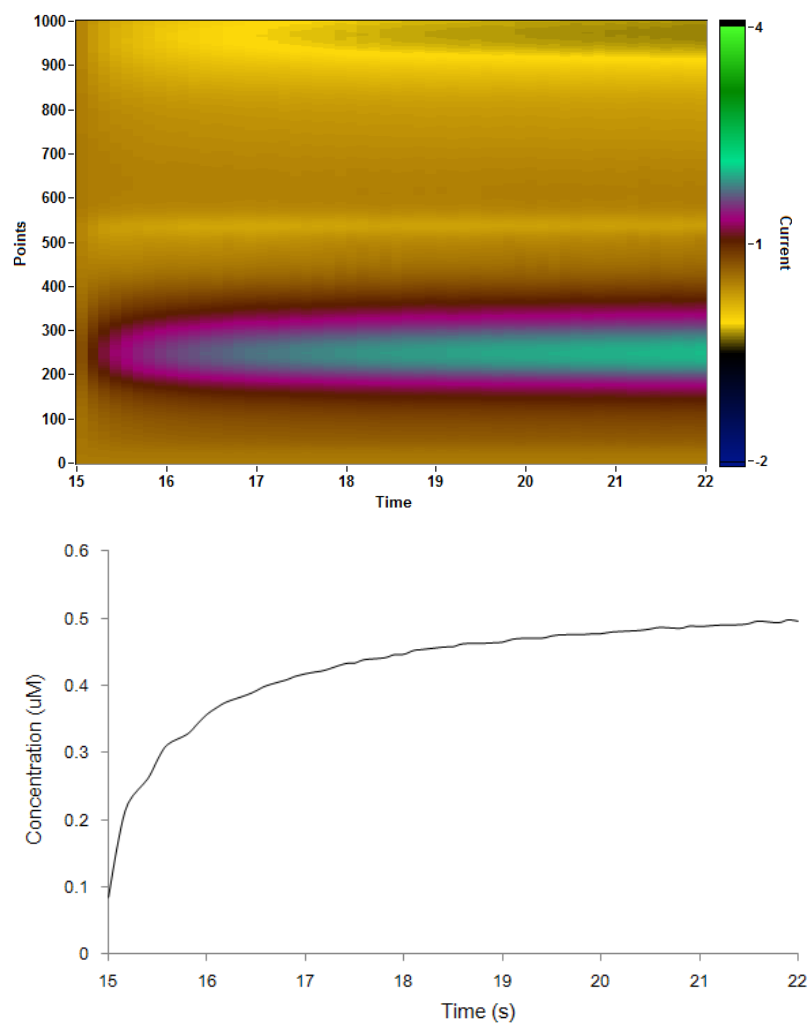


Figure 5.5: FSCV recording started the same time as the holding potential is turned ON, demonstrating the real-time adsorption of dopamine on the working electrode. This also validates the existence of basal dopamine in the dorsal striatum

Then the - 0.4 V holding potential is turned ON at the same time FSCV recording starts. The adsorption of dopamine is encouraged from this time point. As can be observed from Figure 5.5, obvious dopamine signature oxidation current and reduction current appears soon from the start of the recording, and the amplitude of these currents continuously grow in time. From the converted dopamine concentration plot, we can see that the increase due to adsorption of dopamine is nonlinear, similar to a logarithmic shape. Kinetics of the adsorption behavior of dopamine at carbon electrode surface have been studied [8], but is not within the scope of this thesis.

5.2.3 Differences of dopamine concentrations in dorsal striatum and the cortex

The above section proved the capability of the implantable probe to measure endogenous dopamine. To show the regional differences of the dorsal striatum and the cortex, we did continuous FSCV recording sessions while moving the probe with a micro-manipulator in live transgenic mouse brain. Because when lowering the probe, the motion has to be kept very subtle to minimize mechanical stress on the 7 μm diameter carbon fiber, the comparison of dopamine difference cannot be down in this procedure. However, when retracting the probe from dorsal striatum back into the cortex, movement can be relatively fast, making it possible to watch the dopamine response with FSCV recording, and understand the differences between the two regions.

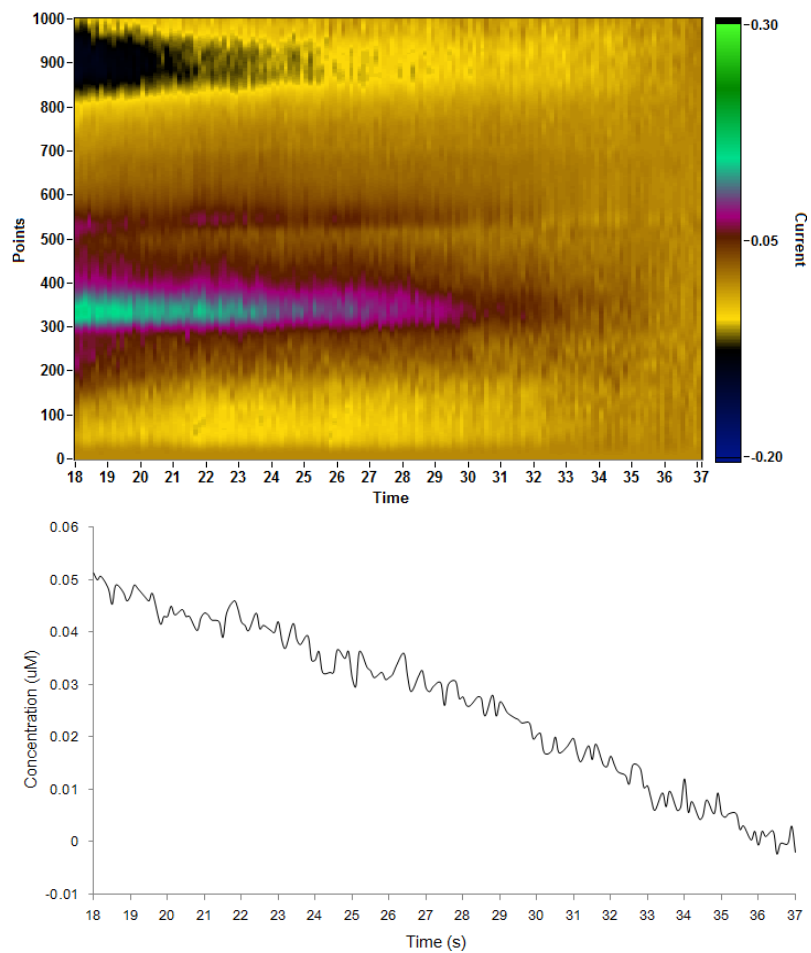


Figure 5.6: FSCV signals as the probe is retracted from dorsal striatum back into the cortex, showing decreased dopamine signal.

To perform this experiment, we firstly kept the neuro-chemical probe at the depth around 2500 μm from the surface of the brain, i.e. in the dorsal striatum. The FSCV recording is turned ON. Then in the fine motion mode of the micro-manipulator we moved the probe up at a speed of roughly 100 μm per second, until the depth reading is 500 μm from the brain surface where probe was in the cortex. As shown in Figure 5.6, we took the end of the recording as the background for FSCV. Dopamine oxidation and reduction current can be observed at the beginning of the recording, and steadily decreased over tens of seconds time as the probe was raised into the cortex. Note that at the end of the FSCV recording, dopamine red-ox currents cannot be seen, but does not mean there's no dopamine present. Since we set the end of the experiment as the background level, the background subtracted color plot certainly shows no activity at the end. What can be observed is a concentration difference of dopamine as the probe went from striatum to cortex. In fact, dopamine also present in the cortex, especially the medial forebrain cortex [1], but often at a lower level than in NAc and striatum.

In sum, the observation of dopamine concentration gradient validates probe's locations in the brain, also demonstrates its capability of detecting baseline dopamine concentration changes. While measuring the adsorption of dopamine potentially provide us with some information of absolute value of dopamine baseline concentration in the dorsal striatum, since the adsorption amount could be proportional to the absolute amount of extracellular dopamine.

5.3 Optogenetically induced *in vivo* dopamine activity

The brain in an live animal is an intact, closed system that is not by nature affected by external artificial inputs. It has been a major goal to understand and potentially perturb this closed system in the neuroscience research. Here in this work, we don't interact directly through neuronal spiking and electric potentials with the intact brain, but we use external stimulations to make the neurons release more neurotransmitter dopamine.

In this section, we demonstrate the optogenetically induced dopamine activity through these two-way neuro-chemical probes. The FSCV recording from figure 5.7 is from an animal chronically implanted with a neuro-chemical probe in the dorsal striatum. During the recording experiment, the animal was brought to a cage around the FSCV instruments and directly connected to the setup, including the 473 nm blue laser. The laser was controlled by analog input device, and an 6 seconds long optical stimulation train consisting of 10 ms light pulses applied at 16 Hz is delivered into the brain. The stimulation started at 40 s in the figure. One can observed an obvious elevated dopamine oxidation and reduction current from 40 s to 46 s. The converted dopamine concentration plot shows the same trend. It also appears that the dopamine activity has a tail that gradually diminishes in tens of seconds. Therefore, an optical stimulation train delivered through our novel two-way probe successfully

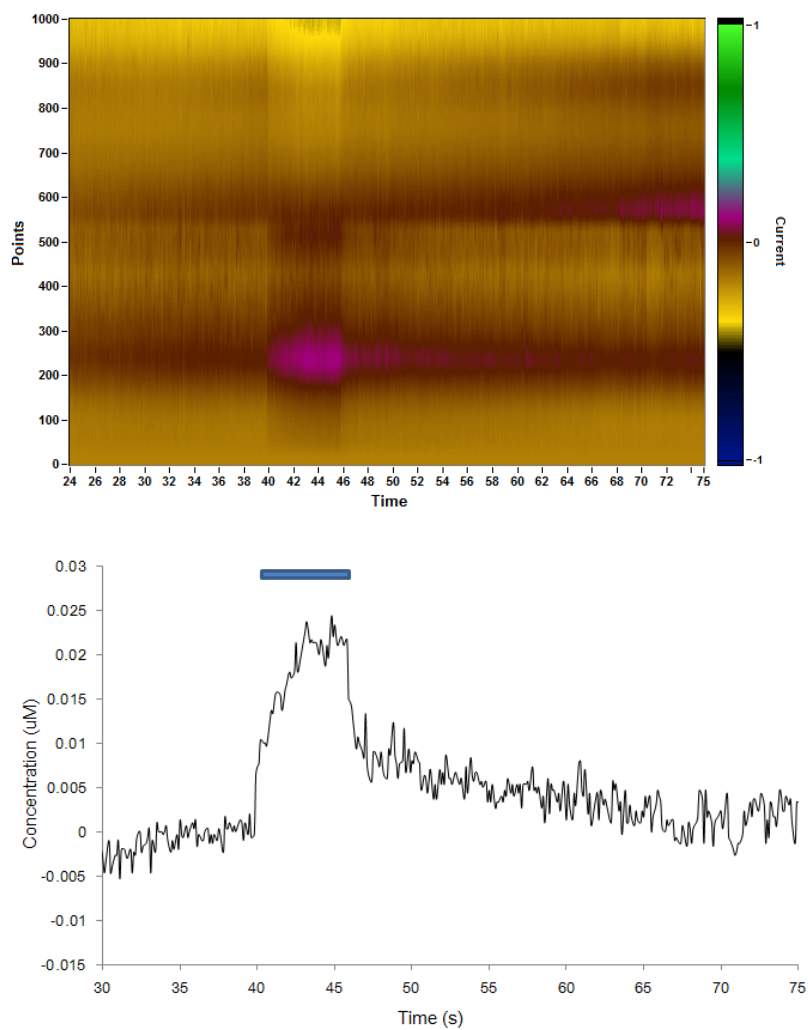


Figure 5.7: Upper panel: FSCV 2D plot. Lower panel: calculated dopamine concentration.

elevated extracellular dopamine concentration in the intact brain while the animal is alive, while simultaneously record such activity.

The importance of using external stimulations to induce dopamine release in a live animal is that it serves as a method of 'write-in' to the closed neuronal circuits. In this case, by 'writing-in' dopamine signals, animal's behavior can be potentially influenced by researchers. For example, artificially induced dopamine release in the NAc can work as a virtual reward signal. It's possible to influence the animal to develop different preferences in places or foods depending on their association with external stimulation.

5.4 Dopamine activity in an environment with external physical-stress induction

In addition to optogenetically induced dopamine activity in an live animal, we also performed proof-of-concept behavior related study of dopamine activity to demonstrate the utility of this chronic implantable neuro-chemical probe. Specifically, we created an physical stress environment and watch for changes in endogenous dopamine activity.

We induce physical stress by the tail pinch method, which is adapted in previous publications related to stress research. The animal is firstly moved to recording chamber and connected with FSCV instrumentation. We also fix the head plate to

the holder to limit animal's movement since tail pinch can cause animal's physical reaction. Because the potential adaptation effect of any stress experiments, the tail pinch is performed at the beginning of each day's FSCV recording session, well before any optogenetic stimulation and other experiments. After FSCV baseline is stable, recording starts and tail pinches lasting for 6 s are suddenly applied to the tail of the mouse.

As in Figure 5.8, from the FSCV signals, tail pinch started a train of activity. The red-ox currents during the activity appear at the usual locations for dopamine signals. The episodically nature of recorded signals indicates the neuro-chemical fluctuation is more complex in a live and awake animal. This is possibly resulting from varies simultaneous neuronal activity in the dorsal striatum. Note that dorsal striatum receives massive neuronal projections from the mid-brain area such as the substantia nigra. It also have numerous connections to the neurons in the cortex, which are actively coordinating motor behaviors. These inter-connected neural circuits create sophisticated neuro-chemical responses especially in an awake animal, and even more if under artificially induced physical stressful situation.

In the potential future work, to understand more of the detailed mechanism of these complex neuro-chemical response *in vivo* in a physically stressed animal, additional advanced electro-physiology recording study is required. Single neuron spiking activity and local field potentials at the location of FSCV recording should be recorded. Then we can put together the electro-physiology signal and FSCV signal

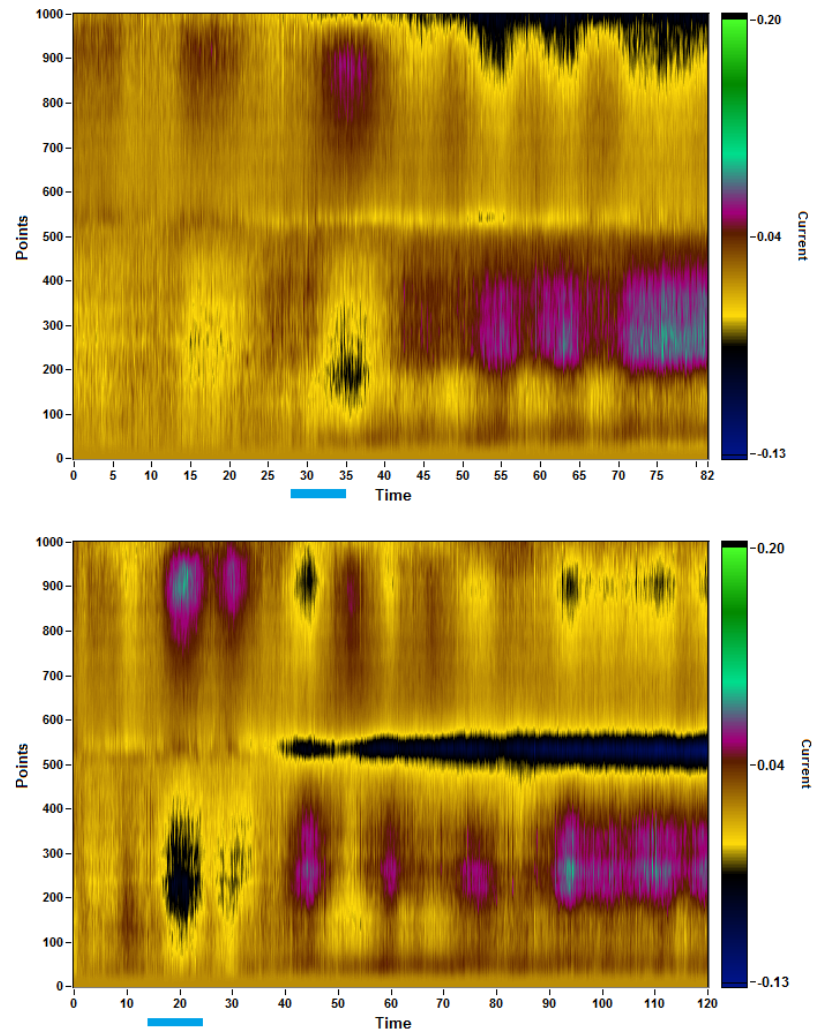


Figure 5.8: Tail pinch stress applied as indicated by the blue stripe. Activities observed following the stress induction.

to reveal the correlations between the two, so that research questions such as if an increased neuronal spiking rate causes fluctuation in extracellular dopamine concentration, or if the beta-band activity in striatum correlates with dopamine.

5.5 Conclusions

In summary, we successfully designed and deployed a chronic implantable neurochemical probe that is capable of delivering light stimulation and recording FSCV signals simultaneously. The endogenous dorsal striatal dopamine has been investigated and compared to the cortex. Optogenetic stimulation delivered directly through the optical fiber in this implanted probe can effectively induce elevated dopamine concentration in live transgenic mice through cell-type specific excitation. While the probe is also capable of monitoring complex real-time neuro-chemical patterns in animals under physical stress. In general, our novel electro-chemical tool and the *in vivo* optogenetic experiment framework opens up opportunities of interrogating neurotransmitter dynamics in the intact brain of behaving animals.

Chapter 6

Discussion and conclusions

In this thesis, we covered a few closely related topics, leading to a detailed electrochemical study of neuro-chemical dynamics in live brain tissue. Both the sliced and intact transgenic mouse brain was used as the experimental subject, while utilizing optogenetic tools to selectively stimulate a single type of cells - dopaminergic neurons. We successfully evoked physiological dopamine concentration fluctuation in various conditions. The development of a chronic implantable neuro-chemical probe that is capable of delivering light stimulation enables us to chronically monitor the neuro-chemical concentration in real time in live, behaving animals.

To be in more detail, the transgenic animal model we used in this work is unique. It was developed so that ChR2 is expressed by specifically targeting dopaminergic neurons through dopamine transporter - Cre recombinase. By optogenetic stimulation of the tissue in forebrain area such as the NAc and dorsal striatum, dopaminergic cell terminals were directly excited through the opsin, inducing a transient high concentration of dopamine (can be up to 700 nM in a slice). This optically induced dopamine release events had features similar to those induced by electrical pulses, i.e. oxidation current at 0.6 V in the cyclic voltammogram, similar peak concentration levels, and similar time profiles of release and uptake. We found optogenetically induced terminal dopamine release in this transgenic animal model appears to be very effective and controllable. In a brain slice, the light power required to induce measurable dopamine release is remarkably low at 0.09 mW/mm². This light power is much lower than typical values used in the literature across *in vitro* and *in vivo* mammalian

studies (10 mW/mm² [68], 3-255 mW/mm² [23]). We demonstrated that optogenetics has the capability to scale dopamine levels readily by varying the light power, pulse width, and shape of waveforms, which is helpful in mimicking the dopamine release level that occurs in natural behaviors where the dopamine concentration is smaller and more variable than those elicited by electrical stimulation [18].

6.1 Light stimulation modulated dopamine release

Across Chapter 3 we demonstrated optical modulation of extracellular dopamine levels. We experimented systematically with numerous stimulation parameters in the brain slices. The reason for this controllable dopamine release level with optogenetics is related to the characteristics of the light gated ion channel ChR2. With increasing light power delivered, the number of photons incident on an individual ChR2 protein per second increases linearly [34]. Assuming a constant channel open probability in one 'hit', more opsin molecules will be activated at the dopamine neuron terminals under higher light power. This results in action potential generation or membrane depolarization leading to increased recruitment of dopamine axons and terminals.

In the case of our optical 'ramp' experiment, adding a ramp as a leading edge to an otherwise square pulse dramatically decreases the level of dopamine release. During the ramp, due to gradually increasing photon density, the opsins on dopamine terminals will be activated at statistically varying times instead of being activated

simultaneously as when subjected to a square pulse. By contrast, a 'non-ramp' simple square pulse turns on a high photon density abruptly leading to synchronized excitation of a large number of opsins, which causes more dopamine axons to be recruited and therefore higher dopamine release. A previous study also showed how bursting-style electrical stimulation at the median forebrain bundle evoked far greater dopamine efflux than temporally equally spaced stimulation [32]. We therefore speculate that the following is likely a general property of terminal dopaminergic response: more synchronized excitations, either through opsins or midbrain synaptic inputs, will result in higher dopamine release. This also suggests that lower physiological dopamine levels may not necessarily result from damage of dopamine neurons, but can be also due to loss of input synchrony. Future intracellular current validation experiments can serve to confirm this speculation.

6.2 Specificity of neuro-chemicals

Electro-chemistry techniques such as cyclic voltammetry provide very rich information about the redox reaction process of electro-active molecules at the carbon electrode surface. This information includes the position of the oxidation current peak, position of the reduction current peak, width and amplitude of the redox peaks, and the ratio of the reduction peak to oxidation peak. Different electro-active chemical species can be distinguished based on these features. In particular, in fast-scan cyclic voltammetry the high chemical specificity is able to distinguish dopamine, serotonin, and ascorbic

acid. Phillips et al. in 2003 [56] demonstrated that for FSCV, the only chemical species cannot be separated from dopamine is norepinephrine which fortunately barely present in NAc and striatum. For ascorbic acid in particular, the oxidation compound - dehydroascorbic acid is not stable enough to generate a reduction peak under FSCV, therefore causing a reduction-to-oxidation peak amplitude ratio around zero [56]. In addition, under fast scan CV, the oxidation current of ascorbic acid ranges across a wide range of the potential; Robinson et al. in 2003 [61] have demonstrated the voltammetry response of ascorbic acid, dopamine, serotonin etc (Fig 4), and have shown the distinct features of these chemicals.

Our optogenetics construct provide an unique advantage in eliciting a single type of neurotransmitters. Due to the cell-type specificity, only the dopamine neuron terminals are excited through membrane protein response to light stimulation. In our brain slice study, the dopamine neuron cell bodies do not present in the same slice as the their projection terminals. Therefore the stimulated dopamine release we observed in nucleus accumbens is an isolated effect, where only the cell terminals (containing dopamine vesicles) are subject to membrane potential activation. In this way, light interact with minimal local cellular structures.

As for most of the non-neurotransmitter chemicals in the brain, they have a much longer time scale in terms of extracellular concentration fluctuations. Our observed light induced dopamine release events are in time scale of a maximum of 2s. While

non-neurotransmitter chemicals do not fluctuate in this time scale, so that background subtraction in FSCV successfully removed non-neurotransmitter chemical interference. Ascorbic acid concentration in the brain is typically stable; in a study where researchers use pharmacology methods to induce a change in the ascorbic acid concentration [14], the concentration change lasts for around 90 s. This demonstrates the slow speed of non-neurotransmitter activity in the brain tissue.

6.3 In vivo dopamine activity

The dopamine dynamics observed in the intact brain appear to be different than the response in brain slices. Background activity can be seen in the FSCV color plot in the dorsal striatum of an live animal even if there is no external stimulation, by light or physical stimulation, exists. This is likely a result of the endogenous neuronal activity in the intact brain. More specifically, neuronal connections from the dorsal striatum or NAc to the midbrain regions such as SNc and VTA, as well as to the cortex. Therefore, understands the dopamine response *in vivo* can be more difficult. Nevertheless, we observed stable optogenetically evoked dopamine concentration change from our chronically implanted neuro-chemical probe. We hope to utilize this novel probe to monitor more of the dopamine activity in real-time in freely behaving animals at varies behavioral and physiology conditions. One potential interesting research topic is to monitor the development of the dopamine deficits in Parkinsonian disease conditions, which is known to cause degeneration in dopaminergic projections

in the striatum area. Furthermore, combining our novel neuro-chemical sensing probe with other electrophysiology and pharmacology tools can be very powerful in some specific research areas.

The electro-chemical neurotransmitter research, in general, is still a burgeoning area of neuroscience. Many questions remain unanswered at this stage. I believe the development of novel electro-chemical techniques and tools can greatly catalyze the research in this field. While the investigation conducted in this thesis focuses on several specific scientific research questions, it is nevertheless a stepping stone towards understanding the complex intricacies of the brain. The detailed understanding of the neurotransmitters through electro-chemistry will eventually contribute to the big picture of understanding the entire sophisticated electrical and chemical system of the human brain.

Appendix A

Investigating induced brain rhythms through optogenetics

In this appendix, we demonstrate the observation of interesting brain rhythms induced by optogenetic stimulation and recorded by intracortical multichannel electrophysiology techniques. These brain rhythms are in the gamma range (40 - 80 Hz) and travel in the primate neo-cortex as spatiotemporal waves. Targeted brain tissue was transduced by viral injection with the red-shifted opsin C1V1(T/T). Constant (1-s square pulses) and ramp light stimulations induced narrowband gamma oscillations even beyond the light stimulation volume, via network interactions. Despite stimulation-related modulation in spiking rates, neuronal spiking remained highly asynchronous during induced gamma oscillations. This work provides an important demonstration for probing spatiotemporal dynamics in the intact brain during various physiological and behavioral conditions.

A.1 Background on brain’s gamma oscillations

In neural computation and in cortical neuron communications, spatiotemporal gamma oscillations are hypothesized to play important roles [33]. In addition, disruption of these spatiotemporal oscillations may play a role in neurological and neuropsychiatric disorders. Recent studies have used optogenetic stimulation to probe the mechanisms and neural circuits underlying the generation of gamma oscillations in neocortex [15]. In particular, mouse models have been used to demonstrate the generation of gamma oscillations in the somatosensory cortex, by activation of either fast-spiking interneurons [16] or layer 2-3 pyramidal cells with continuously incrementing light stimuli

[3]. Despite these advances, most optogenetic studies have focused on rodent models and little is known about the generation of transient gamma oscillations in primate neocortex. In addition, rather than utilizing micro-electrode arrays to cover an area over extended cortical regions, most previous studies have been focused on independent electrode recordings of a few neurons and LFPs around the optical stimulus sites thereby limiting the assessment of the spatiotemporal features of transient gamma oscillations, especially regarding their propagation as cortical waves and the roles of network activity through cortical circuits.

In this chapter, we studied how transient gamma oscillation spatiotemporal patterns can be generated in primate large-scale neocortical networks, using a novel technique to record neuronal ensembles spiking activity and high-density LFPs during simultaneous optogenetic stimulation [76]. Specifically, the new probe used a microelectrode array for ensemble recordings, integrated with a plastic optical fiber (POF) in the center, whose flexibility was critical for chronic implantation into the primate brain. We expressed the red-shifted opsin C1V1(T/T) under the control of the CaMKII promoter in either primary motor cortex (MI) or ventral premotor cortex (PMv) in two macaque monkeys. Under two time profiles of optical stimulation (constant and ramp) during subjects' awake resting states, we investigated the generation of transient gamma oscillations both within the direct light stimulated area, and outside the area via network interaction. Our findings showed that these oscillations were induced above a critical excitation threshold, while spiking activity remained

mostly asynchronous, despite the induced narrowband gamma oscillations. These optically induced gamma oscillations tended to propagate in stereotypical spatiotemporal patterns consisting mostly of concentric expanding waves as demonstrated by vector field (optical flow) and time delay analyses.

A.2 Experimental methods

1. Viral injections and array implantation

Polymer optical fiber microelectrode array (POF-MEA) was fabricated with a 4 X 4 mm microelectrode array (Blackrock Microsystems, UT) with 96 silicon-based electrodes and a polymer optical fiber using methods described in our previous work [76]. Two macaque monkeys (subject T, 6kg and subject P, 7kg) were chronically implanted with POF-MEA arrays in the motor cortex in MI hand area (subject T) and in PMv (subject P), respectively. Injections of the viral vector (AAV5-CaMKII-C1V1(T/T)-eYFP) were performed at three sites (set 1-2 mm apart in the shape of an equilateral triangle approximately at the center of the array). At each site, 2 μ l of viral solution were injected at three different depths (1, 2, 3 mm). Despite the preferential expression of the CaMKII promoter in excitatory cells, previous studies using an AAV5 with various promoters in non-human primates have shown transduction in excitatory but also inhibitory neurons [23]. Array implantation was performed immediately following viral injections to facilitate positioning of the array aligned to the injection sites.

2. Electrophysiological recordings and optical stimulation

Neural recordings were done through a Cerebus multi-channel data acquisition system (Blackrock Microsystems, UT). The optical stimulation was controlled by a custom program written in Labview (National Instruments), sending an analog output to both the laser and the Cerebus data acquisition system for synchronization. In the stimulation protocols during awake resting states, we used constant pulses and light ramps. In particular, 4s long voltage ramps were used for analog modulation of the laser output, which attained a maximum optical power of 6 mW at the end of the ramp. Measurements using a photo-diode indicated that the optical output was slightly sub-linear with respect to the input voltage. Although this could affect the threshold values obtained using ramps, the qualitative results reported here are unaffected.

3. LFP spectral analysis and pairwise phase consistency (PPC) between neuronal spiking and LFPs

Spectral analysis was done in Matlab (Mathworks) using the Chronux toolbox (<http://chronux.org>). Raw data were low-pass filtered with a cutoff frequency of 300 Hz by a 9th order Butterworth filter to yield LFPs. Time-frequency spectrograms were generated through multi-taper methods with a half-bandwidth $W = 5$ Hz, a time window $T = 300$ ms and a number of tapers $K=2TW-1 = 2$, and averaged across trials in each session. Power spectral density was computed over a period of 900 ms during or before optical stimulation and averaged over trials. We used the

power spectrum theoretical confidence intervals provided by the Chronux toolbox. Amplitude of gamma power was determined by averaging the spectral power in the gamma band (40 – 80 Hz).

In addition to power spectrum analyses, we also examined the spectral coherence between single-neuron spiking and LFPs. Recent studies have examined the bias in spike-field coherence estimators, especially in the case of small sample spike trains. In particular, Vinck et al. [75] proposed an alternative measure called the pairwise phase consistency. That is the approach taken here to assess the strength of the phase-locking of neuronal spiking to LFP ongoing oscillations. Chance level distribution for PPC values was estimated via a random resampling approach based on jittering spike times under a uniform distribution in [-50, 50] ms.

4. Spatiotemporal pattern analysis

Time delays across the array were computed as time differences of the peaks in gamma band LFPs (40-60 Hz, subject T) between each electrode and a reference electrode. The electrode on the array with the earliest peak onset was used as reference. Corresponding delay maps were computed during single 20-ms gamma cycles, and averaged over all gamma cycles during multiple trials (N=54). Propagation patterns were identified based on the Horn-Shunk method, a computer vision algorithm classically used to extract the optical flow, or apparent motion, between two consecutive frames. Optical flow methods (Horn-Shunk or similar) have been used

previously to study the spatiotemporal dynamics of neural signals. We used this algorithm to estimate wave vector fields from gamma bandpass-filtered LFPs, specifically in two examples illustrating expanding concentric and spiral wave patterns. First, we applied a 2D linear interpolation of bandpass LFPs on a refined grid formed by repeatedly dividing the intervals 3 times in each dimension. Then we applied the Horn-Schunck algorithm on the interpolated signal (100 iterations; smoothing parameter $\alpha=0.6$). Finally, we averaged the obtained wave vector fields over time during each 20 ms gamma cycle. To further quantify the occurrence of the dominant wave pattern, i.e. expanding concentric waves, the estimated wave vector field was compared with the radial direction vector at each electrode (direction from the center of the array towards the electrode position) in each gamma oscillation cycle. If more than 60% of the sites all showed their wave vector pointing within plus-minus 35 degree of their radial directions in a given gamma cycle, the corresponding spatial pattern was defined as one expanding wave pattern event. Only sites where gamma oscillations were induced by light were included in the computation. The first 150ms after light stimulation onset and the last 50ms in a 1s stimulus were excluded from the analyses to rule out influence of light artifacts.

5. Neural point process modeling

Neuronal action potentials were initially sorted using an automated spike sorter in matlab [72] and then manually examined in Offline Sorter (Plexon). Signal-to-noise ratio (SNR) was calculated as the ratio of spike amplitude compared to the

95% confidence interval for the 5 voltage measurements preceding each spike. Sorted action potentials with a SNR ≥ 1 were used in this study. A point process framework developed by Truccolo et al. in 2005 [70] was used to estimate a generalized linear model of the intensity function (instantaneous spiking rate; 1-ms time resolution) of a given neuron conditioned on the amplitude envelope and phase of the optogenetically-induced gamma oscillations. Gamma amplitude and phase were obtained via a Hilbert transform of the band-pass-filtered LFPs (40-80 Hz). Given an estimated conditional intensity function, the probability of spiking in each 1-ms time bin and the related Receiver Operating Characteristic (ROC) curves were computed. Based on the area under the curve (AUC), we estimated the power of induced gamma amplitude and phase to predict neuronal spiking. Predictive power was defined as $2 \times (\text{AUC} - 0.5)$ and was computed under a five-fold cross-validation scheme.

5. Statistical tests

To compute spatial distribution maps of induced gamma, in each electrode the presence of optically-induced gamma oscillations was determined by comparing gamma power (averaged over 40 to 80 Hz) during and before the 1 s constant light stimulation. Otherwise stated, p-values were calculated via random permutation tests ($n = 104$) and subject to multiple testing corrections, which were implemented via the False Discovery Rate approach (FDR), for dependent samples. In all hypothesis tests, we used a significance level of 0.01.

A.3 Optogenetic stimulation above a critical intensity level induces narrow band gamma oscillations

We recorded 3 sessions in the motor cortex in each of the two opsin expressing macaque subjects (subject T, area M1; subject P, area PMv). Beyond these 6 passive recording sessions in which the subjects were in awake resting states, 5 additional sessions in Subject T were recorded where a visually-guided reach-and-grasp task was performed under applied perturbation of optogenetic stimulus. Sessions were recorded in different days with same stimulation parameter and recording settings to ensure consistency. During each session, subjects were head-fixed in a custom primate chair with a food tray blocked by a lifting door for implementation of the task. Light was delivered through the polymer optical fiber integrated on the MEA into targeted neocortical region with estimated 6 mW maximal intracortical power A.1. The modeled dependence of light spatial distribution on the particular optical stimulation power in neocortex and under MEA is shown in A.1.

We applied two light stimulation time profiles, constant and increasing ramp, respectively, to examine the induction of gamma band activity in primate motor cortex. A constant stimulus profile consisting of a single 1-second square pulse per trial was applied in all 6 recording sessions for both subjects. Single trial raw LFP signals, average (across trials) LFP spectrograms and power spectral densities showed

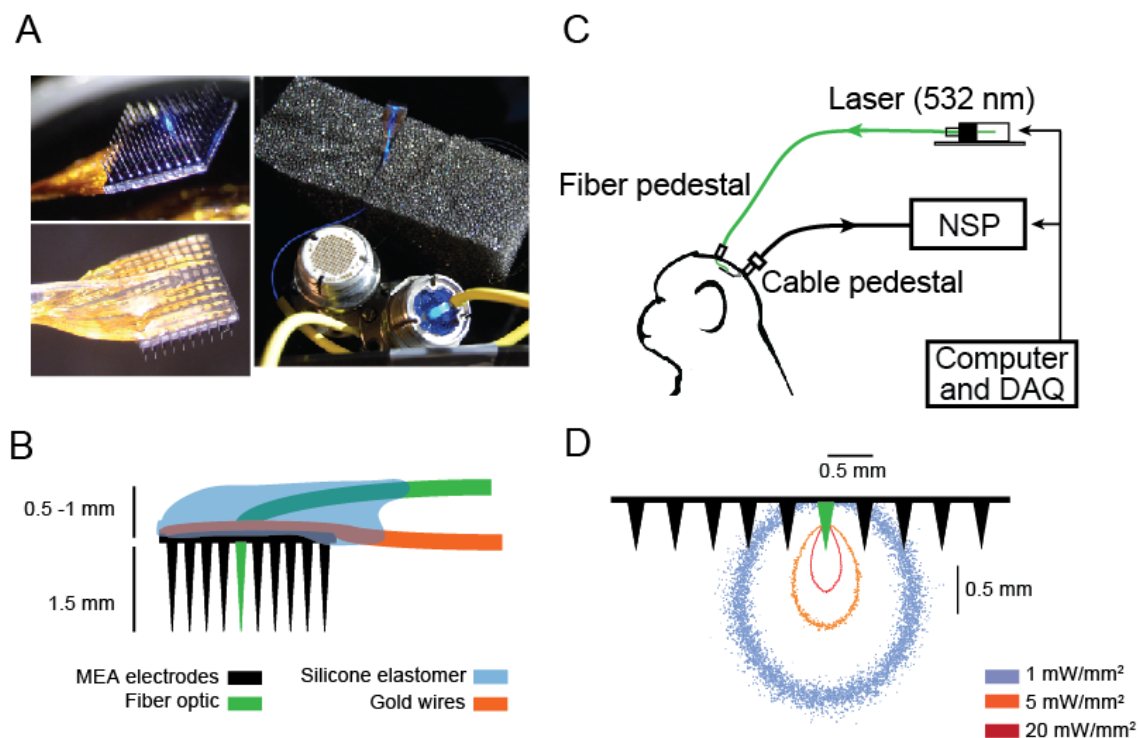


Figure A.1: Polymer optical fiber microelectrode array (POF-MEA). (A) POF-MEA viewed from the electrode side (top left), from the pad side (bottom left), and attached to two pedestals (Cereport, Blackrock Microsystems) for optical and electrical connections respectively (right). (B) Schematics of the POF-MEA; an optical fiber (green) was integrated around the center of the 10 X 10 MEA. (C) Neural recording and optical stimulation setup. (D) Monte-Carlo simulations of light distribution in the brain under 6 mW laser power shows iso-intensity contours at 1 (blue), 5 (orange), 20 (red) mW, respectively. (For illustration purpose, microelectrode separation, but not length, is on scale.)

clear induced narrowband gamma oscillations A.2. Induced oscillations in subject T had a mean frequency of 50 Hz, with higher values for subject P around 76 Hz. Induced gamma oscillations occurred immediately after stimulation onset and remained throughout the entire stimulation period, decreasing to background level after stimulation ended. The increase in the corresponding gamma power, with respect to the background gamma power measured in the 1-second period preceding stimulation onset, was significant ($p < 0.01$; random permutation test) in all sessions for both subjects in the examples shown in A.2.

To more closely examine the dependence of induced gamma oscillations on light stimulation power, the increasing ramp stimulation profile was applied in two sessions in subject T (Methods). This stimulation profile was repeated in 30 trials in each session. Through examination of simultaneously recorded LFPs from the POF-MEA, we observed the onset of 40-80 Hz LFP oscillations after a certain optical stimulation intensity was reached A.3. Gamma-band LFP power was enhanced as the light intensity further increased. This pattern of gamma oscillations onset with increasing light intensity was reliably reproduced across sessions and trials. The onset of optogenetically induced gamma LFP activity was determined by the time at which the power in the 40-80 Hz frequency band arose above the 95% confidence interval of the corresponding power during the preceding non-stimulation period.

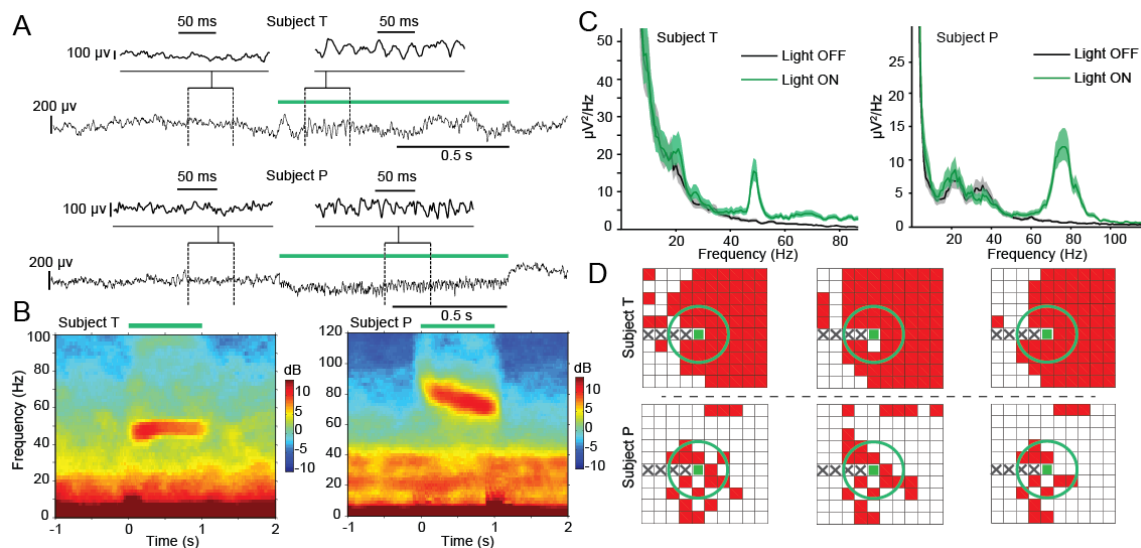


Figure A.2: Gamma oscillations induced by constant (square) pulse light stimulation. (A) Low-pass (< 300 Hz) filtered LFPs from two representative recording sites in subjects T (Top) and P (Bottom). (B) Trial-averaged (n=54; one session) LFP spectrograms for the corresponding LFP channels shown in (A), for subjects T and P respectively. (C) Trial-averaged LFP power spectral density based on the time interval [0.1, 0.9] s during stimulation (green curve). The black curve shows the power spectral density computed for a 0.8 s time window preceding the stimulation onset. (D) Spatial distribution of optically-induced gamma activity over the arrays in subjects T and P, all 6 sessions. Red squares indicate channels in which gamma band LFP power (40-80 Hz) increased during the stimulation period ($p < 0.01$; random permutation test with FDR correction for multiple testing).

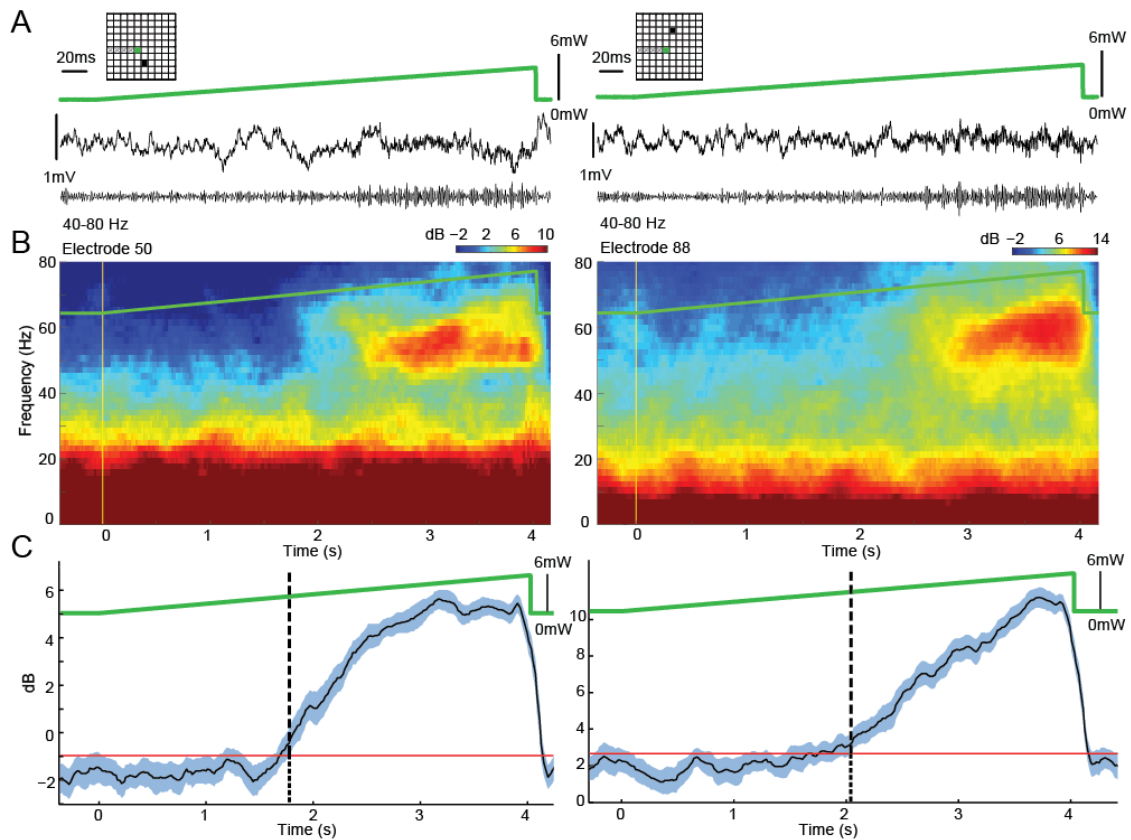


Figure A.3: Gamma oscillations induced by ramp light stimulation. (A) LFP (Top: ≈ 300 Hz; Bottom: 40-80 Hz) from two representative microelectrodes during a 4-second long light ramp. Inset shows the position of electrode. (B) Trial-averaged ($n=36$) spectrograms showed elevated LFP power in the gamma band (40-80 Hz) during the late stage of the light ramp. (C) Evolution of gamma power during light ramps (blue solid line: mean across trials, shaded area: 95% confidence interval). Onset of optogenetically-induced gamma oscillations, detected as the lower CI bound crossing the 99% percentile (red line) of the baseline gamma power, occurred once a critical light stimulation level was reached (2.67 mW and 3.06 mW).

A.4 Induced gamma engage a larger network beyond the direct light stimulation region

The simultaneous multichannel recording capability of the POF-MEA allowed us to track optically-induced transient gamma LFP oscillations in the 4 mm X 4 mm neocortical region surrounding the optical stimulation site. These oscillations were observed across a wide area of the recorded neocortical patch in both subjects. 80.0% and 23.4% of recording electrodes, in subject T and subject P respectively had a significant increase ($p < 0.01$; random permutation test with FDR multi-test correction) in 40-80 Hz LFP power during the 1-second stimulation. This difference in proportion across the two subjects might reflect the extent of opsin expression, differences in local connectivity and/or alignment between the stimulation site and viral injection.

According to previous intra-cortical light scattering simulations, recording electrodes within around 1 mm distance from the optical fiber are under direct light stimulation (using a threshold of 1 mW/mm² [4]). Thus, considering that laser light stimulation was delivered locally through single polymer optical fiber at the center of the array, induced gamma LFP oscillations were distributed not only within, but also well outside the volume of direct light stimulation, such as corner electrodes 2.6 mm away from the optical fiber tip. Thus the light-induced gamma oscillations from the peripheral recording electrodes on the array resulted from indirect recruitment of larger network activity rather than from direct activation of local circuits of

opsin-expressing neurons.

A.5 Spatiotemporal patterns (waves) of optogenetically-induced gamma oscillations

We examined the induced gamma oscillations in the time domain at each electrode site across the array. Band-pass-filtered LFPs (40-60 Hz in subject T and 60-80 Hz in subject P) in spatially separated electrodes revealed systematic differences in the time delays of induced gamma oscillations A.4. When averaged across all trials, these delays in gamma oscillations were spatially organized across the array, indicating horizontal cortical wave propagation.

To further reveal the spatial features of the induced propagating gamma waves, amplitudes of band-pass-filtered LFPs across all 95 electrodes in subject T (where a larger proportion of sites with induced gamma occurred) were mapped onto the microelectrode array site and over sequential time frames covering one gamma cycle (20 ms for subject T). Two wave propagation patterns were observed during the 1s square-pulse light-stimulation periods (supplementary movie). One of the patterns consisted of expanding concentric waves originating at the electrodes close to the light stimulation site. In the other pattern, anti-clockwise spiral waves centered near the optical stimulation site were observed A.4. The former pattern, expanding concentric

wave, was clearly the dominant spatiotemporal feature of the induced gamma oscillation in this subject, appearing in more than 60% of the overall light stimulation period (61.9% out of 660 gamma cycles in N=54 1s square-pulses, Methods; see also supplementary movie). In addition, the delay map averaged over gamma cycles and trials resembled the transient delay maps of the expanding concentric wave A.4.

A.6 Neuronal spiking during induced gamma oscillations

We examined recorded neuronal spiking activity in both subject T (M1) and subject P (PMv) during and outside the optogenetic stimulation period. Spiking activity of single units were sorted in the datasets of all 6 sessions from the two subjects (n=59, 52, 47 in subject T; n=56, 55, 46 in subject P). Neuronal spiking activity with both increased and decreased firing rates during the course of the 1s square pulse light stimulation were observed over a wide range of electrode positions on the array. Example raster plots and PSTHs are shown in A.5. Since optical activation of C1V1(T/T) results in neuronal excitation / depolarization, the observed decreased firing rates likely resulted from inhibitory effects mediated by network interactions. The proportion of neurons that showed increased and decreased firing rates during stimulation were determined to be 32% and 14% in Subject T, respectively, while in Subject P they were 17% and 22%, respectively. Again, we conjecture that these

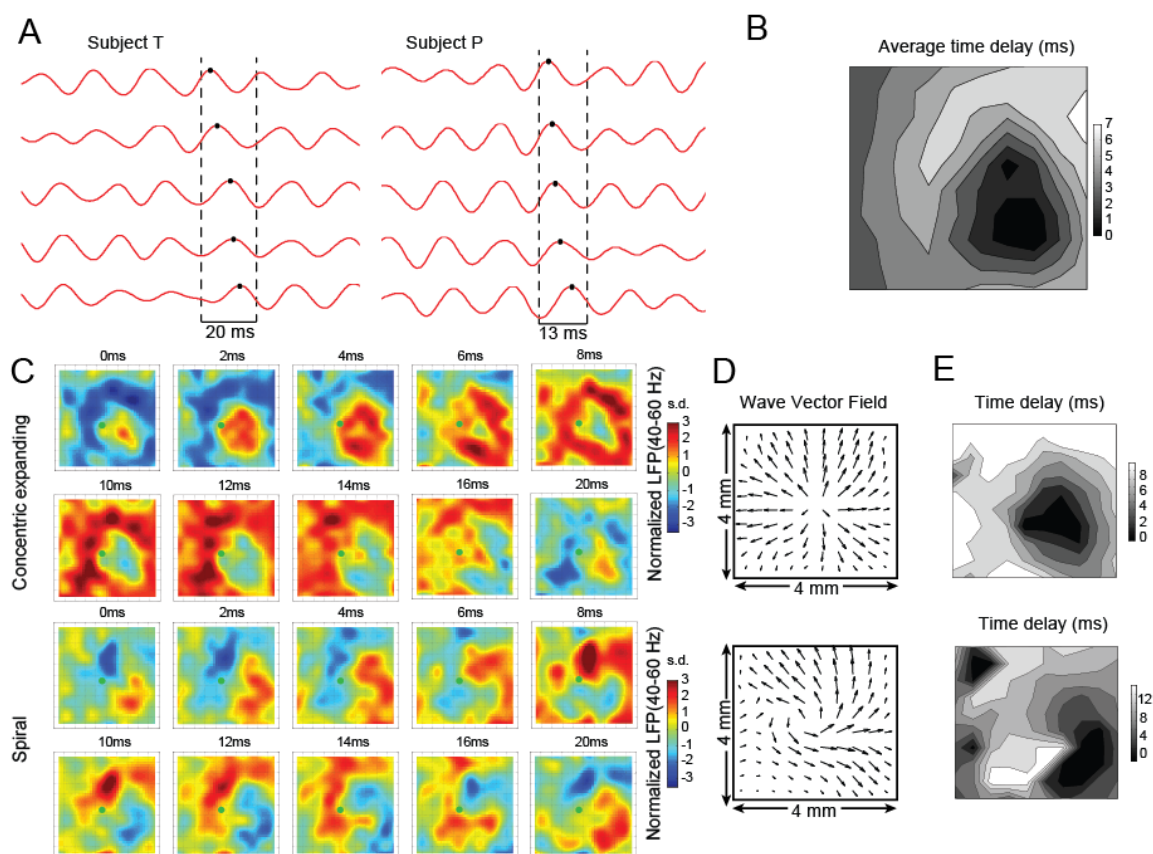


Figure A.4: Spatiotemporal patterns of optogenetically-induced gamma waves. (A) During stimulation, gamma band LFPs showed time delays between different electrodes. (B) Contour map of time delay at each electrode (subject T) with respect to the electrode with the shortest latency, averaged across all gamma cycles from 54 trials. (C) Snapshots of LFP amplitude maps (40-60 Hz, subject T) during a single gamma cycle of 20 ms. Top: Gamma waves propagate in an expanding concentric pattern. Bottom: Spiral pattern. (D) Different patterns of wave propagation illustrated by the averaged wave vector field evaluated via the Horn-Schunck method corresponding to the same sets of data shown in (C). (E) Contour map of transient time delay.

differences across the two subjects might reflect differences in local opsin expression and the recorded populations by the array.

To reveal the relationship between neuronal spiking activity and the simultaneous induced gamma-band LFP oscillations on the same electrode, pairwise phase consistency (PPC [75]) was computed A.6. Only electrode sites where increase in gamma power was statistically significant were included in the analysis. Despite the strong induced narrowband gamma LFP oscillations in these electrodes, only a subset of neurons showed elevated PPC values above chance levels in the specific gamma frequency band (40-80 Hz). The distribution of chance level PPC values was estimated via random resampling based on jittering the spike times (Methods). Nevertheless, even in this subset with statistically significant PPC, PPC values were relatively low indicating weak phase-locking of neuronal spiking to induced gamma LFP oscillations. Overall, although neuronal spiking rates could be largely modulated by light stimulation and many neurons' interspike time interval (ISI) distribution showed a peak corresponding to gamma frequency A.6, neuronal spiking remained highly asynchronous.

To complement the PPC analysis, we fitted neural point process models [70] to quantify the power of the instantaneous amplitude envelope and phase of the optogenetically induced gamma band oscillations to predict neuronal spiking. Instantaneous amplitudes and phases were obtained by taking the Hilbert transform of the band-pass filtered gamma LFP in the same electrode site as the modeled neuron. A point

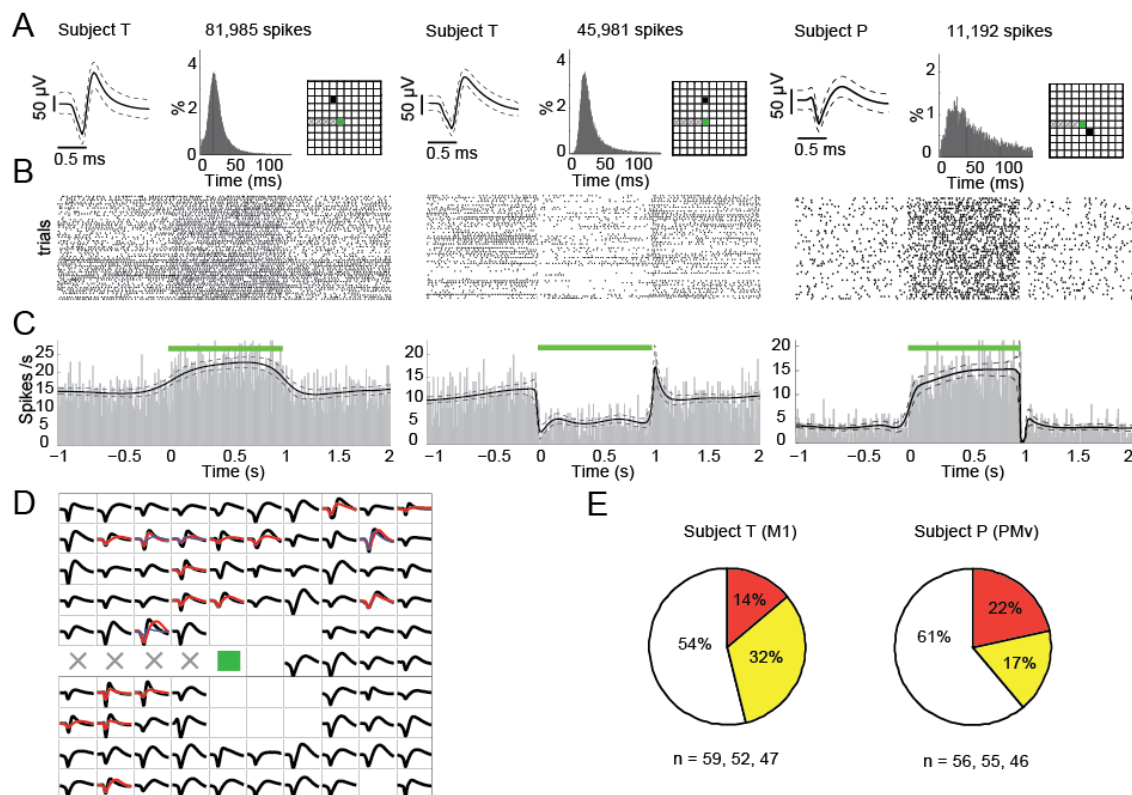


Figure A.5: Modulation of neuronal spiking rates during optogenetically-induced gamma LFP oscillations. (A) The action potential waveforms, ISIs and recording sites for three representative neurons recorded from the two subjects are shown. (B) Corresponding raster plots for each neuron ($n=54$ trials). (C) Corresponding PSTHs estimated via Bayesian adaptive regression splines showing either substantial increase or decrease in spike rates during optical stimulation. The dashed-curves indicate the 95% confidence intervals. (D) Average waveforms of all recorded neurons on the array. Units on the same electrode are shown in different colors. (E) Proportion of neuronal recordings that showed an increase (yellow), decrease (orange), or no change (white) in spiking rates during optical stimulation.

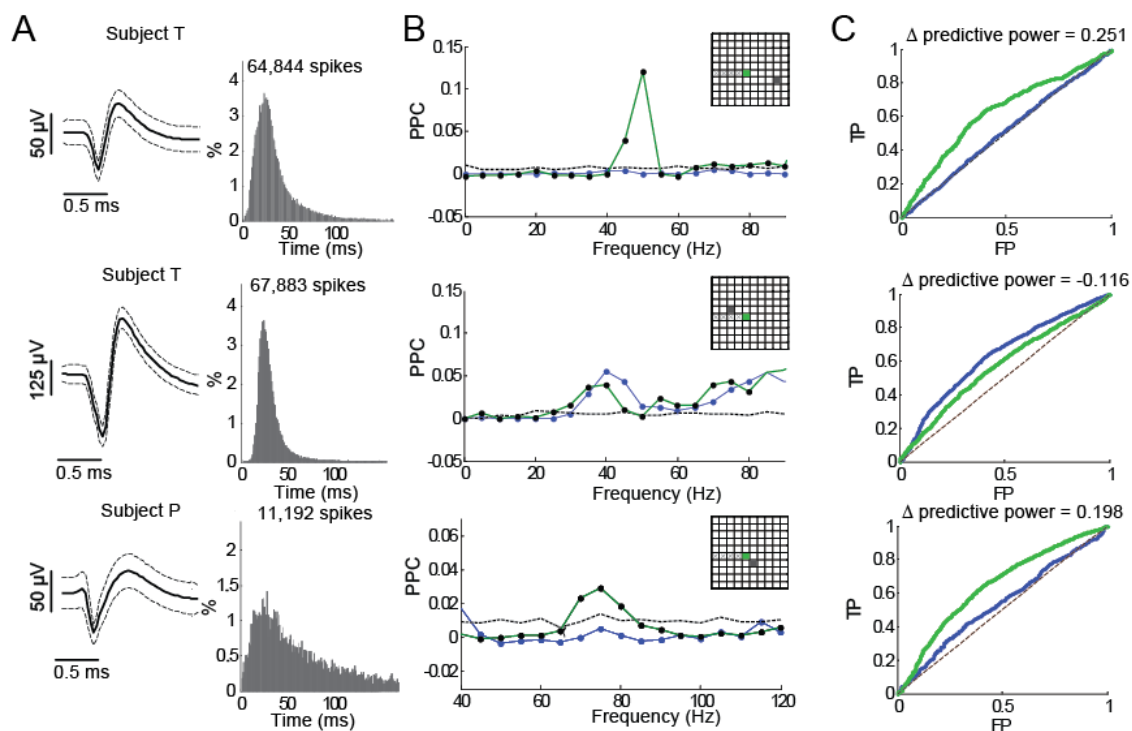


Figure A.6: Spike-LPF pairwise phase consistency analysis and predictive power of optogenetically-induced gamma oscillations on neuronal spiking. (A) Waveforms and ISIs of 3 examples of recorded neuronal spiking. (B) Corresponding pairwise phase consistency (PPC) analysis quantifying the phase-locking of neuronal spiking to LFP oscillations during the 1 s before light stimulation (blue) and during the 1 s optical stimulation period (green). The dashed line shows the 95% confidence interval for the PPC chance level. (C) ROC curves assessing prediction of spiking for the corresponding three neurons using a point process model where the instantaneous rate was modeled as a function of the amplitude envelope and phase of induced gamma. The diagonal dashed line indicates chance level prediction. Blue and green ROC curves correspond to the baseline and stimulation periods, respectively.

process framework was used to fit generalized linear models (GLMs) of the instantaneous spiking rate (conditional intensity function) conditioned on the instantaneous gamma amplitude and phase. Given an estimated GLM, the probability of the modeled neuron to spike in every 1ms time bin and the corresponding ROC curves were computed A.6. Based on the area under the ROC curve, the predictive power, ranging from 0 (no prediction) to 1 (perfect prediction), was computed. Predictive power was computed under a five-fold cross-validation scheme. Predictive power was computed both for the 1-second period preceding stimulation onset (baseline period) and for the 1-second stimulation period. Overall, our analyses based on PSTHs, PPC and GLM predictive power suggest varied and complex relationships between neuronal spiking and the optogenetically induced collective dynamics characterized by narrowband gamma oscillations.

A.7 Discussion and conclusions

In this appendix we have demonstrated that constant optogenetic stimulation based on the C1V1(T/T) opsin can induce sustained narrow-band gamma LFP oscillations in non-human primate motor cortex. Induced gamma oscillations were observed both in primary motor and ventral premotor cortices. These induced oscillations engaged larger cortical networks in the 4 X 4 mm recorded neocortical patches beyond the direct light stimulation domain. The larger network gamma activity was organized in spatiotemporal patterns consisting primarily of expanding concentric waves and other

occasional patterns such as spiral waves. Optical stimulation modulated the firing rate of 46% and 39% of recorded neurons in subjects T and P, respectively. Rate modulation effects showed either a substantial increase or decrease in firing rates. Despite this stimulation-related modulation effect in firing rates, neuronal spiking remained largely asynchronous with respect to the optogenetically induced gamma oscillations, as assessed by measures of phase-locking (pairwise phase consistency) and neural point process predictive power. Overall, our study provides new findings on gamma oscillations induced via optogenetics. The fact that these gamma oscillations were generated by a very simple (constant) stimulation pattern supports the predisposition of neural circuits to generate gamma oscillations under driving inputs in primate motor cortex.

The particular optogenetic construct we used (CaMKII promoter and AAV5 viral vector) is known to express primarily in pyramidal neurons and to a lesser degree in inhibitory interneurons. Thus, although we take the view that gamma oscillations were induced primarily via optical stimulation of pyramidal neurons, we cannot rule out the role of direct optical stimulation in inhibitory interneurons. We considered further analyses based on classifying the recorded neurons into putative pyramidal and inhibitory interneurons. Based on this classification, one could attempt to infer potentially distinct roles for putative pyramidal and inhibitory interneurons in the generation of optogenetically induced gamma LFP oscillations. We also note that

optogenetics in primates is presently a less developed subject than for mouse models (transgenic lines, Cre-recombinase strategies, etc). Progress in this area can be expected to yield better cell type-specific access to cortical circuits in primate brains.

With respect to the induced gamma LFP, neuronal spiking remained largely asynchronous oscillations even though these oscillations were strong and narrowband. This was demonstrated by the weak phase-locking of spiking to the induced gamma LFPs, and by the low gamma amplitude and phase power to predict neuronal spiking. One could expect that under these narrowband oscillations the phase-coupling should be much stronger. However, similar observations have been made in various neural systems and different conditions. For example, Truccolo et al. in 2014 [69] have reported human focal epileptic seizures characterized by sustained narrowband (40 – 60 Hz) gamma oscillations where neuronal spiking also remains highly asynchronous. Furthermore, previous mathematical and computational modeling Brunel et al. in 2003 [11] have demonstrated that narrowband sustained gamma LFP oscillations can indeed emerge at the collective dynamics levels even though neuronal spiking, in both pyramidal and inhibitory interneurons, remains highly irregular and asynchronous.

The combination of optogenetic stimulation and microelectrode array recordings as presented here provides an important approach for probing spatiotemporal cortical dynamics in primates, both in healthy conditions and in neurological disorders. We are currently working on further developing the capabilities of this tool by allowing, for example, multiple optical stimulation sites on the microelectrode array. In this

way, new studies can be extended to the application of complex spatiotemporal stimulation patterns at multiple recording sites, to probe neural dynamics across multiple temporal and spatial scales.

References

- [1] E D Abercrombie, K a Keefe, D S DiFrischia, and M J Zigmond. Differential effect of stress on in vivo dopamine release in striatum, nucleus accumbens, and medial frontal cortex. *Journal of neurochemistry*, 52(5):1655–1658, 1989.
- [2] Antoine R Adamantidis, Hsing-Chen Tsai, Benjamin Boutrel, Feng Zhang, Garrett D Stuber, Evgeny A Budygin, Antonello Bonci, Karl Deisseroth, and Luis De Lecea. Optogenetic Interrogation of Dopaminergic Modulation of the Multiple Phases of Reward-Seeking Behavior. *Journal of Neuroscience*, 31(30):10829–10835, 2011.
- [3] Hillel Adesnik and Massimo Scanziani. Lateral competition for cortical space by layer-specific horizontal circuits. *Nature*, 464(7292):1155–60, April 2010.
- [4] Alexander M Aravanis, Li-Ping Wang, Feng Zhang, Leslie a Meltzer, Murtaza Z Mogri, M Bret Schneider, and Karl Deisseroth. An optical neural interface: in vivo control of rodent motor cortex with integrated fiberoptic and optogenetic technology. *Journal of neural engineering*, 4(3):S143–56, September 2007.

- [5] Benjamin R Arenkiel, Joao Peca, Ian G Davison, Catia Feliciano, Karl Deisseroth, George J Augustine, Michael D Ehlers, and Guoping Feng. In vivo light-induced activation of neural circuitry in transgenic mice expressing channelrhodopsin-2. *Neuron*, 54(2):205–18, 2007.
- [6] Majid Arvand and Navid Ghodsi. A voltammetric sensor based on graphene-modified electrode for the determination of trace amounts of l-dopa in mouse brain extract and pharmaceuticals. *Journal of Solid State Electrochemistry*, 17(3):775–784, November 2012.
- [7] C.E. Bass, V. P. Grinevich, A.D. Kulikova, K.D. Bonin, and E.A. Budygin. Terminal effects of optogenetic stimulation on dopamine dynamics in rat striatum. 214(2):149–155, 2013.
- [8] B D Bath, D J Michael, B J Trafton, J D Joseph, P L Runnels, and R M Wightman. Subsecond adsorption and desorption of dopamine at carbon-fiber microelectrodes. *Analytical chemistry*, 72(24):5994–6002, December 2000.
- [9] Edward Boyden. A history of optogenetics: the development of tools for controlling brain circuits with light. *F1000 Biology Reports*, 3(May):1–12, 2011.
- [10] Jeffrey M Brown, Glen R Hanson, and Annette E Fleckenstein. Cocaine-induced increases in vesicular dopamine uptake: role of dopamine receptors. *The Journal of pharmacology and experimental therapeutics*, 298(3):1150–1153, 2001.

- [11] Nicolas Brunel and Xiao-Jing Wang. What determines the frequency of fast network oscillations with irregular neural discharges? I. Synaptic dynamics and excitation-inhibition balance. *Journal of neurophysiology*, 90(1):415–430, 2003.
- [12] Evgeny A Budygin, Carrie E John, Yolanda Mateo, and Sara R Jones. Lack of cocaine effect on dopamine clearance in the core and shell of the nucleus accumbens of dopamine transporter knock-out mice. *The Journal of neuroscience : the official journal of the Society for Neuroscience*, 22(10):RC222, 2002.
- [13] D R Bull, P Palij, M J Sheehan, J Millar, J a Stamford, Z L Kruk, and P P Humphrey. Application of fast cyclic voltammetry to measurement of electrically evoked dopamine overflow from brain slices in vitro. *Journal of neuroscience methods*, 32(1):37–44, 1990.
- [14] J. Cammack, B. Ghasemzadeh, and R. N. Adams. The pharmacological profile of glutamate-evoked ascorbic acid efflux measured by in vivo electrochemistry. *Brain Research*, 565(1):17–22, 1991.
- [15] Jessica a Cardin, Marie Carlén, Konstantinos Meletis, Ulf Knoblich, Feng Zhang, Karl Deisseroth, Li-Huei Tsai, and Christopher I Moore. Driving fast-spiking cells induces gamma rhythm and controls sensory responses. *Nature*, 459(7247):663–7, June 2009.
- [16] Jessica a Cardin, Marie Carlén, Konstantinos Meletis, Ulf Knoblich, Feng Zhang, Karl Deisseroth, Li-Huei Tsai, and Christopher I Moore. Targeted optogenetic

- stimulation and recording of neurons in vivo using cell-type-specific expression of Channelrhodopsin-2. *Nature protocols*, 5(2):247–54, February 2010.
- [17] Dipesh Chaudhury, Jessica J Walsh, Allyson K Friedman, Barbara Juarez, Stacy M Ku, Ja Wook Koo, Deveroux Ferguson, Hsing-Chen Tsai, Lisa Pomeranz, Daniel J Christoffel, Alexander R Nectow, Mats Ekstrand, Ana Domingos, Michelle S Mazei-Robison, Ezekiell Mouzon, Mary Kay Lobo, Rachael L Neve, Jeffrey M Friedman, Scott J Russo, Karl Deisseroth, Eric J Nestler, and Ming-Hu Han. Rapid regulation of depression-related behaviours by control of midbrain dopamine neurons. *Nature*, 493(7433):532–6, January 2013.
- [18] Jeremy J Clark, Stefan G Sandberg, Matthew J Wanat, Jerylin O Gan, Eric a Horne, Andrew S Hart, Christina a Akers, Jones G Parker, Ingo Willuhn, Vicente Martinez, Scott B Evans, Nephi Stella, and Paul E M Phillips. SI_Chronic microensors for longitudinal, subsecond dopamine detection in behaving animals. *Nature methods*, 7(2):126–129, 2010.
- [19] Roshan Cools. Role of dopamine in the motivational and cognitive control of behavior. *The Neuroscientist*, 14(4):381–395, August 2008.
- [20] F H Crick. Thinking about the brain. *Scientific American*, 241:219–232, 1979.
- [21] Charles A Dackis, M D, Charles P O Brien, and D Ph. Cocaine dependence : a disease of the brain ’ s reward centers. *journal of substance abuse treatment*, 21:111–117, 2001.

- [22] Karl Deisseroth. Optogenetics. *Nature Methods*, 8(1):26–29, 2011.
- [23] Ilka Diester, Matthew T Kaufman, Murtaza Mogri, Ramin Pashaie, Werapong Goo, Ofer Yizhar, Charu Ramakrishnan, Karl Deisseroth, and Krishna V Shenoy. An optogenetic toolbox designed for primates. *Nature neuroscience*, 14(3):387–97, 2011.
- [24] Boadie W Dunlop and Charles B Nemeroff. The Role of Dopamine in the Pathophysiology of Depression. *Arch gen psychiatry*, 64:327–337, 2007.
- [25] J D Erickson, M K Schafer, T I Bonner, L E Eiden, and E Weihe. Distinct pharmacological properties and distribution in neurons and endocrine cells of two isoforms of the human vesicular monoamine transporter. *Proceedings of the National Academy of Sciences of the United States of America*, 93(10):5166–5171, 1996.
- [26] Sarah J Farnsworth, Trent J Volz, Glen R Hanson, and Annette E Fleckenstein. Cocaine alters vesicular dopamine sequestration and potassium-stimulated dopamine release: the role of D2 receptor activation. *The Journal of Pharmacology and Experimental Therapeutics*, 328(3):807–812, 2009.
- [27] D. L. Felten and J. R. Sladek. Monoamine distribution in primate brain. V. Monoaminergic nuclei: Anatomy, pathways and local organization. *Brain Research Bulletin*, 10(2):171–284, 1983.

- [28] Lief Fenno, Ofer Yizhar, and Karl Deisseroth. The Development and Application of Optogenetics. *Annual Review of Neuroscience*, 34(1):389–412, 2011.
- [29] Ingmar H Franken, Jan Booij, and Wim van den Brink. The role of dopamine in human addiction: from reward to motivated attention. *European journal of pharmacology*, 526:199–206, December 2005.
- [30] Paul A. Garris, John R. C. Christensen, George V. Rebec, and R. Mark Wightman. Real-Time Measurement of Electrically Evoked Extracellular Dopamine in the Striatum of Freely Moving Rats. *Journal of Neurochemistry*, 68(1):152–161, November 1997.
- [31] Paul A Garris, Michaux Kilpatrick, Melissa A Bunin, Darren Michael, Q David Walker, and R Mark Wightman. Dissociation of dopamine release in the nucleus accumbens from intracranial self-stimulation. *Nature*, 398(6722):67–69, 1999.
- [32] F.G. Gonon. Nonlinear relationship between impulse flow and dopamine released by rat midbrain dopaminergic neurons as studied by in vivo electrochemistry. *Neuroscience*, 24(1):19–28, January 1988.
- [33] Alexander Gray, Mehdi Balooch, Stephane Allegret, Stefan De Gendt, and Wei-E Wang. Optical detection and characterization of graphene by broadband spectrophotometry. *Journal of Applied Physics*, 104(5):053109, 2008.
- [34] Nir Grossman, Konstantin Nikolic, Christofer Toumazou, and Patrick Degenaar. Modeling study of the light stimulation of a neuron cell with channelrhodopsin-2

- mutants. *IEEE transactions on bio-medical engineering*, 58(6):1742–1751, June 2011.
- [35] Zengcai V. Guo, S. Andrew Hires, Nuo Li, Daniel H. O’Connor, Takaki Komiyama, Eran Ophir, Daniel Huber, Claudia Bonardi, Karin Morandell, Diego Gutnisky, Simon Peron, Ning-long Xu, James Cox, and Karel Svoboda. Procedures for Behavioral Experiments in Head-Fixed Mice. *PLoS ONE*, 9(2):e88678, 2014.
- [36] Michael L A V Heien, Amina S Khan, Jennifer L Ariansen, Joseph F Cheer, Paul E M Phillips, Kate M Wassum, and R Mark Wightman. Real-time measurement of dopamine fluctuations after cocaine in the brain of behaving rats. *Proceedings of the National Academy of Sciences of the United States of America*, 102(29):10023–10028, 2005.
- [37] Michael L a V Heien, Paul E M Phillips, Garret D Stuber, Andrew T Seipel, and R Mark Wightman. Overoxidation of carbon-fiber microelectrodes enhances dopamine adsorption and increases sensitivity. *The Analyst*, 128(12):1413–9, December 2003.
- [38] M.J. Higgins and T.W. Stone. Bicuculline-resistant paired-pulse inhibition in the rat hippocampal slice. *British Journal of Pharmacology*, 109(4):1164–1168, August 1993.
- [39] Sara R Jones, Joshua D Joseph, Larry S Barak, Marc G Caron, and R Mark

- Wightman. Dopamine neuronal transport kinetics and effects of amphetamine. *Journal of neurochemistry*, 73(6):2406–2414, 1999.
- [40] K T Kawagoe, J B Zimmerman, and R M Wightman. Principles of voltammetry and microelectrode surface states. *Journal of neuroscience methods*, 48(3):225–40, July 1993.
- [41] Samuel P Kounaves. Voltammetric Techniques. *Handbook of Instrumental Techniques for Analytical Chemistry*, pages 709–726, 1997.
- [42] W G Kuhr, a G Ewing, W L Caudill, and R M Wightman. Monitoring the stimulated release of dopamine with in vivo voltammetry. I: Characterization of the response observed in the caudate nucleus of the rat. *Journal of neurochemistry*, 43(2):560–9, August 1984.
- [43] Chang Lin Liang, Tom T Wang, Kate Luby-Phelps, and Dwight C German. Mitochondria mass is low in mouse substantia nigra dopamine neurons: implications for Parkinson’s disease. *Experimental neurology*, 203(2):370–80, February 2007.
- [44] Yao Lu, Nicolette Driscoll, Ilker Ozden, Zeyang Yu, and Arto V. Nurmikko. Modulating dopamine release by optogenetics in transgenic mice reveals terminal dopaminergic dynamics. *Neurophotonics*, 2(3):031207, 2015.
- [45] Yao Lu, Wilson Truccolo, Fabien Bertrand Paul Wagner, Carlos E. Vargas-Irwin, Ilker Ozden, Jonas B. Zimmermann, Travis May, Naubahar Agha, Jing Wang,

- and Arto V Nurmikko. Optogenetically-Induced Spatiotemporal Gamma Oscillations and Neuronal Spiking Activity in Primate Motor Cortex. *Journal of Neurophysiology*, 2015.
- [46] Linda Madisen, Tianyi Mao, Henner Koch, Jia-min Zhuo, Antal Berenyi, Shigeyoshi Fujisawa, Yun-Wei a Hsu, Alfredo J Garcia, Xuan Gu, Sebastien Zanella, Jolene Kidney, Hong Gu, Yimei Mao, Bryan M Hooks, Edward S Boyden, György Buzsáki, Jan Marino Ramirez, Allan R Jones, Karel Svoboda, Xue Han, Eric E Turner, and Hongkui Zeng. A toolbox of Cre-dependent optogenetic transgenic mice for light-induced activation and silencing. *Nature Neuroscience*, 15(5):793–802, 2012.
- [47] Monique a Makos, Kyung-An Han, Michael L Heien, and Andrew G Ewing. Using In Vivo Electrochemistry to Study the Physiological Effects of Cocaine and Other Stimulants on the *Drosophila melanogaster* Dopamine Transporter. *ACS chemical neuroscience*, 1(1):74–83, January 2010.
- [48] Vivien Marx. Microscopy: seeing through tissue. *Nature Methods*, 11(12):1209–1214, 2014.
- [49] James R. Melchior, Mark J. Ferris, Garret D Stuber, David R. Riddle, and Sara R. Jones. Optogenetic versus electrical stimulation of dopamine terminals in the Nucleus accumbens elicits local modulation of presynaptic release. *Journal of Neurochemistry*, pages n/a–n/a, 2015.

- [50] Arben Merkoçi, Martin Pumera, Xavier Llopis, Briza Pérez, Manel del Valle, and Salvador Alegret. New materials for electrochemical sensing VI: Carbon nanotubes. *TrAC Trends in Analytical Chemistry*, 24(9):826–838, October 2005.
- [51] a. Nimmerjahn. Surgical Implantation of a Head Plate in Mice in Preparation for In Vivo Two-Photon Imaging of Microglia. *Cold Spring Harbor Protocols*, 2012(5):pdb.prot069278–pdb.prot069278, 2012.
- [52] C Warren Olanow. The scientific basis for the current treatment of Parkinson’s disease. *Annual review of medicine*, (55):41–60, January 2004.
- [53] Ilker Ozden, Jing Wang, Yao Lu, Travis May, Joonhee Lee, Werapong Goo, Daniel J O’Shea, Paul Kalanithi, Ilka Diester, Mohamed Diagne, Karl Deisseroth, Krishna V Shenoy, and Arto V Nurmikko. A coaxial optrode as multifunction write-read probe for optogenetic studies in non-human primates. *Journal of neuroscience methods*, 219(1):142–54, September 2013.
- [54] T D Parsons, J R Coorsen, H Hortmann, A K Lee, F W Tse, and W Almers. The Last Seconds in the Life of a Secretory Vesicle. *Cold Spring Harbor Symposia on Quantitative Biology*, 60:389–396, January 1995.
- [55] A.G. Phillips, C.D. Blaha, and H.C. Fibiger. Neurochemical correlates of brain-stimulation reward measured by ex vivo and in vivo analyses. *Neuroscience & Biobehavioral Reviews*, 13(2-3):99–104, June 1989.

- [56] P E Phillips, Donita L Robinson, Garret D Stuber, Regina M Carelli, and R Mark Wightman. Real-time measurements of phasic changes in extracellular dopamine concentration in freely moving rats by fast-scan cyclic voltammetry. *Methods Mol Med*, 79:443–464, 2003.
- [57] Paul E M Phillips, Pamela J Hancock, and Jonathan a Stamford. Time window of autoreceptor-mediated inhibition of limbic and striatal dopamine release. *Synapse (New York, N.Y.)*, 44(1):15–22, April 2002.
- [58] James G Roberts, Leyda Z Lugo-morales, Philip L Loziuk, and Leslie A Sombers. *Real-Time Chemical Measurements of Dopamine Release in the Brain*, volume 964. 2013.
- [59] D.a. Robinson. The electrical properties of metal microelectrodes. *Proceedings of the IEEE*, 56(6):1065–1071, 1968.
- [60] Donita L Robinson, Michael L a V Heien, and R Mark Wightman. Frequency of dopamine concentration transients increases in dorsal and ventral striatum of male rats during introduction of conspecifics. *The Journal of neuroscience : the official journal of the Society for Neuroscience*, 22(23):10477–10486, 2002.
- [61] Donita L Robinson, B Jill Venton, Michael L a V Heien, and R Mark Wightman. Detecting subsecond dopamine release with fast-scan cyclic voltammetry in vivo. *Clinical chemistry*, 49(10):1763–73, October 2003.

- [62] Mitchell F Roitman, Garret D Stuber, Paul E M Phillips, R Mark Wightman, and Regina M Carelli. Dopamine operates as a subsecond modulator of food seeking. *The Journal of neuroscience : the official journal of the Society for Neuroscience*, 24(6):1265–71, February 2004.
- [63] Wolfram Schultz. Behavioral dopamine signals. *Trends in neurosciences*, 30(5):203–10, May 2007.
- [64] Roger Sperry. Some effects of disconnecting the cerebral hemispheres. *Bioscience Reports*, 2(5):265–276, 1982.
- [65] Jonathan A Stamford, Zygmunt L Kruk, Peter Palij, and Julian Millar. Diffusion and uptake of dopamine in rat caudate and nucleus accumbens compared using fast cyclic voltammetry. *Brain Research*, 448:381–385, 1988.
- [66] Garret D Stuber, Thomas S Hnasko, Jonathan P Britt, Robert H Edwards, and Antonello Bonci. Dopaminergic terminals in the nucleus accumbens but not the dorsal striatum corelease glutamate. *The Journal of neuroscience : the official journal of the Society for Neuroscience*, 30(24):8229–8233, 2010.
- [67] B E Kumara Swamy and B Jill Venton. Carbon nanotube-modified microelectrodes for simultaneous detection of dopamine and serotonin in vivo. *The Analyst*, 132(9):876–84, September 2007.
- [68] Sarah Threlfell, Tatjana Lalic, Nicola J Platt, Katie A Jennings, Karl Deisseroth,

and Stephanie J Cragg. Striatal dopamine release is triggered by synchronized activity in cholinergic interneurons. *Neuron*, 75(1):58–64, July 2012.

- [69] W. Truccolo, O. J. Ahmed, M. T. Harrison, E. N. Eskandar, G. R. Cosgrove, J. R. Madsen, a. S. Blum, N. S. Potter, L. R. Hochberg, and S. S. Cash. Neuronal Ensemble Synchrony during Human Focal Seizures. *Journal of Neuroscience*, 34(30):9927–9944, 2014.
- [70] Wilson Truccolo, Uri T Eden, Matthew R Fellows, John P Donoghue, and Emery N Brown. A point process framework for relating neural spiking activity to spiking history, neural ensemble, and extrinsic covariate effects. *Journal of neurophysiology*, 93(2):1074–1089, 2005.
- [71] Hsing-chen Tsai, Feng Zhang, Antoine Adamantidis, Garret D. Stuber, Antonello Bonci, Luis De Lecea, and Karl Deisseroth. Phasic firing of dopamine...SI. *Science*, 324(May):1080, 2009.
- [72] Carlos E Vargas-irwin, Gregory Shakhnarovich, Payman Yadollahpour, M K John, Michael J Black, and John P Donoghue. motor cortex populations. 30(29):9659–9669, 2011.
- [73] B. Jill Venton, Hui Zhang, Paul a. Garris, Paul E. M. Phillips, David Sulzer, and R. Mark Wightman. Real-time decoding of dopamine concentration changes in the caudate-putamen during tonic and phasic firing. *Journal of Neurochemistry*, 87(5):1284–1295, November 2003.

- [74] Trisha L Vickrey, Barry Condron, and B Jill Venton. Rapid Detection of Endogenous Dopamine Changes in *Drosophila melanogaster* using Fast-Scan Cyclic Voltammetry. *Analytical chemistry*, 81(22):9306–9313, 2009.
- [75] Martin Vinck, Marijn van Wingerden, Thilo Womelsdorf, Pascal Fries, and Cyriel M a Pennartz. The pairwise phase consistency: a bias-free measure of rhythmic neuronal synchronization. *NeuroImage*, 51(1):112–22, May 2010.
- [76] Jing Wang, Fabien Wagner, David a Borton, Jiayi Zhang, Ilker Ozden, Rebecca D Burwell, Arto V Nurmikko, Rick van Wagenen, Ilka Diester, and Karl Deisseroth. Integrated device for combined optical neuromodulation and electrical recording for chronic in vivo applications. *Journal of neural engineering*, 9(1):016001, February 2012.
- [77] R M Wightman, C Amatore, R C Engstrom, P D Hale, E W Kristensen, W G Kuhr, and L J May. Real-time characterization of dopamine overflow and uptake in the rat striatum. *Neuroscience*, 25(2):513–523, 1988.
- [78] R Mark Wightman, Michael L a V Heien, Kate M Wassum, Leslie a Sombers, Brandon J Aragona, Amina S Khan, Jennifer L Ariansen, Joseph F Cheer, Paul E M Phillips, and Regina M Carelli. Dopamine release is heterogeneous within microenvironments of the rat nucleus accumbens. *The European journal of neuroscience*, 26(7):2046–54, October 2007.

- [79] R Mark Wightman and Donita L Robinson. Transient changes in mesolimbic dopamine and their association with 'reward'. *Journal of Neurochemistry*, 82(4):721–735, 2002.
- [80] Q Wu, M E Reith, R M Wightman, K T Kawagoe, and P A Garris. Determination of release and uptake parameters from electrically evoked dopamine dynamics measured by real-time voltammetry. *Journal of neuroscience methods*, 112(2):119–133, 2001.
- [81] Jordan T Yorgason, Rodrigo a España, and Sara R Jones. Demon voltammetry and analysis software: analysis of cocaine-induced alterations in dopamine signaling using multiple kinetic measures. *Journal of neuroscience methods*, 202(2):158–64, November 2011.
- [82] Matthew K Zachek, Jinwoo Park, Pavel Takmakov, R Mark Wightman, and S Gregory. Microfabricated FSCV-Compatible Microelectrode Array for Real-time Monitoring of Heterogeneous Dopamine Release. *Analyst*, 135(7):1556–1563, 2010.
- [83] Shengli Zhao, Catarina Cunha, Feng Zhang, Qun Liu, Bernd Gloss, George J Augustine, and Guoping Feng. Improved expression of halorhodopsin for light-induced silencing of neuronal activity. *Brain Cell Biol.*, 36(1-4):141–154, 2008.